ANALYSIS OF ENERGY REQUIREMENTS IN STIRRED MEDIA MILLS

by

RICHARD JOHN TAMBLYN

A thesis submitted to
The University of Birmingham
for the degree of
DOCTOR OF ENGINEERING

School of Chemical Engineering
College of Engineering and Physical Sciences
The University of Birmingham
August 2009

Abstract

Vertically stirred media mills represent an important tool for the comminution of a range of industrial minerals. In this work, calcium carbonate is ground to size ranges below 2 µm in an Imerys stirred media mill. The role of grinding media on the efficiency is considered, and with the use of a novel, rod shaped grinding media, significant energy savings in ultrafine wet grinding are seen. This is proven to be an effect attributable to the shape of the grinding media, rather than the density of the grinding media. After a comprehensive efficiency analysis of the performance of a range of spherical and rod shaped media, further investigations are made through analysis of flow patterns within the mill using Positron Emission Particle Tracking (PEPT). Data collected from PEPT has given new insights into the distribution of material and kinetic energy within the mill, as well as an understanding of the effect of media density and motor speed in relation to the efficiency of the grinding. Furthermore, investigations are made into dry grinding of talc using the stirred media mill, which is subsequently soaked in water to give a low energy route to high surface area of the mineral.

For my grandparents...

An dyscudhansowdhym yu an moyha a vry re be gusulyes dhym der ow dyfygyansow.

The most important of my discoveries have been suggested to me by my failures.

Sir Humphry Davy, Scientist and Cornishman.

Acknowledgements

I would like to thank a number of people for their help and advice with this thesis. At the university, the guidance and supervision of Neil Rowson and Richard Greenwood, for the technical advice, encouragement and the opportunities they have granted me.

I would also like to thank the supervision I have received from everyone at Imerys – Jarrod Hart for his advice and enthusiasm and our lengthy (often philosophical) discussions about my work. Dave Skuse and Dave Gittins have also been great sources of support throughout my time there.

The rest of the New Technology Group at Imerys have all allowed a wealth of knowledge and experience to benefit this work, especially John Slater for all of the help with polymer testing in the earlier points in this work, as well as Mark Windebank for his many ideas and contributions to the grinding project. Elsewhere at Imerys I thank the Physical Testing, Analytical Chemistry and Microscopy groups for all of the help with test work.

I also thank Serafim Bakalis, Andy Ingram and Xianfeng Fan at the University of Birmingham for all of their help with either running the PEPT experiments and or for their advice with data analysis. Thanks to James Bowen for the help with the AFM images.

Thanks to the other EngD students at Imerys, Rachel, Paul, Steve and Yao for your friendship and company. Finally, I would like to thank all of the support I have received from all of my family, my girlfriend Marie, as well as friends at Imerys, Birmingham and elsewhere.

TABLE OF CONTENTS

TABLE OF FIGURES

List of Tables

1 INTRODUCTION

1.1 Project Introduction

Innovation in grinding represents opportunities for energy saving and process optimisation, as well as the potential for creating new mineral functionality. This work examines stirred media mills are at the forefront of comminution processes, both within Imerys and in the wider mineral processing community.

Across the whole of minerals industry, comminution is the largest consumer of energy, estimated at 29% of total energy demand [1], and as much as 0.5% of global energy consumption [1]. However, the thermodynamic efficiency of grinding (i.e. the fraction of input energy transferred to surface area generation) is known to be very low, and estimated at between 0.1 – 1.0% [2] for grinding in size ranges below 1 μm. Therefore there is great possibility for optimisation of the grinding in order to save energy and thus reduce costs and the carbon footprint of the process.

The high shear environment of a grinder is also known to promote chemical reactions, which may not otherwise occur. This field, mechanochemistry, is now established as a means for both synthesising new particles and modifying existing materials [3]. Together

with the potential energy and cost savings, this adds a further dimension to the driving force behind research into stirred media mills.

The stirred media mill (also known as a 'sand grinder') is essentially a stirred vessel, filled with a grinding media (generally ceramic, spherical balls approximately 1 mm in diameter) which is fed with a mineral, generally in a slurry form. This may either be a batch or a continuous process, and it is common that a batch arrangement can be used at the lab scale, whilst full scale equipment are almost universally continuous.

1.1.1 Grinding Marble at Imerys

Calcium Carbonate, in the form of marble is a key product for Imerys, with production up to 7.5 Mt *per annum* [4]. There are a range of end applications for the mineral, however, the large volume end users include the paper industry, and as functional additives for the polymer industry [5]. The marble is mined as large, coarse pieces of rock, with sizes up to several metres in diameter. In order to transform this material to a form which is suitable for the end application, a number of beneficiation steps take place. The key components to these steps are the crushing and milling of the mineral to the required particle size, as summarised in Figure 1-1.

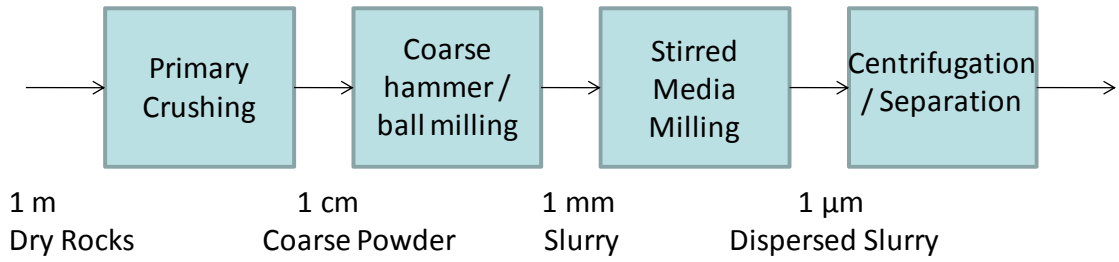

Figure 1-1: Summary of the processing steps in the beneficiation of calcium carbonate.

The large rocks are dry mined from the ground, and jaw crushed into manageable, centimetre scale pieces. After this stage, the material may be shipped to a central processing site where the remainder of the processing occurs. With Imerys, this is often the preferred economic option, as the products from several mines can be processed at one plant, which may be conveniently located close to the customer, or to a major port.

The coarse powder can then be dry ground by hammer milling or ball milling to a powder less than 1 mm. At this stage, the powder can be dispersed in water, and fed into a cascade of stirred media mills (known within Imerys as 'sand grinders'). The series of sand grinders produces progressively finer particle size distribution in the slurry. Additionally, grinders for ultrafine grinding may use a smaller median diameter of grinding media. Figure 1-2 shows a photograph of multiple cascades of grinders, from an Imerys plant.

Figure 1-2: Photograph of three cascades of grinders, at an Imerys plant.

The slurry is fed to the top of the grinder, and after moving through the rotating bed of media, it exits the grinder through a bottom screen arrangement, as seen in Figure 1-3. These screens are not designed to classify the slurry, and are solely intended for retention of the grinding media. Depending on the desired grade of product, an Imerys plant will use up to six grinders in a cascade, and there can be an overall reduction in median particle size from 50 μm to below 1 μm for the finest products.

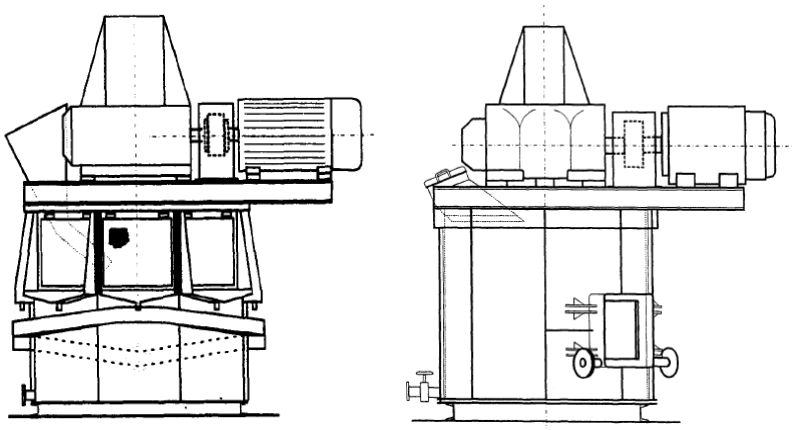

Figure 1-3: Schematic of the ECC top-screen (left) and bottom-screen (right) sand grinders [6].

After grinding, there is usually a centrifugation stage to remove any large pieces of unground marble or broken grinding media. There may also be an air flotation stage which is designed to remove any organic contaminant material from the slurry by exploiting the difference in surface chemistry between product and contaminant.

Within this thesis, the wet grinding work concentrates on understanding the role of the grinding media on the performance and flow characteristics of a lab scale grinder. This examines a range of commercially available spherical media, including the current *status quo* within Imerys, examining the role of different the media density on the performance. Furthermore, a new development which is a major theme of this thesis, is the use of rod shaped grinding media, as developed within the company. By making a large change in the design of grinding media from spherical (or near-spherical) material to ceramic rod shaped particles it is seen that a significant improvement is made on the process efficiency. This

work investigates the benefits of this media, and attempts to characterise the flow patterns in order to better understand the phenomenon.

1.1.2 Dry grinding of talc

This thesis also examines a different use of the lab scale stirred media mill – as a tool for dry grinding. Talc is chosen as a mineral to grind for these experiments, due to an interest in a patent published by Nanomat [7] which detailed the production of a high surface area talc, through a combination of dry grinding and subsequent wet grinding. However, when approached the company was unable to provide a large sample of the material, and did not understand the process through which the material had been generated. In this thesis, the wet grinding stage is replaced with a simple soaking in water, which still generates an unexpected rise in surface area. Rather than optimising the process for surface area generation, the focus here is on characterisation of the material before and after processing, in order to understand the mechanism which is occurring.

1.2 Commercial Benefits

1.2.1 Ground Calcium Carbonate

This review looks at the market for Ground Calcium Carbonate (GCC) before examining the specific potential benefits from the grinding media technology investigated in this thesis. For an in depth review of the markets, including a break down by country and by company, the interested reader is pointed towards the review by Roskill Information Services, 2005 [8].

Imerys is a large supplier of calcium carbonate as a bulk commodity, however, it is a highly competitive market, and currently Imerys are not the largest volume supplier to the paper industry – which represents a large proportion of the market for the mineral as seen in Figure 1-4. The market break down which is shown in Figure 1-5 uses slightly older data (from 2004), but demonstrates the market position which Imerys holds with respect to volumes of calcium carbonate. With such bulk commodities, where volumes are high and prices are low any savings in processing costs can help give a producer of carbonates a competitive edge over rivals.

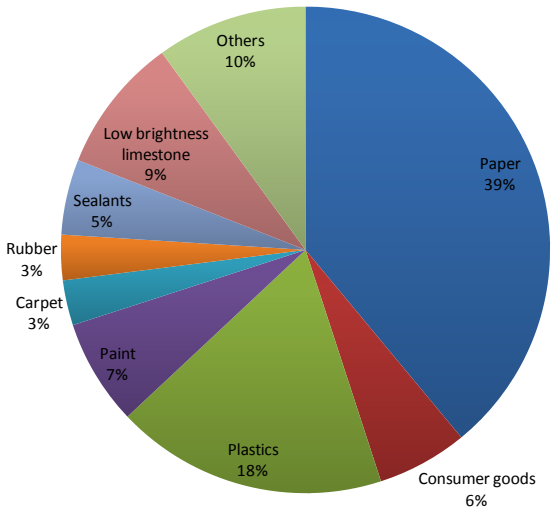

Figure 1-4: Global markets for Ground Calcium Carbonate (GCC) as of 2004 [5].

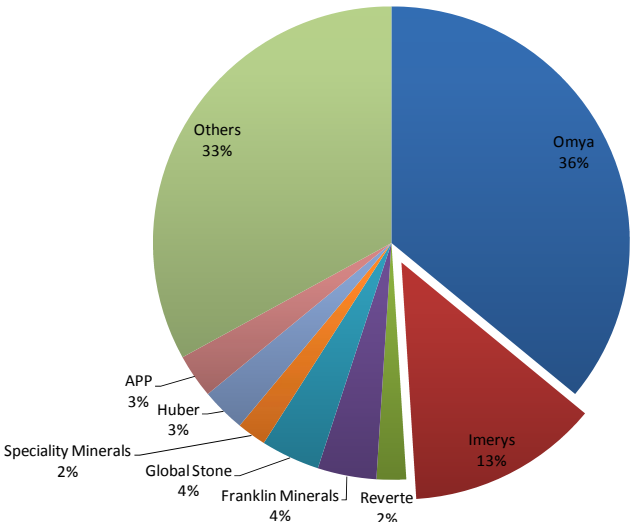

Figure 1-5: Leading producers of GCC in 2004. Data Source, O'Driscoll, 2007 [5].

The fiercely competitive market means that it is undesirable to make large capital investments for the purpose of improving efficiency. For the processing of Ground Calcium Carbonate (GCC), two of the major costs are the energy for grinding and expenditure on dispersants. Rising energy costs have increased pressure on Imerys for the grinding minerals, which may not be feasible to be absorbed by the customer. With a progressively declining global paper industry [9] causing a reduction in demand, this problem is only exacerbated. This produces an interesting financial balance: there are limited funds available for major capital expenditures on the processing routes; however, there is an immense pressure for process optimisation in order to reduce costs.

The favourable solution to this problem is to make a modification to the processing route without incurring significant capital expenditure. This could be achieved through one of the following approaches:

- **Optimising Operating Parameters:** Many of the parameters of the plant can be adjusted in order to optimise the efficiency, such as the weight fraction of mineral in the slurry, process flow rates, media volume concentration or the chosen feed material source. However, in a mature industry with experienced chemical engineers this optimisation has already taken place, and there are few opportunities to improve the process significantly.
- **Small adjustments to grinder:** There are opportunities for modification of the grinder which do not require large capital expenditure. For example it may be possible to modify baffles – or introduce new ones – which could compress flow and improve grinder efficiency. This is an area where there has been some research at Imerys, however there can be difficulties in scaling any new developments from the lab scale grinder to full scale production line.
- **Choose a more cost efficient dispersant:** As the dispersant is a significant cost, it may be possible to choose alternative suppliers and different chemistries for the dispersant in order to save costs. However, there may be a trade off between a cheaper dispersant and a reduction in performance and maintenance of a good slurry rheology. This is an area of ongoing research within Imerys.
- **Change the grinding media:** Although the consumption rate is low, grinding media is essentially an operating expenditure, as the high shear environment in the grinder causes abrasion of the media as well as size reduction of the mineral. The

current grinding media is chosen by Imerys on the basis of giving sufficient performance at a low cost. There is a large potential for a different grinding media which could give an improved efficiency over the *status quo*. The economic balance of a new grinding media (which may well be more expensive) would have to account for the improved efficiency and reduction in wear rate. This is the key area of research which is central to this thesis.

1.2.2 High Surface Area Talc

Although the global supply of talc is not as high as GCC, it is still a key industrial mineral, in terms of both volume and sales. The global market is estimated at 9.0 Mt [4], and this is dominated by supply from China and the US, as is shown in Figure 1-6. The supply of talc from China continues to grow, due in part to discovery of new sources, as well as the abundance of cheap labour[4], which reduces costs of the hand sorting of the raw material.

Talc is used in a number of applications, although this thesis focuses on the application in plastics, where it increases stiffness and adds dimensional stability, leading to use in the following fields [4]:

- Appliance panels and window housing.
- White kitchen goods.
- Plastic furniture.
- Automobile appliances, such as plastic trim, hub caps and fuel tanks.

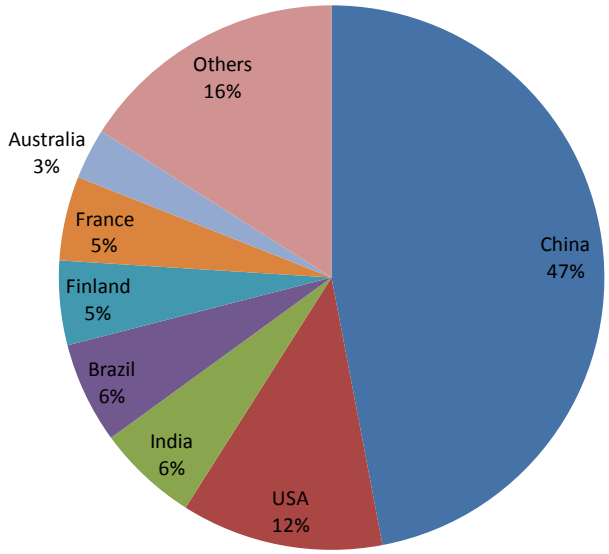

Figure 1-6: Global distribution of the supply of talc. Data from 2004 [4].

Talc is also found in a number of other fields, which usually exploit the aspect ratio (talc naturally forms platy particles) and surface chemistry of the mineral. These are summarised in Figure 1-7 for the US market. It is seen that although still a significant market, application in plastic represents much lower volumes than many of the other key applications.

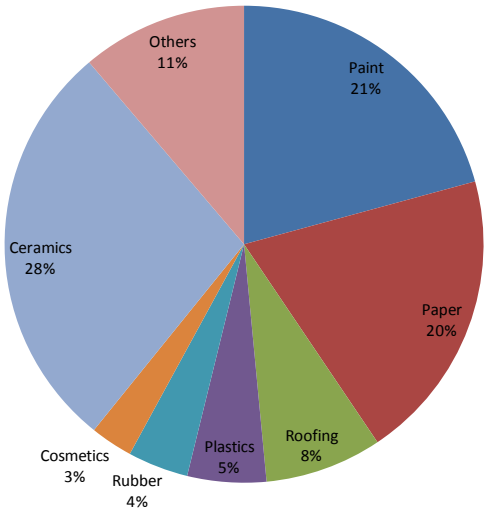

Figure 1-7: Distribution of the application for talc in the USA. Data from 2004 [4].

When dealing with the high surface area talc, which is formulated within this thesis, the benefits in plastic are suggested as being due to the higher surface area and greater number of fine particles, which could increase the stiffness and flexural modulus without having negative effects on the impact strength of the compound [10]. If there was a systematic benefit to talc made through the methods which are detailed in this thesis, then there would be a significant market edge for any company competing for the market for talc in plastics, which accounts for over 35,000 t of material *per annum*. Furthermore, if the effects are significant, than the product can be sold at a premium into these markets.

There may be further benefits of a high surface area talc which are not reviewed or examined within this thesis. For example, talc is used in the paint industry to help control viscosity whilst improving the covering power and reinforcing the dried paint [4]. It may be

envisaged that a higher surface area material would offer different viscosity control and a different interaction with the organic solvents which are present.

In summary, the production of high surface area talc could prove to have a significant market value, and there may be a number of applications where this could be a disruptive technology. However, in order to achieve this, the material would have to be proven to perform to the required standard and consistently. Furthermore, the value gained from the high surface area must more than offset the processing costs from the dry grinding and soaking stages which are detailed in this thesis.

1.3 Objectives of this work

In the broadest sense, this thesis aims to improve understanding and to further the potential of the Imerys sand grinder. More specifically, the initial focus, in Chapter 5, is on the role of the grinding media in the wet milling of calcium carbonate slurries in order to improve efficiency. This is performed by reviewing a range of commercial spherical media, as well as proving the benefits of a new rod shaped media which has been developed within Imerys. As well as simply looking at the performance with respect to size reduction, other secondary factors are considered, namely the contamination from media to product, the effect on the product brightness, and the wear rates of the media.

As well as this approach, a more detailed examination of the process is made through the use of Positron Emission Particle Tracking (PEPT). This is a tool for examining the flow patterns within the mill and investigating the role of the grinding media on the various flow parameters. The relationships of these parameters with the media density and the efficiency of the grinding are then explored in Chapter 6.

Finally in Chapter 7, there is a focus on the dry grinding of minerals for the generation of a high surface area material, which could represent an innovative use for an Imerys sand grinder, or indeed for alternative dry grinding approaches. The material generated through this work is tested in an end application – as a reinforcing filler in a polypropylene matrix, where its effectiveness is considered compared to an unfilled matrix as well as a matrix filled with unground material.

1.4 References

[1] Tromans D. Mineral comminution: Energy efficiency considerations. Minerals Engineering 2008;21:613.
[2] Fuerstenau DW, Abouzeid AZM. The energy efficiency of ball milling in comminution. International Journal of Mineral Processing 2002;67:161.
[3] Balaz P. Mechanochemistry in Nano Science and Engineering: Springer, 2008.
[4] Harben PW. Industrial Minerals Handybook: A Guide to markets, specifications and prices: Metal Bulletin PLC, 2002.
[5] O'Driscoll M. A bright carbonate future. Industrial Minerals. London, 2007. p.24.
[6] Lofthouse CH, Johns FE. The svedala (ECC International) detritor and the metals industry. Minerals Engineering 1999;12:205.
[7] He JD, Christopher. Methods of providing nano-talc powders. In: USPTO, editor. US: Nanomat Inc., 2004.
[8] The Economics of Ground Calcium Carbonate. London: Roskill Information Services, 2005.

[9] Lehtovaara MK, Matti; Suojapelto, Kimmo; Kassi, Tuomo. Market Opportunities for Paper Industry in Radio Frequency Identification. Technology Business Research Centre, Research Reports. Lappeenranta: Lappeenrante University of Technology, 2009.
[10] Rothon R, editor Particulate-filled polymer composites: Longman, 1995.

2 Literature Review

2.1 Introduction to particle breakage

Particle breakage is can be considered to occur by one of four methods [1]:

- **Impact** – sudden shock force acting on the particle. Resulting in a very wide size distribution. Typical in a tumbling ball mill.
- **Compression –** Steady application of opposing normal forces resulting in a wide particle size distribution. Typical of a jaw crusher.
- **Attrition –** Removal of many fine particles the exterior of a much larger particle through particle-particle contact.
- **Abrasion –** Size reduction of particles through shear forces from the fluid medium.

The relative importance of these different modes of breakage will depend on the size of the material being used, as well as the equipment being used for the grinding. Figure 2-1 gives a representation of this energy, where it is clear that for grinding materials to a size below 1 µm, the mass normalised amount of energy required is many order of magnitudes higher than for particles which may only be one order of magnitude coarser.

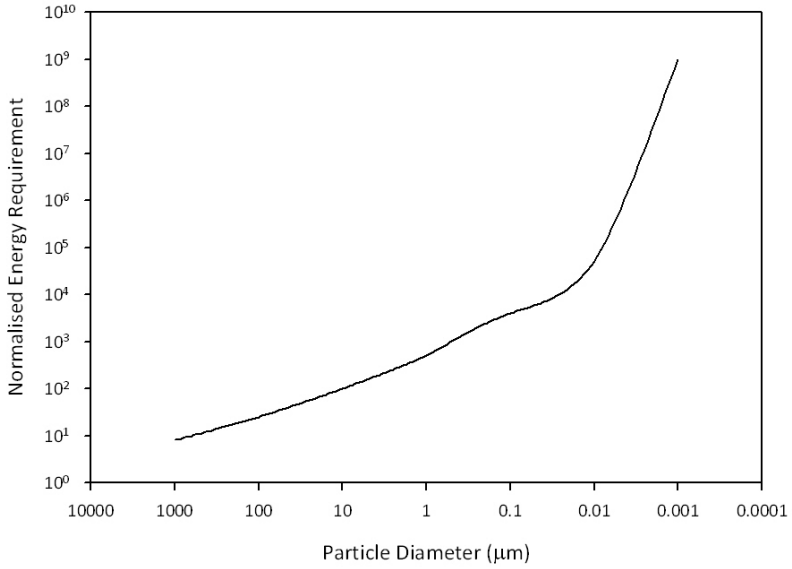

Figure 2-1: Representation of grinding energy per mass to reduce size by 10% [2].

Perhaps the most common correlation for the energy required to achieve a size reduction is Bond's Law:

$$E_B = C_B \left(\frac{10}{\sqrt{x_p}} - \frac{10}{\sqrt{x_f}} \right) \qquad \textbf{(2.1)}$$

Where E_B is the predicted energy required, x_p is the product size, x_f is the feed size and C_B is the material specific Bond Work Index. These correlations are used widely in industry for grinding materials from several metres down to approximately 50 μm[2]. However, there are clearly limitations to the law which is a generic approximation and does not account for factors such as the equipment being used and the mode of breakage. This makes is unsuitable for ultrafine grinding, where efficiency is lower and energy demand is higher, and also where the specific shape, cleavage and mineralogy of the mineral becomes important.

From the perspective of the mill performance, an often cited measure of mill efficiency is the energy density [3]. Authors state that a higher energy density is beneficial to mill performance, and that horizontal mills such as the IsaMill® (Xstrata) gives an improved efficiency due to a higher energy density (≈1000 kW/m^3 rather than 100 kW/m^3 for the stirred media mill at both lab and pilot scale). Whilst it may be beneficial to maintain a high energy density, the work contained in this thesis will argue that this is a poor measure as it denigrates systems which have local areas of very high energy density and a good slurry circulation.

2.2 Developments in the Stirred Media Mill

The stirred media mill which is used in this thesis, is a vertically stirred mill developed within English China Clays (ECC, now Imerys). In 1964 the laboratory scale grinder was developed in-house [4], which was subsequently developed into pilot and full scale production equipment for clay grinding. These grinders for clay grinding had a top-screen approach, and are still sold under license by Metso Minerals. The development of bottom screen grinders for the high solids grinding of calcium carbonate was completed in 1972 [4]. The design has essentially stayed the same in this time, with modifications being made to some of the materials of construction (such as polyurethane liners) and to the motors themselves. The final key change in the operation of the ECC sand grinder is the introduction of ceramic grinding media in place of natural sand, for the improvement of process efficiency [4].

Beyond Imerys, there have been numerous other developments within stirred media milling, and perhaps the most significant of these is the Isa Mill [5], developed for the liberation of ultrafine material for the metal ore industry. In the Isa Mill, the rotating shaft is horizontally mounted, allowing for much larger mills to be made in areas where plant footprint is not a concern. Within this metal industry, stirred media mills, or similar, are used for a number of metal ore applications where ultrafine grinding is required to maximise liberation of the ore from the gangue. These include the zinc [6], copper[7], gold [8], iron [9] and lead [10] industries. The benefits of these fine sizes of liberation are comprehensively reviewed by Grano, 2009 [11], which also analyses the effect of other chemical aspects of the grinding environment including the dissolved material in the water and the surface coating of the grinding media.

The vertically stirred media mill as a tool for the metals industry is reviewed by the original designers [12] where the advantages of the design are discussed. Although now 10 years old, the listed advantages are still relevant now:

- Lower capital costs.
- Higher energy efficiency.
- Small footprint.
- Lower maintenance costs through fewer moving parts.

The authors also demonstrate that the grinder is an effective tool for the reduction of particle sizes from over 20 µm to below 5 µm, which is an important region for applications which require flotation of ultrafine material [11].

Aside from Imerys' own applications in industrial minerals, other manufacturers have developed the vertically stirred mill with a higher aspect ratio (i.e. tall with a narrower diameter). A comparison between the ECC sand grinder and the Hosokawa Pearl Mill® is given in Figure 2-2 where the fundamental change in aspect ratio can be seen. Although there have been many published works [13, 14] demonstrating the uses of the Pearl Mill®, there is little work available comparing the relative merits of the two mills. From the perspective of an industrial minerals application, this may be due to major competitors, such as Omya and Imerys, using different mills without a cross comparison of technology being feasible or realistic.

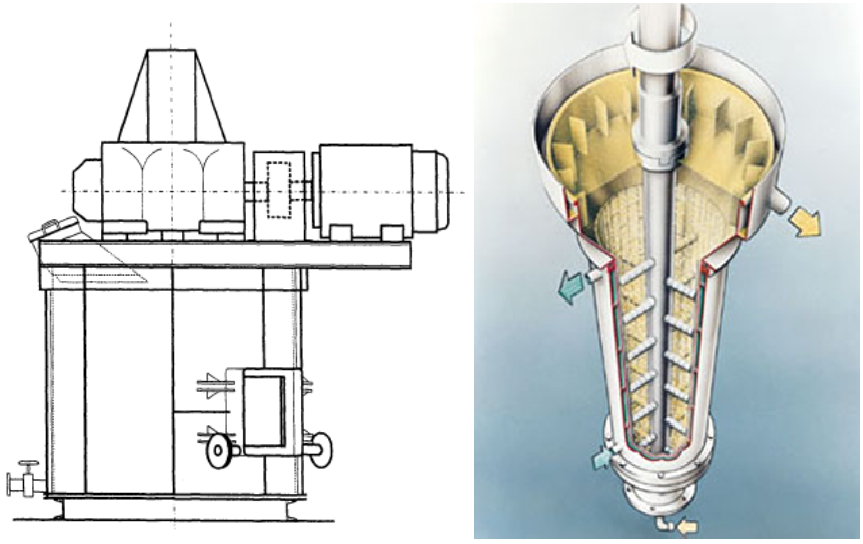

Figure 2-2: Comparative schematic of the ECC bottom screen sand grinder [12] (left) and the Hosokawa Pearl Mill [15].

Further to industrial minerals and metalliferous grinding, other applications for the stirred media mill are reported, although these are largely much smaller volumes. These applications include dental glass [16], zirconia [17], gibbsite [18], and for stabilised nano-particles [19]. In such applications, it is not the efficiency or footprint of the grinder which is the reason for its use; it is the ability to closely control all of the operating parameters in order to generate the precise conditions required for such a high specification product.

For the grinding of all minerals, there is a plethora of research examining the role of various process parameters on the grind efficiency. In this review, the grinding media is dealt with in detail, whilst for the effect of slurry rheology and dispersion, reviews by Forssberg [20] amongst others [21-26] are recommended. Further parameters, such as the role of scale up and impeller speed are reviewed by Jankovic [27].

2.3 Developments in grinding media

Literature searches for grinding media give many references to media for tumbling ball mills as well as the more intense ultrafine grinding in stirred media mills. This review concentrates on finer grinding media for stirred media mills, as relevant to this thesis, however some consideration will be given to larger media in ball mills, when examining the effect of media shape.

2.3.1 Density and Composition

Historically, sand has been used as the grinding media of choice for many stirred media mills. This has a number of advantages, in being very cheap and available close to the mine site [3]. For low intensity applications, the performance is reported as being acceptable [28] and it is still used in some plants within Imerys. However, in high intensity environments, there is a clear need to move to higher specification grinding media [3, 29, 30], and within Imerys this has focused on a move to ceramic media [31].

A commercial review of the evolution of ceramic grinding media is given by Graves [32], where it is suggested that the viability of media is reliant on density and mechanical properties, as well as the microstructure of the material. For grinding to finer particle sizes, the surface roughness is claimed to be important as the size of the product becomes comparable to the scale of the surface features. A key conclusion of this paper is that the hardness of the product should be less than that of the media in order to reduce media wear, however, there are few assertions as to the effect of the density and hardness on the efficiency of grinding.

Becker *et al.* [33] report the comminution of alumina and silicon carbide with a range of grinding media including alumina (Al_2O_3), zirconia (ZrO_2), mixed oxides and steel. The investigation into grind efficiency with the various media does not show a strong effect of the media type, although there is some evidence for an improved performance of the ceramic media against the steel. It is possible that this lack of a clear media effect is related

to the authors' choice of mineral – both alumina and silicon carbide are themselves hard media, and therefore the experiments could be grinding both media and product simultaneously.

A lot of the research into stirred media mills has focussed on horizontal equipment such as the IsaMill® (Xstrata), which is used in many industries, including the high growth areas of platinum group metals [5, 10, 34, 35]. Farber *et al.* [35] test a commercial media with densities of 3.8, 4.2 and 6.2 g/cm^3 for the communition of a platinum ore in a lab scale IsaMill. Their work demonstrates that the relationship between media size and efficiency is not linear, and in the given experiments there appears to be an optimum size of approximately 2 mm. However the work would benefit from additional data points in the determination of this maximum. Furthermore, the role of density is shown to be somewhat ambiguous, and there is not a precise relationship shown, alluding to the possibility that there are further media properties to consider.

2.3.2 Media Shape

To date, there has been no reported research on rod shaped media for stirred media mills, with media of the 1-2 mm size dimension. For this reason the rod shaped media discussed in this thesis is the subject of a patent application in conjunction with Imerys. However, the use of cylindrical (or other) shaped media is established in other comminution processes and results are reported for the tumbling ball mill as far back as 1973 [36]. In this paper, cylinders with an aspect ratio of 1.24-1.60 and a length of 19.0 mm are compared with

2.54 mm diameter steel balls and similar volume hexagonal prisms. Although the data do not represent a comprehensive data set, there is evidence of differences in grinding between the media shape, results are finer with spheres than any other media, but the author argues that alternative shaped media offer different benefits with respect to the width of particle size distributions.

More recently, there have been a number of publications examining the use of cylinders or 'cylpebs' (heavily rounded cylinders [37-40]). These novel shaped particles are argued to provide an improved breakage rate, and this is demonstrated well for dry grinding in a tumbling mill by Ipek [38]. Cylpebs are seen to produce faster breakage rates, and this is especially noted for the coarser (100-1000 μm) fractions. However, if the media is to be viable, the improved efficiency must not be to the detriment of the media wear rates. Yildirim [41] investigates the effect of the media shape on wear rates, through a comprehensive mathematical model, based on the erosion over the surface. It is not clear that this approach recognises that corners or the cylinders may be more susceptible to wear than other areas, but nevertheless there appears to be good corroboration between the model and the given data.

There has been little other work in the field of novel shaped grinding media. Some work has been reported on the milling kinetics of fragmented spherical media [42] although this is more concerned with explaining existing phenomena rather than exploiting the shape of these broken fragments. It is also recognised that much larger rod shaped media do exist

in, for example, rod mills, which use long (over 300 mm) and thick (over 30 mm) rods in tumbling mills for the comminution of larger particles [43].

2.4 Motion in a stirred media mill

The stirred media mill is a multiphase system, consisting of a discrete, macroscopic solid phase (media) with a microscopic mineral phase dispersed in water, and a free surface between this mixture and the air, through a central vortex. Attempts to investigate this system can be divided into those based on a mathematical model for the motion within the mill, alongside experimental analysis of the system. The root of the difficulty lies in choosing which component of the multiphase system to monitor – as there have been few approaches to consider all aspects together.

2.4.1 Experimental investigation into stirred mill flow patterns

The key to the investigation of flow in a stirred mill is non-invasive measurement of the properties. This approach is often hampered by the opacity of any grinder arrangement. There has been some work by Rydin *et al.,* 1993 [44] using a cinematographic approach to investigating flow, and this work required modifying the grind chamber to a clear plastic construction. This work makes an excellent foray into motion of the media in a mill, and examines separation of grinding beads and velocities. However, the use of steel balls means that there are limitations as to what can be investigated, and the only useful data are of bead motion at the wall. As this cannot be proven, on the given evidence, to be representative of the whole chamber, or that it is the key area of the mill to consider, it is

difficult to use the results for furthering understanding. However, the benefit of this approach is that there has been very little modification made an existing experimental set up, suggesting that whatever information can be gleamed is representative of a known experiment.

There have been approaches by Schwedes and co-workers [45-49] to extend this optical approach through decreasing opacity in the system. The work reported in 1999 [48], again uses a transparent mill chamber as well as glass beads and a refractive index matched silicone fluid. The arrangement is known as Particle Image Velocimetry (PIV) and is shown to give very good data on the motion in this system. The radial symmetry of the system is exploited to give velocity profiles from impeller to wall, and it is shown that the highest velocity achieved is close to the impeller tip (reaching up to 40% of the tip speed) and furthermore the velocity gradients are at least one order of magnitude higher at the tip than at any other region within the mill. The unfortunate compromise which has to be made in this analysis is that complete modification of the whole apparatus is required in order to generate data. These compromises still allow a generic investigation into motion within a mill, but it is impossible to ascertain what the effect of changing any parameters would be in a real mill, as that is not possible in this arrangement.

Other approaches have been made to avoid altering the process, Clermont, 2008 [50] demonstrates a non-invasive technique for investigating motion in a ball mill, through fitting an electrical impedance measurement device within the lining of the mill, and back-

calculating the relative position of the balls and the slurry. This technique gives good analysis of the relative location of these components within the mill, but does not give details of the specific motion of the individual grinding beads.

The final approach that has been researched is that which is also followed in this thesis, the use of Positron Emission Particle Tracking (PEPT). This is applied by Conway-Baker *et al.* [51, 52] for investigating the motion of grinding media within the mill. This paper makes an initial investigation into flow patterns within the mill, and the effect of motor speed and impeller design. Changes in occupancy (i.e. where the tracked particle spends time in the chamber) are examined with different motor speeds. However, there has not been any further interpretation of the data, and the images are given as longitudinal slices, rather than radial integrations, and do not exploit the symmetry of the system. The advantage of this system is that there is no requirement to modify the existing experimental set up whatsoever. As there is not an optical approach, the PEPT camera can be used with opaque mill chambers, as well as opaque slurry and grinding media. A review of PEPT in related applications is given in Section 2.5.

2.4.2 Mathematical Modelling of stirred mill flow patterns

Mathematical modelling of a system avoids the compromises frequently made in experimental observation, as seen with the optical techniques in Section 2.4.1, or the costs associated with techniques such as PEPT. It also offers the potential to investigate the

effect of any number of process parameters, including the impeller design and the mill configuration.

2.4.2.1 Discrete Element Modelling

Discrete Element Modelling (DEM) is a tool for modelling interactions between solid particles, and can therefore be applied to the grinding media in a stirred mill. There is much literature on the subject [34, 53-57] all of which produce a representation of the movement of the grinding beads. However, there are key limitations which exist for all of these works. Primarily, there is little attention paid to the slurry, which is considered to be a simple Newtonian fluid. In reality of course, this is a complicated two phase mixture, which can have complex rheology [20]. This omission means that shear fields within the fluid are effectively ignored, despite these forces being sufficient to cause particle breakage [48]. Additionally, limitations due to computer power cause models to be restricted in the number of particles which can be used, and the shape – which is limited to spherical particles. For these reasons, it is considered that although some correlation has been shown between experimental data (from PEPT) and DEM modelling [51, 52], the models simply confirm broad trends in flow patterns and require further integration with experimental data in order to aid process design.

2.4.2.2 Fluid mechanics approach

Other authors have concentrated on the behaviour of the fluid rather than the grinding media. Blecher *et al.* [46] examine fluid flow around a tip, and found a good correlation

with experimental data. The image which is reproduced in Figure 2-3 shows that correlation with PIV, however there is only a qualitative similarity. The small area which is used for this analysis relies on symmetry between several impeller tips within the grinder. In reality this is unlikely to be a fair assumption to make, as gravitational forces causes differences in conditions at the different impeller tips.

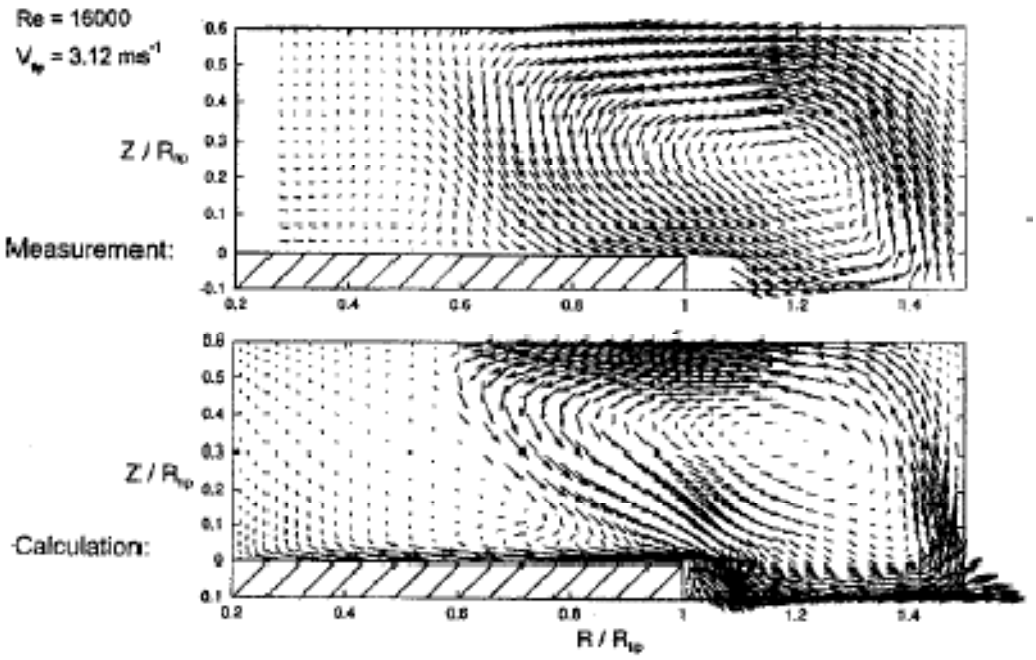

Figure 2-3: Comparison of the flow around an impeller tip from measurement by PIV (top) and fluid mechanics modelling (bottom) [49].

2.4.2.3 Population balance approach

Population balance equations [58] have also been used for the modelling of grinding systems by a number of authors and is reviewed by Frances, 2004 [59]. The approach uses a statistical analysis of collisions between particles, as well as for the breakage functions of the particles (i.e. the probability of fracture, and the particle size distribution of the

fractured particles). The benefit of this technique is that the focus is on the media, which is the aspect which all investigators ideally wish to understand. However, the pitfalls of the technique, as highlighted [59, 60] are the functions for the selection of particles and their breakage. This is further complicated by inconsistencies in the behaviour of a natural mineral product, as is the nature of Imerys' grinding.

2.4.2.4 *Detailed examination of models by Kwade* et al.

Although several different approaches for the modelling of a stirred media mill have been discussed, the approach by Kwade *et al.* [45-47, 61-67] has become the most established. The first consideration is that particle fracture is induced by stress events during the collision of two grinding beads. Therefore, a stress frequency, SF, within the mill can be considered (independent of the mineral), and a time to achieve the required particle size of product, t_g. Therefore the total number of stress events, SN is the product ($SN = t_g \cdot SF$). The stress number can also be considered from equation (2-2):

$$SN = \frac{N_c P_s}{N_p} \tag{2-2}$$

Where N_c is the number of collisions, P_s is the probability of a particle being caught and stressed at contact, and N_p the number of feed particles in the mill. The number of collisions in the grind is considered proportional to the motor speed (rpm) grind time and the number of grinding beads present, N_{GM}:

$$N_c \propto n.t_g.N_{GM} \propto n.t_g.\left(\frac{V_{GC}.\varphi_{GM}.(1-\varepsilon)}{\left(\frac{\pi}{6}\right).d_{GM}^3}\right) \tag{2-3}$$

In equation (2-3) the number of grinding beads has been devolved into a function of the volume of the grinding chamber, V_{GC}, the mill fill fraction, φ_{GM}, the media porosity,ε and the diameter of the grinding media, d_{GM}.

The authors then argue that the probability of a collision for grinding hard materials is proportional to the diameter of the grinding bead, through the schematic shown in Figure 2-4.

$$P_s \propto d_{GM} \tag{2-4}$$

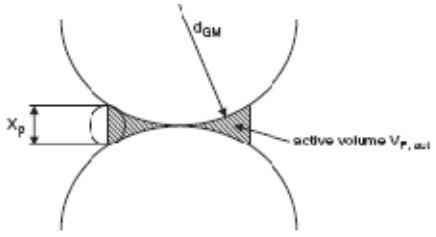

Figure 2-4: Demonstration of the active volume between colliding particles [67].

Finally, the number of particles can be considered as quotient of the total volume of particles, $V_{P,T}$, and the volume of an individual particle (assumed to be spherical). This can be expressed with existing terms, if the volumetric solids content of the slurry is considered, C_V.

$$N_P \propto \frac{V_{P,T}}{V_T} = V_{GC}.\frac{(1-\varphi_{GM}(1-\varepsilon)).C_V}{V_P} \tag{2-5}$$

For a proportionality relationship, the authors combine equations (2-3) - (2-5), to arise at the following expression:

$$SN \propto \frac{\varphi_{GM}(1-\varepsilon)}{(1-\varphi_{GM}(1-\varepsilon)).C_V}.\frac{nt}{d_{GM}^2} \quad (2\text{-}6)$$

It is interesting to note at this juncture, the dependence on the media voidage, ε, because for rod shaped grinding media, there is a different packing fraction, ε_r, than there is for spheres. If the rods were further considered then the length, L, and cross sectional diameter, d_x, could be considered, and equation (2-6) would instead appear as:

$$SN_R \propto \frac{\varphi_{GM}(1-\varepsilon_r)}{(1-\varphi_{GM}(1-\varepsilon_r)).C_V}.\frac{nt}{d_x^2} \quad (2\text{-}7)$$

If rod shaped media is to be compared with spherical media, the time to achieve a given stress number can be derived by setting the ratio of equations (2-6) and (2-7) to be unity.

$$t_r = \frac{\varepsilon_r(1-\varepsilon)-1-\varepsilon_r}{\varepsilon(1-\varepsilon_r)-1-\varepsilon}.t \quad (2\text{-}8)$$

From equation (2-8) it can be seen that this model for the stress number shows the time for grinding is highly dependent on the packing fraction of the media, and differences in packing between the rods and the spheres are highly significant.

The authors extend the theory by considering the stress energy of a collision, which is determined by the kinetic energy of the faster of the two colliding beads. At this stage there are a number of assumptions made (direct quotes from [66]):

1. Only single particles are stressed intensively between two grinding media and therefore, the stressed particle volume does not depend on the size of the grinding beads.
2. The tangential velocity of the grinding beads is proportional to the tip speed of the disks [*impellers*].
3. The mill size and geometry stay constant.
4. The displacement of the suspension between two approaching grinding media causes no essential decrease of the media velocities and, thus, of the kinetic energy of the two grinding media.
5. The elasticity of the feed material is much smaller than that of the grinding beads and, therefore, the kinetic energy of the beads is nearly completely transferred to the feed particles and not partly consumed by the deformation of the beads.

These assumptions lead to the expression given in (8) for the stress energy (SE).

$$SE \propto d_{GM}.\rho_{GM}.v_t^2 \qquad (2\text{-}9)$$

Where ρ_{GM} is the density of the grinding media, and v_t is the tip speed of the impeller.

This analysis is shown within the literature to be a useful tool, however there are clear limitations. The first assumption given above suggests that only one particle would be trapped between the two grinding beads. Given that the system can have up to 78 wt.% mineral in the slurry, and that the particles are several orders of magnitude smaller than the media, it seems unlikely that this assumption would hold. The second assumption is that the tangential velocity of the beads is proportional to the tip speed of the disk

impellers. This directly effects equation (2-9), and although the work within this thesis focuses on pin impellers rather than disk impellers, the work shown here, as well as others [52] does not confirm this assumption.

Assumption 4 suggests that the displacement of the fluid is an insignificant energy requirement. With a number of systems with higher viscosity slurries (such as the high solids grinding of calcium carbonate) this is unlikely to hold, and in later work the authors have incorporated a modifying factor to account for this [67].

An overall criticism of this approach to the stirred media mill is the assumption that all comminution is through impact fracture. However, as discussed by Prasher [1] there are three modes of fracture: abrasion, compression and impact (see Section 2.1). There is no evidence given within the literature which confirms that this is the dominant mode of fracture, and in fact there is some evidence (which is not conclusive) that abrasion becomes key with the fine grinding [68].

2.5 Related applications of Positron Emission Particle Tracking (PEPT)

The only previous use of PEPT for the sand grinder system has been discussed in Section 2.4.1, and this work has been extended in this thesis. However, there has been work conducted in analogous systems with high speeds and radial symmetry. An in depth review into this previous work is beyond the scope of this thesis, however the paper by Parker

[69] discusses much of this work. It is sufficient to surmise that PEPT has been successfully applied to many of the applications shown in Table 2-1, and there are many analogies here with the stirred media mill. Studies of occupancy, velocity profiles and shear are not novel, however their application and interpretation for the stirred media mill do represent new insights.

Table 2-1: Summary of past PEPT work in systems analogous to the grinder.

Application	Authors and references	Analogy to sand grinder
Mixed Vessel	Guida, 2009 [70] Jones, 2007 [71] Fishwick, 2005 [72] Kuo, 2005 [73] Barigou, 2004 [74]	Vertically stirred vessel with good radial symmetry.
Granulator	Hassanpour, 2007, '09 [75, 76] Ng, 2007, '08 [77, 78] Bridgwater, 2004 [79] Chiti, 2007 [80]	Radially symmetric system where shear is key to efficiency.
Rotating Drums	Ingram, 2005 [81] Parker, 2005 [82] Cox, 2003 [83]	Applications for milling, and mixing due to radial motion.

2.6 Dry grinding of talc

The intense mechanical treatment of a mineral through dry grinding can result in alterations to the mineral structure which are well documented [84-87]. When platy minerals such as talc or kaolinite are ground, the initial grinding is seen to increase surface area and decrease particle size, however extended grind times, the crystallinity of the mineral is reported to decrease and agglomeration occurs, resulting in a coarse, amorphous phase [85].

With intense dry grinding of kaolinite, formation of hydrogen gas is reported [88] which is attributed to the mechanochemical reaction of surface water with radicals formed by bond rupture on the surface. Specifically considering the surface chemistry, Infra-Red (IR) studies of the surface bonding in kaolinite [89, 90] have shown that disruption and rearrangement can occur.

With respect to talc, structural properties have been studied, as well as the optical properties of the treated material, where it is seen that optical properties improved concomitantly with grinding time [91]. Mechanochemically activated talc which is subsequently leached in an acid solution has been shown to produce a porous structure with a extremely high surface area [92]. However the resulting material can no longer be described as a talc mineral having been fundamentally transformed into a porous silica.

2.7 References

[1] Prasher CL. Crushing and Grinding Process Handbook: John Wiley & Sons, 1987.

[2] Klimpel RR. Introduction to the Principles of Size Reduction of Particles by Mechanical Means. Gainesville, Florida: NSF Engineering Research Center for Particle Science & Technology, 1997.

[3] Wills BAN-M, T.J. Wills' Mineral Processing Technology. Oxford: Elsevier, 2007.

[4] Falcon-Steward HR. A Review of the technology of ultrafine wet grinding in agitated media mills. Imerys Internal Research Report, 1989.

[5] Woodall PE, Udo. Attrition mill. In: USPTO, editor, vol. 5797550. US: Mount ISA Mines Ltd., Erich Netzsch GmbH & Co, 1998.

[6] Burgess F, Reemeyer L, Spagnolo M, Ashley M, Brennan D. Ramp up of the Pasminco Century Concentrator to 500 000 tpa zinc metal production in concentrate. Eighth Mill Operators' Conference, Proceedings 2003;2003:153.

[7] Filippou D, St-Germain P, Grammatikopoulos T. Recovery of metal values from copper-arsenic minerals and other related resources. Mineral Processing and Extractive Metallurgy Review 2007;28:247.

[8] Labrooy SR, Linge HG, Walker GS. Review of Gold Extraction from Ores. Minerals Engineering 1994;7:1213.
[9] Ding ZY, Yin ZL, Liu L, Chen QY. Effect of grinding parameters on the rheology of pyrite-heptane slurry in a laboratory stirred media mill. Minerals Engineering 2007;20:701.
[10] Johnson NW, Gao M, Young MF, Cronin B, Australasian Inst MIN, Met AIM, Met. Application of the ISAMILL (a horizontal stirred mill) to the Lead-Zinc Concentrator (Mount Isa Mines Ltd) and the mining cycle. Annual Conference of the Australasian-Institute-of-Mining-and-Metallurgy on the Mining Cycle (AusIMM 98). Mount Isa, Australia, 1998. p.291.
[11] Grano S. The critical importance of the grinding environment on fine particle recovery in flotation. Minerals Engineering 2009;22:386.
[12] Lofthouse CH, Johns FE. The svedala (ECC International) detritor and the metals industry. Minerals Engineering 1999;12:205.
[13] Tusar M, Tusar L, Zupan J. The optimisation of energy consumption and time in colour pigment grinding with pearl mills. J. Mater. Process. Technol. 2006;171:48.
[14] Strazisar J, Runovc F. Kinetics of comminution in micro- and sub-micrometer ranges. International Journal of Mineral Processing 1996;44-45:673.
[15] Hosokawa Micron. http://www.hosokawa.co.uk/anr.php. Accessed March 2009.
[16] Vital A, Zurcher S, Dittmann R, Trottmann M, Lienemann P, Bommer B, Graule T, Apel E, Holand W. Ultrafine comminution of dental glass in a stirred media mill. Chemical Engineering Science 2008;63:484.
[17] Adam J, Drumm R, Klein G, Veith M. Milling of zirconia nanoparticles in a stirred media mill. Journal of the American Ceramic Society 2008;91:2836.
[18] Alex TC, Kumar R, Roy SK, Mehrotra SP. Stirred Bead Mill Grinding of Gibbsite: Surface and Morphological Changes. Advanced Powder Technology 2008;19:483.
[19] Sommer M, Stenger F, Peukert W, Wagner NJ. Agglomeration and breakage of nanoparticles in stirred media mills - a comparison of different methods and models. Chemical Engineering Science 2006;61:135.
[20] He MZ, Wang YM, Forssberg E. Slurry rheology in wet ultrafine grinding of industrial minerals: a review. Powder Technology 2004;147:94.
[21] He M, Forssberg E. Influence of slurry rheology on stirred media milling of quartzite. International Journal of Mineral Processing 2007;84:240.
[22] He MZ, Wang YM, Forssberg E. Parameter effects on wet ultrafine grinding of limestone through slurry rheology in a stirred media mill. Powder Technology 2006;161:10.
[23] Jankovic A, Sinclair S. The shape of product size distributions in stirred mills. Minerals Engineering 2006;19:1528.
[24] Mende S, Stenger F, Peukert W, Schwedes J. Mechanical production and stabilization of submicron particles in stirred media mills. Powder Technology 2003;132:64.
[25] Garcia F, Le Bolay N, Trompette J-L, Frances C. On fragmentation and agglomeration phenomena in an ultrafine wet grinding process: the role of polyelectrolyte additives. International Journal of Mineral Processing 2004;74:S43.
[26] Sakthivel S, Krishnan VV, Pitchumani B. Influence of suspension stability on wet grinding for production of mineral nanoparticles. Particuology 2008;6:120.
[27] Jankovic. A review of regrinding and find grinding technology - the facts and myths. Metso Minerals Website.

[28] Loveday BK, Dong H. Optimisation of autogenous grinding. Minerals Engineering 2000;13:1341.
[29] Orumwense AO. Effect of media type on regrinding with stirred mills. Minerals & Metallurgical Processing 2006;23:40.
[30] Gedevanishvili S, Deevi SC. The effect of ZrO2 grinding media on the attrition milling of FeAl with Y2O3. Mater. Sci. Eng. A-Struct. Mater. Prop. Microstruct. Process. 2004;369:236.
[31] Payton D. Comparison of pilot scale GK and ECCI type grinders when using Carbolite ceramic media and sand. Imerys Internal Research Report, 2000.
[32] Gale Graves BF. Evolution of Ceramic Grinding Media. Industrial Minerals: IM, 2007.
[33] Becker M, Schwedes J. Comminution of ceramics in stirred media mills and wear of grinding beads. Powder Technology 1999;105:374.
[34] Yang RY, Jayasundara CT, Yu AB, Curry D. DEM simulation of the flow of grinding media in IsaMill. Minerals Engineering 2006;19:984.
[35] Farber BY, Knopjes L, Bedesi N. Advances in ceramic media for high energy milling applications. Minerals Engineering;In Press, Corrected Proof.
[36] Kelsall DF, Stewart PSB, Weller KR. Continuous grinding in a small wet ball mill. Part V. A study of the influence of media shape. Powder Technology 1973;8:77.
[37] Shi F. Comparison of grinding media--Cylpebs versus balls. Minerals Engineering 2004;17:1259.
[38] Ipek H. The effects of grinding media shape on breakage rate. Minerals Engineering 2006;19:91.
[39] Lameck NS, Kiangi KK, Moys MH. Effects of grinding media shapes on load behaviour and mill power in a dry ball mill. Minerals Engineering 2006;19:1357.
[40] Ipek H. Effect of grinding media shapes on breakage parameters. Particle & Particle Systems Characterization 2007;24:229.
[41] Yildirim K, Austin LG. The abrasive wear of cylindrical grinding media. Wear 1998;218:15.
[42] Lameck NS, Moys MH. Effects of media shape on milling kinetics. Minerals Engineering 2006;19:1377.
[43] Richardson JFH, J.H. Coulson & Richardson's Chemical Engineer. Oxford: Butterworth-Heinemann, 2002.
[44] Rydin R, Maurice D, Courtney T. Milling dynamics: Part I. Attritor dynamics: Results of a cinematographic study. Metallurgical and Materials Transactions A 1993;24:175.
[45] Becker M, Kwade A, Schwedes J. Stress intensity in stirred media mills and its effect on specific energy requirement. International Journal of Mineral Processing 2001;61:189.
[46] Blecher L, Kwade A, Schwedes J. Motion and stress intensity of grinding beads in a stirred media mill .1. Energy density distribution and motion of single grinding beads. Powder Technology 1996;86:59.
[47] Kwade A, Blecher L, Schwedes J. Motion and stress intensity of grinding beads in a stirred media mill .2. Stress intensity and its effect on comminution. Powder Technology 1996;86:69.
[48] Theuerkauf J, Schwedes J. Theoretical and experimental investigation on particle and fluid motion in stirred media mills. Powder Technology 1999;105:406.
[49] Theuerkauf J, Schwedes J. Investigation of motion in stirred media mills. Chemical Engineering & Technology 2000;23:203.

[50] Clermont BdH, B. Optimization of mill performances using on-line ball and pulp measurements. In: Wills BA, editor. Comminution. Falmouth, UK: Minerals Engineering International, 2008.
[51] Barley RW, Conway-Baker J, Pascoe RD, Kostuch J, McLoughlin B, Parker DJ. Measurement of the motion of grinding media in a vertically stirred mill using positron emission particle tracking (PEPT) Part II. Minerals Engineering 2004;17:1179.
[52] Conway-Baker J, Barley RW, Williams RA, Jia X, Kostuch J, McLoughlin B, Parker DJ. Measurement of the motion of grinding media in a vertically stirred mill using positron emission particle tracking (PEPT). Minerals Engineering 2002;15:53.
[53] Kim S, Choi WS. Analysis of ball movement for research of grinding mechanism of a stirred ball mill with 3D discrete element method. Korean Journal of Chemical Engineering 2008;25:585.
[54] Kim S, Chung H, Choi H. Analysis of Grinding Rate Constant on a Stirred Ball Mill Using Discrete Element Method Simulation. Journal of the American Ceramic Society 2009;92:531.
[55] Powell MS, McBride AT. A three-dimensional analysis of media motion and grinding regions in mills. Minerals Engineering 2004;17:1099.
[56] Cleary PW, Sinnott M, Morrison R. Analysis of stirred mill performance using DEM simulation: Part 2 - Coherent flow structures, liner stress and wear, mixing and transport. Minerals Engineering 2006;19:1551.
[57] Sinnott M, Cleary PW, Morrison R. Analysis of stirred mill performance using DEM simulation: Part 1 - Media motion, energy consumption and collisional environment. Minerals Engineering 2006;19:1537.
[58] Ramkrishna D. Population Balances: Theory and Applications to Particulate Systems in Engineering: Academic Press, 2000.
[59] Frances C. On modelling of submicronic wet milling processes in bead mills. Powder Technology 2004;143:253.
[60] Bilgili E, Hamey R, Scarlett B. Nano-milling of pigment agglomerates using a wet stiffed media mill: Elucidation of the kinetics and breakage mechanisms. Chemical Engineering Science 2006;61:149.
[61] Breitung-Faes S, Kwade A. Nano particle production in high-power-density mills. Chemical Engineering Research & Design 2008;86:390.
[62] Kwade A. Determination of the most important grinding mechanism in stirred media mills by calculating stress intensity and stress number. Powder Technology 1999;105:382.
[63] Kwade A. Mill selection and process optimization using a physical grinding model. International Journal of Mineral Processing 2004;74:S93.
[64] Kwade A. Wet comminution in stirred media mills - research and its practical application. Powder Technology 1999;105:14.
[65] Muller F. Parameters influencing generation of steep particle size distributions in stirred media mills - stata of knowledge and research. In: Kwade A, editor. Grinding and Dispersing with Stirred Media Mills. Braunschweig, Germany: iPat, 2007.
[66] Stender HH, Kwade A, Schwedes J. Stress energy distribution in different stirred media mill geometries. International Journal of Mineral Processing 2004;74:S103.
[67] Ghadiri MS, A.D.; Hounslow, M.J., editor Particle Breakage. Oxford: Elsevier, 2007.

[68] Hogg R. Breakage mechanisms and mill performance in ultrafine grinding. Powder Technology 1999;105:135.
[69] Parker DJ, Fan X. Positron emission particle tracking--Application and labelling techniques. Particuology 2008;6:16.
[70] Guida A, Fan X, Parker DJ, Nienow AW, Barigou M. Positron emission particle tracking in a mechanically agitated solid-liquid suspension of coarse particles. Chemical Engineering Research & Design 2009;87:421.
[71] Jones JR, Parker DJ, Bridgwater J. Axial mixing in a ploughshare mixer. Powder Technology 2007;178:73.
[72] Fishwick R, Winterbottom M, Parker D, Fan XF, Stitt H. The use of positron emission particle tracking in the study of multiphase stirred tank reactor hydrodynamics. Canadian Journal of Chemical Engineering 2005;83:97.
[73] Kuo HP, Knight RC, Parker DJ, Adams MJ, Seville JPK. Discrete element simulations of a high-shear mixer. Advanced Powder Technology 2004;15:297.
[74] Barigou M. Particle tracking in opaque mixing systems: An overview of the capabilities of PET and PEPT. Chemical Engineering Research & Design 2004;82:1258.
[75] Hassanpour A, Antony SJ, Ghadiri M. Modeling of agglomerate behavior under shear deformation: effect of velocity field of a high shear mixer granulator on the structure of agglomerates. Advanced Powder Technology 2007;18:803.
[76] Hassanpour A, Kwan CC, Ng BH, Rahmanian N, Ding YL, Antony SJ, Jia XD, Ghadiri M. Effect of granulation scale-up on the strength of granules. Powder Technology 2009;189:304.
[77] Ng BH, Kwan CC, Ding YL, Ghadiri M, Fan XF. Solids motion of calcium carbonate particles in a high shear mixer granulator: A comparison between dry and wet conditions. Powder Technology 2007;177:1.
[78] Ng BH, Kwan CC, Ding YL, Ghadiri M, Fan XF, Parker DJ. Granular flow fields in vertical high shear mixer granulators. Aiche Journal 2008;54:415.
[79] Bridgwater J, Forrest S, Parker DJ. PEPT for agglomeration? Powder Technology 2004;140:187.
[80] Chiti F. Lagrangian Studies of turbulent mixing in a vessel agitated by a Rushton turbine: PEPT and CFD. Dept of Chemical Engineering, vol. PhD. Birmingam: University of Birmingham, 2007. p.241.
[81] Ingram A, Seville JPK, Parker DJ, Fan X, Forster RG. Axial and radial dispersion in rolling mode rotating drums. Powder Technology 2005;158:76.
[82] Parker DJ, Fan XF, Forster RNG, Fowles P, Ding YL, Seville JPK. Positron imaging studies of rotating drums. Canadian Journal of Chemical Engineering 2005;83:83.
[83] Cox PW, Bakalis S, Ismail H, Forster R, Parker DJ, Fryer PJ. Visualisation of three-dimensional flows in rotating cans using positron emission particle tracking (PEPT). Journal of Food Engineering 2003;60:229.
[84] Aglietti EF, Porto Lopez J. Physicochemical and thermal properties of mechanochemically activated talc. Materials Research Bulletin 1992;27:1205.
[85] Aglietti EF. The effect of dry grinding on the structure of talc. Applied Clay Science 1994;9:139.
[86] Zbik M, Smart RSC. Influence of dry grinding on talc and kaolinite morphology: inhibition of nano-bubble formation and improved dispersion. Minerals Engineering 2005;18:969.

[87] Pedro J. Sánchez-Soto M. Effects of Dry Grinding on the Structural Changes of Kaolinite Powders. Journal of the American Ceramic Society 2000;83:1649.
[88] Kameda J, Saruwatari K, Tanaka H. H_2 generation during dry grinding of kaolinite. Journal of Colloid and Interface Science 2004;275:225.
[89] Frost RL, Mako E, Kristof J, Horvath E, Kloprogge JT. Modification of Kaolinite Surfaces by Mechanochemical Treatment. Langmuir 2001;17:4731.
[90] Breen C, Illés J, Yarwood J, Skuse DR. Variable temperature diffuse reflectance infrared Fourier transform spectroscopic investigation of the effect of ball milling on the water sorbed to kaolin. Vibrational Spectroscopy 2007;43:366.
[91] Christidis GE, Makri P, Perdikatsis V. Influence of grinding on the structure and colour properties of talc, bentonite and calcite white fillers. Clay Minerals 2004;39:163.
[92] Yang H, Du C, Hu Y, Jin S, Yang W, Tang A, Avvakumov EG. Preparation of porous material from talc by mechanochemical treatment and subsequent leaching. Applied Clay Science 2006;31:290.

3 Experimental Methods

This chapter details the analytical methods and experimental methods common throughout this thesis.

3.1 Size Measurement

3.1.1 Sedigraph

Size measurement through sedimentation, is an established technique based on Stokes' Law of settling, which states that a particle settling velocity is proportional to the density difference between the particle and fluid, the fluid viscosity and the square of the particle diameter. A review of this is given in [1].

Stokes' law for a spherical particle may be expressed by equation (3.1).

$$D = \sqrt{\frac{18\eta u}{(\rho - \rho_0)g}} \qquad \textbf{(3.1)}$$

or

$$D = Ku^{1/2} \qquad \textbf{(3.2)}$$

where D = particle diameter, η = fluid viscosity, u = particle velocity, ρ = particle density, ρ_0 = fluid density, and K is a conglomeration of the parameters seen in equation (3.1). Stokes' law may safely be applied, providing the Reynolds number is below ~0.5, and thus laminar

flow is maintained. Now a particle of diameter D will fall a distance h in a time t, given by equation (3.3).

$$D = K\left(\frac{h}{t}\right)^{1/2} \qquad \textbf{(3.3)}$$

Therefore, after a time, t_1, there will be no particles with a diameter greater than D_1 less than a distance h_1 from the surface. Therefore, if X-rays are used to measure the concentration of particles at corresponding heights from the surface, it is possible to gain a distribution of the size distribution of the powder[2]. This technique is established at Imerys as the standard procedure to measure particle size for quality control purposes. The Sedigraph 5120 (Micromeritics, USA) is used for these purposes.

3.1.2 Dynamic Light Scattering

Dynamic Light Scattering is also used for size analysis of fine particles, giving a diameter related to the sphere of rotation in the fluid. For blocky particles with an aspect ratio close to unity, this diameter is very similar to the sedimentation diameter. For higher aspect ratio materials, such as clay or talc platelets, this diameter is likely to be higher. These techniques are reviewed in [1]. At Imerys, the Mastersizer S (Malvern, UK) is used for this purpose, as well as CILAS 1064 (Cilas, France). Both of these use the established Fraunhofer and Mie algorithms for reconstructing the particle size distributions, depending on the size. The Fraunhofer algorithm is used for coarser particle sizes, whilst Mie

algorithms which account for the different refractive indices are used with material below 2 μm.

3.2 Surface Area

3.2.1 BET Surface Area

When measuring surface area, the most frequently used physical process of that of physisorption, i.e. the adsorption of molecules onto the surface without the formation of a chemical bond. This physisorption behaviour is most commonly modelled with the BET isotherm. The isotherm is named after the scientists, Brunauer, Emmet and Teller who first derived it in 1938, and is shown in equation (3.4).

$$\frac{P}{V(P^{sat}-P)} = \frac{1}{V_m C} + \frac{C-1}{V_m C}\frac{P}{P^{sat}} \qquad \textbf{(3.4)}$$

where:

V is the volume of gas adsorbed at pressure P.

P^{sat} is the saturated vapour pressure at the temperature of the experiment.

V_m is the volume occupied by a monolayer of adsorbate.

C is an established experimental constant.

The BET isotherm is based on the assumptions of the Langmuir isotherm, namely that all possible sites for adsorption are equivalent and that adsorption strength is independent of coverage. The BET isotherm is abundantly used, despite its limitations in some areas. As with Langmuir, the theory assumes that there can be no lateral movement over the surface of the adsorbate, and also that it exerts no lateral force upon the adjacent molecules. Therefore, inaccuracies may be arrived at with highly mobile/interacting surface adsorbates. However, its potential for multilayer adsorption gives it an advantage over many other theories[3].

The main disadvantage of the technique is when very finely porous materials, such as zeolites. BET experiments are most commonly performed using nitrogen gas, which is a small diatomic gas (length ~5 Å). It is also possible to use helium as the adsorbing gas, which is a significantly smaller gas (~1 Å). In zeolitic material, it is possible that there are pores or chambers which helium would pass through, whilst nitrogen would not. Thus there is clearly a limitation when using materials with the finest of pores[4].

Many processes will also use much larger molecules reacting, or adsorbing to the surface, and a common problem experienced in capillary condensation, whereby pores are blocked by build up of larger molecules. The BET isotherm is not elaborate enough to cater for this, and so there may be a discrepancy between the predicted surface area and the volume of reagent which will adsorb onto the surface.

At Imerys, the BET surface area is determined using the TRISTAR equipment, manufactured by Micromeritics (USA). The system is mostly automated, so little must be done by the operator, save for the set up of the operating software. It is however key that the sample is degassed prior to testing, to remove any material which has been adsorbed in prior work, or during storage.

The operation measures the quantity of nitrogen gas which is adsorbed as a monolayer on the test sample. Conditions are sought whereby the surface area of a molecule of gas is accurately known, hence the operation is performed close to the boiling point of the adsorbate. This is achieved by immersing the flask in liquid nitrogen. Volumes adsorbed are determined from accurate pressure measurements, thus the surface area is calculated. Measurement errors are largely attributed to sampling difficulty, at ±3%.

3.2.2 Dynamic Vapour Sorption

In addition to the surface area measurements available at Imerys, Dynamic Vapour Sorption is used to investigate surface features. The DVS Advantage (Surface Measurement Systems UK Ltd.) uses precision gravimetric and vapour pressure measurements to form isotherms in much shorter time scales than traditional adsorption isotherm techniques. This is due to the vapour for adsorption flowing over and past the sample, rather than the traditional static approach [5] and is shown schematically in Figure 3-1.

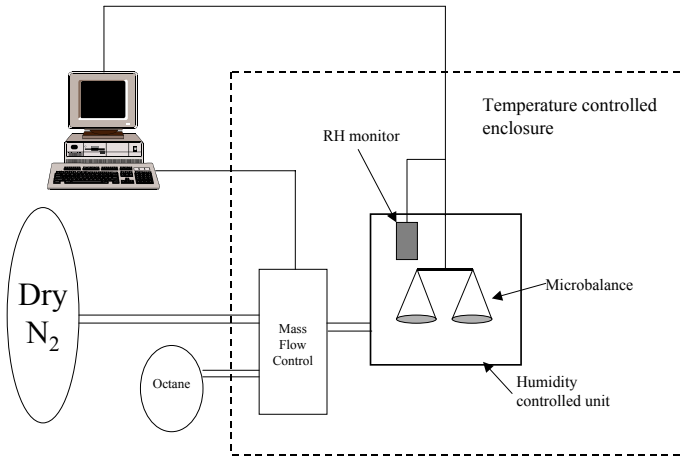

Figure 3-1: Schematic of the DVS equipment

The mass of the sample is measured to an extremely high resolution, and when the rate of mass change is below 0.002 %/min, there is an increase in solvent vapour pressure. For this work, octane is used as a solvent. The recorded data can also be fitted to the BET isotherm to give an additional confirmation of the surface area of a mineral.

3.3 Other Characterisation Methods/Techniques

3.3.1 Powder Brightness Measurement

Powder optical properties are very important to a large number of Imerys applications. For the measurement of brightness and yellowness of Imerys powders, the Datacolor Elrepho (Datacolor, NJ, USA) is used according to ISO standard [6]. The preparation of the powder is important, and if the calcium carbonate sample is presented as a slurry, it is flocculated with 10 ml of a 10 wt.% $CaCl_2$ (Sigma Aldrich, UK). The flocculated slurry is vacuum filtered

in a Büchner funnel (120 mm grade 541 papers from Whatman) and the sample thoroughly dried at 80 °C.

The brightness is defined as the percentage of light with a nominal wavelength of 457 nm which is reflected from 10 g of the pressed powder sample in comparison to a perfect diffuser. The powder yellowness is defined as the difference in the reflectance of a pure diffuser and the pressed powder sample with a light source with a wavelength of 571 nm. The technique is accurate and highly repeatable, with quoted brightness values having an error of ±0.1.

3.3.2 Mercury Porosimetry

Mercury porosimetry is used to investigate porosity of materials. The sample is weighed (0.125 g) and added to the equipment with a sample of mercury, an increasing pressure profile is then applied, progressively increasing from 0.0125 – 190 Pa. Accurate measurement of the system volume is taken as a function of pressure, allowing the volume of material within the pores to be determined. Knowledge of the relationship between mercury pressure and pore diameter [7] enables a full pore size distribution to be ascertained over the range 1000 – 10 nm approximately. At Imerys, the Pascal 240 (CE Instruments) is used for this investigation.

3.3.3 X-Ray Diffraction

The crystallographic composition of talc samples was performed using X-Ray Diffraction (XRD). X-rays focussed onto the sample interfere with the electron cloud of the atoms, and are re-radiated by Raleigh scattering according to Bragg's law of crystallinity[8], as shown in equation (3.5).

$$n\lambda = 2d.sin\theta \quad \textbf{(3.5)}$$

Where λ is the X-ray wavelength, n is an integer multiple for the scattering, d is a characteristic length in the crystal lattice and θ is the angle between incidence and scattering. The system uses wavelengths in the range 5 – 0.1 Å. Due to the experimental arrangement of the X-ray source and detector with respect to the source, 2θ is measured and reported by convention. The peaks in the sweep of 2θ correspond to characteristic lengths in the crystal lattice. When considered together, these give a diagnostic identification of the minerals present. Through the use of standard materials, some quantitative analysis of the composition can be ascertained. Any amorphous material will not be detected by the technique.

In the process at Imerys, 5 g of the sample is milled with a McCrone micronising mill to ensure that all material is below 10 µm in size. This sample is vacuum filtered with a Büchner funnel (120 mm grade 541 paper from Whatman) and dried at 80 °C before being pressed into a circular sample holder. The sample is analysed in a PANalytical X'Pert PRO (PANalytical, Netherlands), enabling the crystalline composition to be ascertained.

3.3.4 X-Ray Fluorescence

X-Ray Fluorescence (XRF) is the spectroscopic analysis of secondary X-rays from the emission of materials excited by high energy X-Rays[9]. This enables the elemental composition (based on oxides) of mineral powders to be determined. Prior to X-ray testing, the loss of ignition of the material is also measured. The remaining material (4.00 g of sample) is mixed with a PVA binder (Sigma Aldrich, UK) and, after mixing, pressed into a disc. This disc is used with the PANalytical Magix PRO XRF (PANalytical, Netherlands) equipment, which is regularly calibrated with a host of reference materials (various metal oxides, spectroscopy grade, Sigma Aldrich, UK). From this data, the composition of the material can be ascertained.

3.4 Microscopy Techniques

3.4.1 Scanning Electron Microscopy

Scanning Electron Microscopy (SEM) is used throughout this work for the investigation of the sub-micron morphology of particles. The key limitation of the technique is the extremely small sampling size. At Imerys, samples are sputtered with a thin layer of gold before being placed in a Jeol 6700F Field-SEM (Jeol, Japan), where magnification can be achieved up to a feature resolution of 1 nm.

3.4.2 Transmission Electron Microscopy

Transmission Electron Microscopy (TEM) is used for the ultrafine investigation of talc in Chapter 7. The system employed is a Jeol 1200EX system (Jeol, Japan), allowing resolution of features below 1 nm.

3.4.3 Atomic Force Microscopy

Atomic Force Microscopy (AFM) is also used for the characterisation of surface features and edge dislocations of talc in Chapter 7. A MultiMode AFM (Veeco, UK) with a NanoScope III camera (Veeco, UK) is used in tapping mode in order to characterise fine surface features of a powder immobilised on a slide. A maximum vertical resolution of 100 nm is used.

3.5 Grinding Equipment

3.5.1 Lab grinder for wet grinding

Lab scale stirred media milling was performed in an Imerys sand grinder. The grinder is shown in Figure 3-2. The impeller can be seen with two pairs of orthogonally mounted pins, inside the chamber. The impeller arms and the chamber lining are all lined with polyurethane to reduce wear, and prevent product discolouration. The chamber is mounted on a freely rotating metal plate, which has a load arm resting against a load cell. This enables measurement of the torque, and thus gives a measure of the energy input into the system. Figure 3-3 shows the measurements of the system layout.

The motor is a 0.55 kW motor (Brook Hansen, UK) with a maximum speed of 1500 rpm, fitted with a variable speed drive control box (Cheetah SM, UK). The rest of the motor and the data logger are made in house by Imerys.

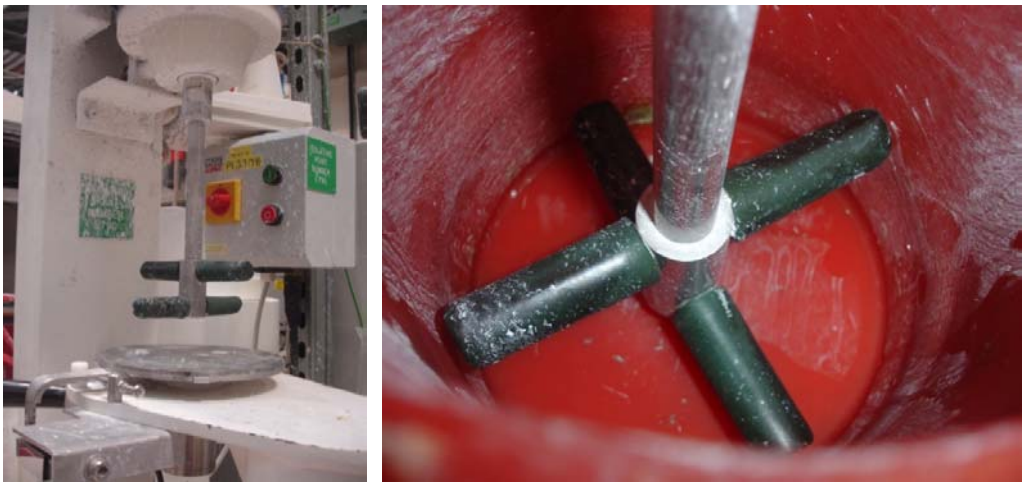

Figure 3-2:Photographs of the grinder (a) without pot and (b) impeller arm inside pot.

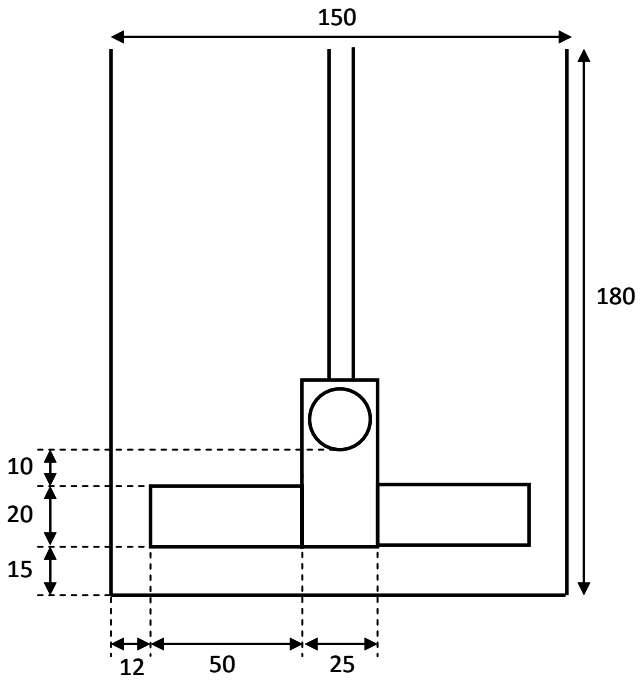

Figure 3-3: Drawing of the grind chamber with full measurements in mm.

This work discusses widely discusses the speed of the motor, quoted in revolutions per minute (rpm). For the purposes of clarification, calibration between motor speed and the impeller tip speed is given in Table 3-1

Table 3-1: Calibration between motor speed and impeller tip speed.

Motor Speed (rpm)	Tip Speed (m/s)
600	3.93
800	5.24
1000	6.54
1200	7.85

For the wet grinding of Calcium carbonate (marble flour), the basic recipe is as follows (NB some parameters may be varied in later work):

- 1500 g Carbolite 16-20 (Carbo Ceramics, USA) media, normalised by density to maintain the same volume of media (Carbolite has a density of 2.71 g/cm^3).
- 250 g tap water.
- 4.5 ml Dispex 2695 sodium polyacrylate (Ciba Specialty Chemicals, UK) dispersant (longer grinds may require further dispersant addition.
- 750 g Marble flour, from Marmara, Turkey (Imerys).

First the water and dispersant are added to the grind chamber, and the media and mineral are dry mixed by hand in a bag. These are then added to the chamber, which is slowly brought up to the required motor speed. Throughout the grind, the power input is monitored, and for longer grinds, water or dispersant may be added as required to compensate for losses through evaporation and fresh surface area generation. The total energy input is monitored in Wh, however comparison of grind are normalised to the dry weight of mineral into kWh/t.

3.5.2 Lab grinding for dry grinding of talc

For the dry grinding experiments, a mill with the same dimensions as given in Figure 3-3 was utilised, except the equipment was fabricated from mild steel, to prevent melting at high temperatures. The recipe for this work is as follows:

- 1500 g Carbolite 16-20 (Carbo Ceramics, USA).
- 300 g talc (Beihai, China).

Whilst the motor speed was maintained at 1410 rpm.

3.5.3 Pilot grinding at Imerys Gothers Pilot Plant

Pilot scale grinding was performed on an 18.5 kW mill at Imerys' Gothers pilot plant, shown schematically in Figure 3-4. Precise specifications are commercially sensitive and may not be published, but the grinder has a diameter of 700 mm and a height of approximately 1000 mm with an octagonal cross section. The screen at the bottom of the grinder retains the media whilst allowing the slurry to recirculate around the system. The height of the flexible exit pipe to the grinder allows for control of the fluid level within the grinder. The impeller arms are arranged as the sets of two pins, each set offset by 120° such that overall there is an impeller arm every 60° over the three sets.

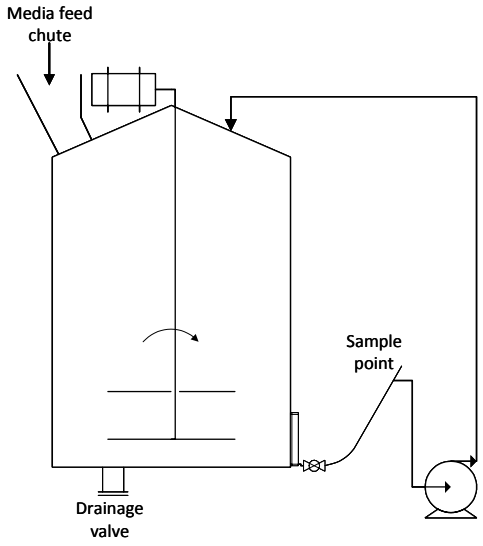

Figure 3-4: Schematic of pilot grinder at Gothers pilot plant.

The grinder was filled with pre-dispersed slurry of Carbital 60 (Imerys, France) with sufficient slurry to maintain the appropriate media volume concentration in the mill after accounting for the slurry in the re-circulating pipe work. The following recipe was observed:

- Grinding media: 249 kg for Carbolite 16-20, 333 kg for Alodur 92 and 386 kg for zirconium silicate (Cenotec).
- 100 L of Carbital 60 dispersed calcium carbonate slurry, 75 wt.% mineral.
- Further dispersant (Dispex 2695) is added as required throughout the grind.

Samples are taken every 25 kWh/t through a valve operated sampling point, where 500 ml was collected for analysis. Slurry density was measured throughout to ensure that the correct mineral solids fraction is maintained during the grind. After the grind was

complete, a 5 L sample was collected, and the remaining slurry was purged to the drain. The media was then thoroughly rinsed with water and dried.

3.6 Positron Emission Particle Tracking (PEPT)

The use of Positron Emission Particle Tracking (PEPT) is now an established technique, based originally on Positron Emission Tomography (PET) from medical physics, the PEPT technique has been developed at the University of Birmingham. Rather than tracking the whole of a fluid, as in PET, PEPT tracks a single particle which has been labelled. For the purposes of this work, a single grinding media particle is labelled by direct irradiation in a 33 MeV ^{3}He beam from a cyclotron. This causes a small proportion of the ^{16}O present in the bead to be converted to the radioactive ^{18}F. For a full description of the labelling technique, see Parker and Fan, 2008 [10]. The ^{18}F then decays through positron emission. The emitted positrons immediately collide with their antiparticle, electrons, resulting in pairs of anti-parallel γ-rays, as shown in Figure 3-5.

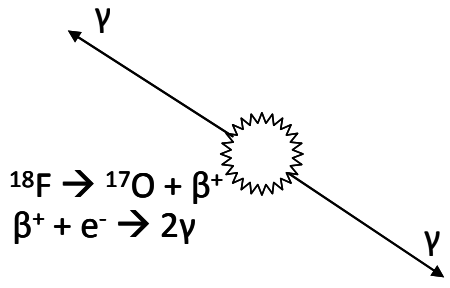

Figure 3-5: Schematic of the release of gamma rays during positron emission

The labelled media particle can be placed in the grinder, which is operated in exactly the same fashion as it would otherwise. The grinder is placed between the two plates of the gamma ray camera, as seen in Figure 3-6. The gamma rays are simultaneously detected by the two cameras, which provides a line of response (LOR) passing close to the tracer particle. The cameras are capable of detecting the LORs of up to 100k gamma rays per second.

Algorithms developed by Parker *et al.* [11, 12] use the multiple LORs which are received and triangulate the position of the labelled particle, as represented in Figure 3-7. The algorithm minimises the sum of perpendicular distances from the tracer location to the LORs. Within such a process, there is inherent scattering of the γ-rays such that not all rays cross close to a single point. The algorithms developed by Parker *et al.*[11, 12] detect these corrupt data and remove them, allowing a calculation for the location of the particle. A key criterion of the algorithm is the maximum permitted interval for data for a given data point. A shorter tolerance leads to more accurate positional resolution, which is especially important in high speed systems. However, if this interval is reduced too far then there may be insufficient data for accurate triangulation. The generated data is a series of (t,x,y,z) information with a data point approximately every 50 ms. This can be further disseminated by the algorithms developed and discussed in Chapter 6. Through this technique, a resolution of the tracer particle to within 1 mm is achievable.

Figure 3-6: Photograph of the lab scale grinder inside the gamma ray camera.

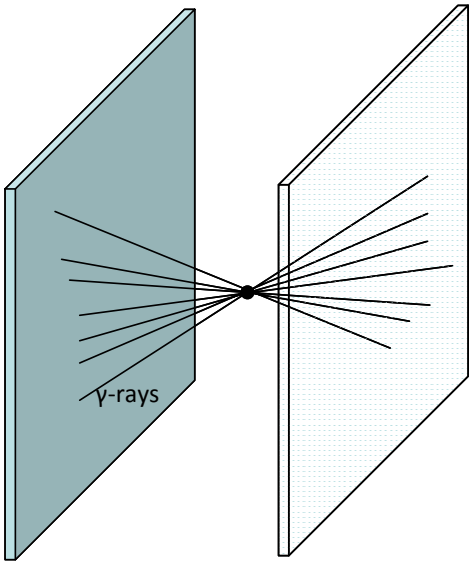

Figure 3-7: Schematic of the process for triangulating the particle location.

3.7 Polymer Processing and Testing

3.7.1 Compounding

Mineral and polymer were first mixed by hand in a bucket to give an approximately homogenous mixture. This material was then added to the feeder of a BakerPerkins MP2030 co-rotating twin-screw extruder (Baker Perkins, UK) with a temperature profile from 160 up to 180 °C (die), screw speed of 300 rpm, and torque ranging 40 % of capacity. The hot compound was continuously cooled in a water bath, before air drying and pelletising. This was performed initially at 30 wt.% mineral filler, however, the material was re-passed through the compounder after 24 hr of conditioning, and at this stage the mineral fraction maybe reduced by further addition of virgin polymer.

3.7.2 Injection Moulding

The pellets from compounding were moulded using a Arburg Allrounder 320M injection moulder (Arburg, Germany), with barrel temperatures 200-230 °C, mould temperature 30 °C, injection rate 35.5 cm^3/s, holding pressure 1000 bar, cooling time as required for solidification. The resulting test pieces are both dog-bone and straight bar pieces, sufficient for the following mechanical testing. After moulding, the test pieces were conditioned by open storage in a room maintained at 23 °C and 50% relative humidity for a minimum of 48 h in accordance with ISO 291.

3.7.3 Mechanical Testing

A range of mechanical testing were performed on the dog-bone and straight bar pieces, in accordance with techniques described in [13].

Impact Testing

Impact testing was performed with a Rosand IFW5 (Fleming, UK) falling weight impact test. For this work both notched and un-notched Charpy impact tests were performed in accordance to ISO 179-2 [14]. For this work, the feed and product of the dry grinding techniques discussed in Chapter 7 are compared with an ultrafine kaolin, Polsperse™ 10 as a control. For each test, 20 specimens are used on test pieces measuring 80x10x4 mm with impact made perpendicular to the flat surface as seen in Figure 3-8.

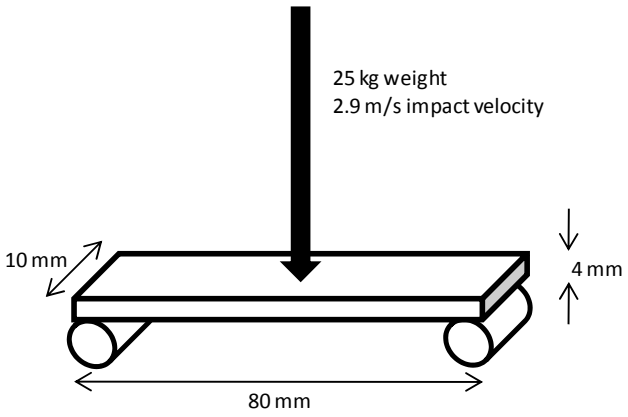

Figure 3-8: Schematic of the measurement of impact properties by falling weight.

The instrumentation then allows computation of the following:

- Impact stress: based on the peak force exerted on the specimen in the direction of movement, and the cross sectional area of the test piece.
- Impact energy: energy required for complete breakage of the test specimen.
- Peak deflection: deflection of the test piece at the peak force.

Both notched and un-notched test pieces are considered, as the notch removes any initiation from the crack propagation.

Tensile Modulus

Tensile modulus is performed with a Hounsfield HK105 tensometer (Hounsfield, UK). For each material, 10 ‘dog-bone’ shaped specimens are held in clamps according to ISO 527-2 [15] and a head speed of 50 mm/min is applied. Load cells measure the applied force against time in order to determine the tensile modulus.

Flexural Modulus

Flexural modulus is measured with a Hounsfield HK105 tensometer (Hounsfield, UK). For each material, 5 ‘dog-bone’ shaped specimens are analysed in accordance with ISO 178 [16]. The test piece is mounted on supports separated by 60 mm and the cross-sectional of the test piece in this region is 10x4 mm. The head speed used is 2 mm/min and the load cell allows measurement of the applied force against time, in order to determine the flexural modulus.

3.8 References

[1] B.A. Wills . Mineral Processing Technology. Oxford: Elsevier, 2007.

[2] P.A. Webb CO. Analytical Methods in Fine Particle Analysis: Micromeritics, 1997.

[3] Coulson R, Bachurst, Harker. Coulson and Richardson's Chemical Engineering: Butterworth-Heinemann, 1991.

[4] S. Ross JPO. On Physical Adsorption: Interscience Publishers, 1964.

[5] Tisserand C, Calvet R, Patry S, Galet L, Dodds JA. Comparison of two techniques for the surface analysis of alumina (Al_2O_3): Inverse Gas Chromatography at Finite Concentration (IGC-FC) and Dynamic Vapor Sorption (DVS). Powder Technology 2009;190:53.

[6] Anon. Measurement of diffuse blue reflectance factor (ISO Brightness). ISO 2470:1999.

[7] Allen T. Particle Size Measurement. London: Chapman and Hall, 1981.

[8] Azaroff LV. X-Ray Diffraction: McGraw-Hill, 1974.

[9] Lifshin E. X-Ray Characterization of Materials: Wiley-VCH, 1999.

[10] Parker DJ, Fan X. Positron emission particle tracking--Application and labelling techniques. Particuology 2008;6:16.

[11] Parker DJ, Hawkesworth MR, Beynon TD. Process applications of emission tomography. The Chemical Engineering Journal and the Biochemical Engineering Journal 1995;56:109.

[12] Parker DJ, Hawkesworth MR, Broadbent CJ, Fowles P, Fryer TD, McNeil PA. Industrial positron-based imaging: Principles and applications. Nuclear Instruments and Methods in Physics Research Section A: Accelerators, Spectrometers, Detectors and Associated Equipment 1994;348:583.

[13] R.Brown. Handbook of Polymer Testing: Marcel Dekker, 1999.

[14] Charpy Impact Strength. In: ISO, editor. ISO179, 2000.

[15] Plastics - Testing Tensile Properties. In: ISO, editor. ISO 572-2, 2000.

[16] Plastics - Determination of Flexural Properties. In: Standardisation IOf, editor. ISO178, 2001.

4 Materials Characterisation

This Chapter characterises the raw materials which have been used throughout this thesis, as well as detailing other chemicals used throughout.

4.1 Minerals

4.1.1 Marble (Calcium Carbonate)

The wet grinding work throughout this thesis is conducted on calcium carbonate as marble. Marble is a form of calcium carbonate ($CaCO_3$) which is metamorphosed from the sedimentary limestone. Limestone is often formed from the remains of biological activity, but may also be formed from a precipitation reaction of lime (CaO) with carbon dioxide [1]:

$$CaO + H_2CO_3 \rightarrow CaCO_3 + H_2O$$

or

$$Ca(OH)_2 + H_2CO_3 \rightarrow CaCO_3 + 2H_2O$$

Metamorphosis of the limestone at pressures over 1000 bar and temperatures from 200-500 °C produces marble through re-crystallisation or solid state reaction. There have been many comprehensive studies on the paragenesis of marble, as well as the common

impurities in the material through the various stages of formation; for an excellent review, the reader is directed towards Chang, Howie and Zussman, 1996 [2].

The Marmara flour is a marble source from the Marmara deposit, Turkey owned by Imerys. After mining from the ground, the marble is jaw crushed into small (millimetre scale) chips before being hammer milled into a dry powder. This is the raw feed to the grinders in the cascade at the plant scale, and thus is an appropriate choice of material as a feed for the wet grinding in these experiments.

The particle size distribution of the feed material is shown in Figure 4-1 where it is seen that there is a mono-modal distribution and a large percentage of material greater than 10 µm. A further summary of the physical parameters is given in Table 4-1. The steepness is also shown in Table 4-1, which is an important measure of the particle size for many Imerys applications, which requires that they are sold with a given fraction of material less than 2 µm as well as a steepness value which demonstrates that there is not an excess of ultrafine or coarse material present.

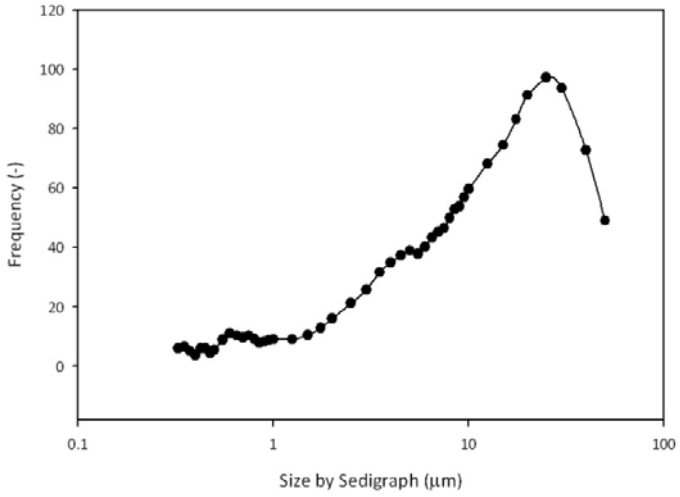

Figure 4-1: Particle size distribution of the Marmara flour by Sedigraph.

Table 4-1: Summary of physical properties of the Marmara flour. Sizes are measured by Sedigraph.

Parameter	Value
d10 (µm)	2.91
d50 (µm)	17.50
d90 (µm)	52.00
Steepness (100*d30/d70)	31.2
Surface Area (m^2/g)	0.68
ISO Brightness	90.7
Yellowness	1.6

The material retains good optical properties, with an ISO brightness of 94.7 and a yellowness of 1.1. This numbers are represent a whiter and less yellow sample than the Marmara flour described in Table 4-1. Although there may be some natural variation in feed, the improved properties of the Carbital 60 are likely to be due to the different

interference of the finer particles with the light, as well as the beneficiation of the product which may have removed some coloured material.

4.1.2 Carbital 60 slurry (Calcium Carbonate)

The pilot scale work in this thesis does not use a dry powder, as was used with the laboratory scale grinding, but a pre-dispersed slurry which is already sold as a product by Imerys. The Carbital 60 production uses the Marmara flour from Section 4.1.1 as a feed, and therefore the mineralogical composition is the same. The slurry is 77 ±1 wt.% solids dispersed in order to minimise viscosity. The key difference is that the slurry has already been ground within a cascade of grinders, so the particles are much finer as seen in Table 4-2. This prevents any sedimentation of material in the re-circulating loop of the pilot grinder, thus reducing any sampling errors as well as decreasing the chances of any blockages within the pipework.

Table 4-2: Summary of size properties for Carbital 60 (measured by Sedigraph)

%< 10 µm	99.4
%< 2 µm	62.3
%< 1 µm	37.9
Median diameter (µm)	1.45
Surface Area (m^2/g)	6.51

The material retains good optical properties, with an ISO brightness of 94.7 and a yellowness of 1.1. This numbers are represent a whiter and less yellow sample than the

Marmara flour described in Table 4-1. Although there may be some natural variation in feed, the improved properties of the Carbital 60 are likely to be due to the different interference of the finer particles with the light, as well as the beneficiation of the product which may have removed some coloured material.

4.1.3 Talc

Talc is an example of a phyllosilicate mineral with a tri-octahedral layered structure. Magnesium ions occupy the octahedral sites between the silica layers, such that there are no vacant sites[3]. The crystal structure is shown in Figure 4-2. The lack of interlayer vacancies reduce the cation exchange capacity of talc compared to other phyllosilicate minerals, and the lack of surface hydroxyl groups gives talc its hydrophobic nature. Talc deposits are generally termed as being either macro- or micro-crystalline, with the macro-crystalline form being much more common, resulting in the familiar form with large individual platelets and a high aspect ratio (thickness:diameter).

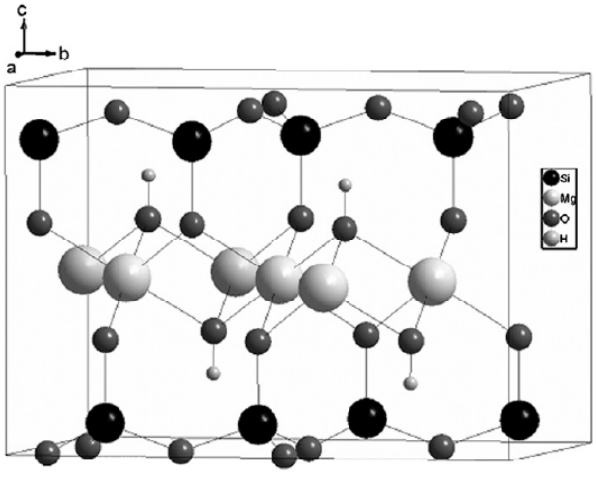

Figure 4-2: Schematic representation of the structure of a talc crystal[4].

The talc chosen for the dry grinding experiments is an exploration sample from Beihai, China. This was selected for its availability as well as the high purity (X-Ray Diffraction shows 97% purity, the remainder is dolomite). The material is presented in rock form (pieces approximately 7 cm in diameter) which is jaw crushed and hammer milled to produce a fine, dry powder. The size properties of the feed talc material are given in Table 4-3. The key physical properties to note are the very high d_{90} by Sedigraph (32.0 μm), indicating a large amount of very coarse material, and the low surface area, suggesting there is not a large amount of ultrafine material. The brightness and yellowness both indicate a very white and pure product.

Table 4-3: Summary of the physical properties of the Beihai talc.

BET Surface Area (m^2/g)	d_{10} by Sedigraph (μm)	d_{50} by Sedigraph (μm)	d_{90} by Sedigraph (μm)	Brightness	Yellowness
3.6	1.3	7.9	32.0	95.0	1.6

4.1.4 Kaolin

For the purposes of the mechanical testing of the polymer compounds in Chapter 7, a control material is used for comparison with the different talc minerals used. For this purpose, Polsperse™ 10 is used. Polsperse™ 10 is an Imerys ultrafine kaolin for the performance minerals sector which has been chemically treated to improve levels of dispersion in non-aqueous systems (exact modification is industrially sensitive). A summary of the properties of the product are given in Table 4-4. The most significant physical

properties to consider are the fine size distribution, with very few coarse particles (≤ 0.2% above 10 µm). Large particles can lead to reduction of impact strength, so this is important. Furthermore, the material has a relatively high surface area (16.0 m^2/g) which indicates there is significant area for interaction with the polymer matrix. The optical properties suggest a material which is lower in brightness than the talc and the calcium carbonates previously discussed, and this is often typical of kaolinite.

Table 4-4: Summary of the physical properties of Polsperse™ 10, an ultrafine Imerys kaolin product.

BET Surface Area (m^2/g)	Size fraction above 10 µm (mass % by Sedigraph)	Size fraction below 1 µm (mass % by Sedigraph)	Brightness	Yellowness
16.0 ± 0.5	0.2	77.0 ± 0.5	87.5 ± 1.0	4.2 ± 0.2

4.2 Grinding Media

A key aspect of this thesis is the development and comparison of grinding media. This section introduces the grinding media which have been used throughout, focussing on the current *status quo* within Imerys, as well as the newly developed media, which this work has been a part of. The alternative commercial media which are used for wet grinding of calcium carbonate are also summarised.

4.2.1 Carbolite 16-20

Carbolite (Carbo Ceramics, US) is widespread in usage throughout Imerys' grinding operations. As well as offering an acceptable grinding performance, it does not have a significant negative effect on the colour properties of the carbonate. The product is principly composed of mullite ($Al_6Si_2O_{13}$) which is a product of the extreme calcinations of calcined clay [5].

4.2.2 Summary of spherical media

The other spherical media which are used in this thesis are summarised in Table 4-5. Although there is some variation in the size ranges, they are chosen to be as close as is possible. There are other characterisations which can be made of the media, given in these product specification sheets given by the suppliers such as material hardness and crush strength. These are not included as the test methods may not be consistent across the different suppliers.

Table 4-5: Summary of the properties of the commercial spherical grinding media used in this work.

Brand Name	Supplier	Principle Composition	Density (g/cm^3)	Colour	Size range (mm)
Carbolite 16-20	Carbo ceramics (US)	Mullite	2.71	Grey	0.85-1.2
Carbo HSP	Carbo ceramics (US)	Alumina based	3.53	Dark Brown	0.85-1.2
Keramax MT1	Magotteaux (Belgium)	Alumina/ zirconia	3.90	Pale yellow	1.0-1.2
Cenobead CZS	Cenotec (Korea)	Zirconium silicate	4.2	White	1.0-1.2
Silibead YS	Sigmund-Lindner	Yttria stabilized zirconia	6.0	Pearlescent white	1.0-1.2

4.2.3 Rod Shaped grinding media

The rod shaped grinding media which are discussed throughout this thesis are manufactured by Imerys, as a development product. They are extruded to have a diameter based on a mesh size of 16 (i.e. 1.00 mm), however there may be some shrinkage of this number during drying and firing. There is a distribution for the length of the rods, based on the mechanism of cutting, but the median length is 3 mm.

For the majority of the wet grinding work at lab and pilot scale, Alodur 92 was used as the rod shaped media. This has a high alumina content, and a dark brown colour, as seen in Figure 4-3, where it can be also seen that after prolonged use, there is some rounding of the corners of the rod shape, and a polishing of the media surface.

Figure 4-3: Microscopy Images of the fresh Alodur 92 (left) and media worn after pilot grinding (right).

Throughout the wet grinding chapter of this thesis, the case is made for whiter rod shaped grinding media, which are subsequently manufactured in the small scale. The recipes are made with three different feed materials, and their densities are summarised in Table 4-6. All of the white recipes use the same proportions of other additives in order to produce the extrudable paste (although green water content may vary).

Table 4-6: Summary of the density and composition of the white rod shaped media.

Name/Principle Composition	Density (g/cm^3)	Colour
Alodur 92 (high alumina)	3.63	Dark brown
Alodur 96 (v. high alumina)	3.75	Brown/Black
Metakaolin	2.71	White
Mineral A	2.91	White/Grey
Mineral B	2.81	White/Grey
Mineral C	3.92	Bright white

4.3 Process Chemicals

4.3.1 Dispersant

The calcium carbonate slurries must be fully dispersed in order to maintain a good viscosity at high solid weight fractions (over 75%). Much work has been done within Imerys on the development of dispersants for these applications[6] and predominantly certain sodium polyacrylate based dispersants are used. Research continues in this area, with the intention of improving performance, but also reducing cost. For the dispersion of calcium carbonate powder in this work, Dispex 2695 (Ciba Specialty Chemicals, UK) is used, which is a commercially sourced sodium polyacrylate.

4.3.2 Polymer for compounding trials

The high surface area talc material is introduced into a polymer, alongside some controls in Chapter 7. For this purpose, polypropylene (PP) is used, which is a commodity polymer used in a range of applications. The polymer chains in PP can have a diverse rangth of length distributions as well as different amount of branching, and this affects their flow properties and thus the end application. For this work, HE125MO grade from Borealis (Austria) was used, which is a homopolymer with good flow properties and stiffness, intended for injection moulding applications.

4.4 References

[1] Tegethoff FWR, J.; Kroker, E. Calcium Carbonate: From the Cretaceous Period into the 21st Century. Basel: Birkhauser, 2002.
[2] Chang LLYH, R.A.; Zussman, J. Non-silicates: Sulphates, Carbonates, Phosphates, Halides. Rock Forming Minerals, vol. 5B. London: Longman Group, 1996. p.101.

[3] Deer WAH, R.A.; Zussman, J. An Introduction to the rock forming minerals: Prentice Hall, 1996.
[4] Douillard JM, Salles F, Henry M, Malandrini H, Clauss F. Surface energy of talc and chlorite: Comparison between electronegativity calculation and immersion results. Journal of Colloid and Interface Science 2007;305:352.
[5] Kim BM, Cho YK, Yoon SY, Stevens R, Park HC. Mullite whiskers derived from kaolin. Ceramics International 2009;35:579.
[6] Vincent B. The effect of adsorbed polymers on dispersion stability. Advances in Colloid and Interface Science 1974;4:193.

5 High Solids grinding of Calcium Carbonate Slurries

5.1 Introduction

Calcium carbonate is a key product for Imerys, where volumes up to 7.5 Mtpa [1] of marble are quarried and ground to a finer particle size for use, predominantly, in the paper industry, although there are further applications in plastics and paints[2]. The grinding process has been developed within Imerys, and is primarily performed with stirred media mills with a high solids fraction slurry (75 wt.% mineral). Grinding with high solids slurry has benefits with respect to plant efficiency, as the rate of work input is raised, thus improving the overall throughput. By selling the product as a high solids slurry, Imerys vastly reduces the transportation costs (as less water is being transported) and also reduces any de-watering costs for the customer. Full plant grinders are run on a fully continuous basis, with a number of grinders in a cascade, however it is possible to work in a batch process to investigate the process at lab and pilot scale.

5.1.1 Use of lab-scale mills

Small scale grinding equipment remains an important tool for the minerals processing industry, both as a mechanism for new product development, and for analytical purposes within process control. At Imerys, the laboratory scale (2 L chamber) grinder is the key piece of equipment when size reduction below 10 µm is required in the wet phase. Within the New Technology Group, this could be a new mineral, outside of Imerys' portfolio, or

Exploration services may look at a new source of an existing mineral or the Process Development team may be testing new dispersants for improved performance, or cost reduction.

The use of a lab scale mill becomes a more useful tool for a large industrial minerals company, when the scale up to full plant equipment is understood. Through English China Clays (ECC) and now Imerys, this scale up is well understood[3], aided by the fact that the first stirred media mills were developed internally by ECC in the 1960's[3].

Despite the understanding of the scale up, there are some key differences with the grinder at production scale. The larger grinders are operated in a continuous mode, with a bottom screen exit point, as is described in Section 5.3. For the majority of products, the grinder will be part of a cascade, whereby the production will get sequentially finer. The batch process of the laboratory grinder does not emulate this exactly, but by considering the overall energy input, it is possible to compare processes via the total grinding energy.

5.1.2 Variables in a small batch grinding process

The variables in a batch grinding process can be separated into three categories: mill, operating parameters and mineral properties.

5.1.2.1 Mill Properties

The properties of the mill are less likely to be altered over the course of experiments as small alterations at lab scale may entail large changes on the plant, which would subsequently involve large capital expenditure. However, they are still very important to the process:

- Mill chamber geometry: the lab scale mill has a cylindrical chamber allowing for the smoothest flow possible. For the ease of construction and, importantly, the ease of replacing the liner[4], production mills have an octagonal cross section.
- Impeller geometry: the size and shape of the mill impeller has a significant effect on the flow within any stirred vessel[5], and within a grinder the shape and number of impeller arms is important, as well as the clearance between impeller tip and wall. Previous studies have looked at the effect of the shape on the flow patterns [6]. The lab grinder has two orthogonal pairs of short rod-shaped pins.
- Material of construction: choice of mill liner and impeller coatings can affect the flow directly (through e.g. slip conditions), but more importantly have varying wear characteristics. Wear of the mill can lead to product contamination (including loss of brightness) and to increased plant downtime whilst replacements are fitted (having significant associated costs). The lab scale grinder is polyurethane lined to minimise contamination, but production mills are lined with various materials. The Gothers pilot grinder is lined with steel only.

- Grinding media: the variation of grinding media properties is the focus of this work, and will be discussed in greater depth. Key variables are the size, shape, density, hardness and wear resistance.

The tables considered in this experimental program are laid out in Table5-1.

Table 5-1: Variables considered in experimental framework.

Variable	Media Considered
Media Shape	Alodur 92, Carbolite
Media Density	4 commercial spherical media, 5 developed rod shaped media
Motor Speed	Alodur 92, Carbolite

5.1.2.2 Operating Parameters

At the lab scale, with a batch grinding process, most of the operating parameters can be set at the required levels. However, at the production scale, there is less flexibility with many variables, as a result of fixed gear motors and a continuous production method. However, most parameters can be proscribed given flexibility in production:

- Motor speed: lab scale grinders have a variable speed drive, to enable full control up to approximately 1500 rpm. The vast majority of Imerys' production grinders do not have variable speed controllers, although it is possible for them to be retrofitted. Production grinders are typically run at a high motor speed (~1410 rpm) to maximise plant efficiency (*N.B.* this does not necessarily equate to grind

efficiency, which may be achieved at lower speeds, the higher speed increases throughput and thus overall plant efficiency)[3]. The motor is geared to give an impeller speed of 132 rpm typically.

- Media Volume Concentration (MVC): internal work at Imerys[3] has shown a significant optimum in the ratio of media to slurry (based on volume) in a stirred media mill. The curve in optimisation may be specific to a given set of operating parameters. In a batch grinder, the MVC is easily controlled simply by specifying which materials are inputted to the system. However, in a continuous grinder, this is less easily controlled, and much more difficult to measure online.
- Slurry properties: the two key properties of the slurry are the weight fraction of mineral and the rheology (hence dispersion). A well dispersed slurry has a lower viscosity, and as a result improves the flow patterns within the mill. The percentage mineral in the slurry also directly affects the viscosity, but there are further benefits for plant efficiency from maintaining a high slurry density, that is the increased mill throughput. In production, as well as in lab scale work, the calcium carbonate slurry begins the grinding process at 75 wt.% solids, which may rise to 78% with evaporation during processing and any downstream flash evaporation. Assuming good dispersion can be achieved, less water in the final product has further benefits for energy savings in transportation.

5.1.2.3 Mineral properties

An understanding of the mineral properties is crucial to the grinding process. Although many of the parameters listed below are fundamental to the mineral and cannot be altered, but others may be controlled by various pre-treatments:

- Particle size: the final required particle size distribution is dependent on the total energy inputted to the system, as well as the initial particle size. For a given grinding media, there may only be a certain size reduction ratio over which it is practical to operate[7]. In carbonate production, pre-milling with hammer mills gives a sufficiently fine product to be fed to the first stage of a cascade of grinders. These grinders have a progressively finer size distribution of grinding media. Additionally, the size of the particles will have a significant effect on the slurry viscosity and the dispersant requirements.
- Mineral hardness/breakage: many parameters are put forward for a characteristic number relating to particle breakage[8], and although these may be approximations, it is true that a given mineral system will have a specific energy for reduction over the size range given.
- Shape properties: with minerals such as kaolin or talc, which are platy in nature, higher aspect ratios can alter slurry rheology. Furthermore, it is likely that a high aspect ratio is intended to be maintained as well as possible over the progression of the grind, and this affects how the grinder is operated[9].
- Surface chemistry: variations in surface chemistry fundamentally alter the dispersion of the mineral in the slurry, and may require further chemical treatment.

As size is reduced, fresh surfaces are exposed, which can also require treatment in order to maintain good dispersion.

5.1.3 Objectives of this chapter

This work focuses on the role of the grinding media in the efficiency of the processing. With lab scale grinding it is possible to rapidly test a number of grinding media over a range of conditions, and because a relatively small mass of media is required, it is possible to test materials which may be too expensive to trial at pilot scale.

The thrust of the work is the invention of a new grinding media, Alodur rods, which represents a step change in the design of grinding media. The extruded material, discussed in Chapter 4, is rod shaped, rather than being spherical.

The market for grinding media is now increasingly populated with higher price, higher performance materials, rather than the lower price, shorter lifetime materials which have been favoured by Imerys[10]. Therefore, included within this work is an examination into the effect of the media specific density on the grinding performance. This is achieved by using a range of products with as closely matched size distribution as possible (based on product specifications). Within this, it is assumed that by changing the composition, there are no significant effects on the efficiency of size reduction. It is accepted that there will be differences in inherent material properties (elasticity, abrasiveness, wear resistance, etc.), but it is assumed that these will have negligible effect on the size reduction of the mineral.

The effects of these properties on other aspects of mineral specification are important, and their effect on *e.g.* mineral brightness will be considered.

5.2 Lab Results

5.2.1 Energy benefits from Alodur 92

When grinding at milder conditions than is used for emulating the production conditions (70 wt.% slurry rather than 75 wt.%), progressive size reduction with energy input is seen, as shown in Figure 5-1.

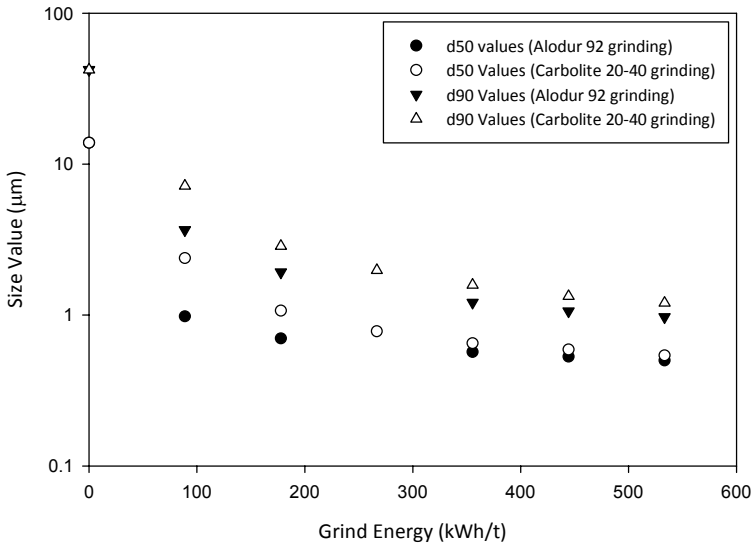

Figure 5-1: Size reduction of Calcium Carbonate samples for the two different media as a function of grind energy. Size measurements are performed by Malvern Mastersizer. Systematic error bars are omitted for clarity, as they are small (< 5%) for all data. Errors from repeat measurements are not made for this exploratory experiment.

Alodur 92 was used as a grinding media in the lab scale grinder over a range of media volume concentrations. As a comparison with existing Imerys technology, Carbolite

spherical media was also used. Existing knowledge within Imerys has shown that the optimum media volume concentration for Carbolite is 52 vol.% media[3], therefore only this ratio is considered, the results are shown in Figure 5-2.

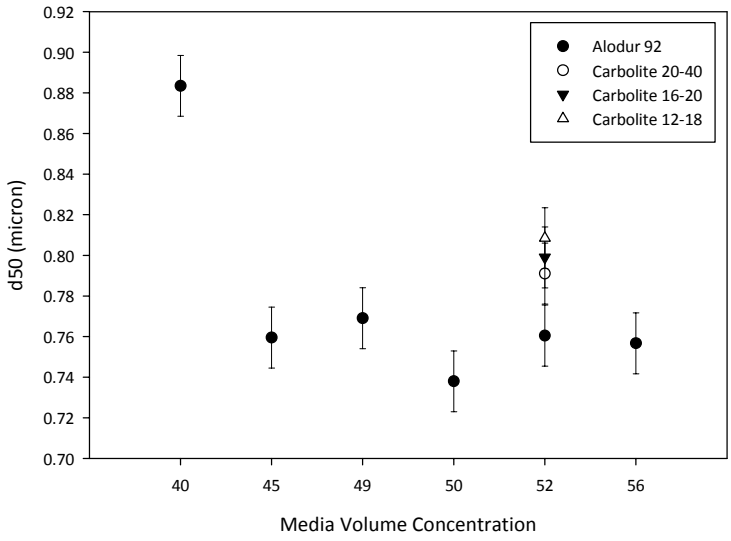

Figure 5-2: d50 of GCC samples ground for 150 kWh/t at 75 wt.% slurry. Sizes measured by Malvern. Error bars are systematic measurement/sampling errors, not from experiment repetition.

It is seen in Figure 5-1 that there can be significant differences in energy efficiency over a long grind depending on the choice of grinding media. The Alodur (rod-shaped) grinding media is seen to reduce the median particle size more rapidly than the Carbolite material, especially in the early stages of grinding. For example, it is seen that to reduce the d_{50} to 1 µm with Carbolite would take approximately 200 kWh/t, whilst with Alodur this would require less than 100 kWh/t. Note that in this initial experiment, a finer grade of Carbolite (20-40#) is used.

The results of Figure 5-2 show the sensitivity of the experiments to the concentration of grinding media in the system. It is seen that not only does the Alodur 92 give a consistently finer d_{50} after 150 kWh/t, this is achieved over the range of media volume concentration from 45 – 56%. This may suggest there would be greater process stability in a full scale plant.

5.2.2 Effect of media density (spheres vs. rods)

The Alodur 92 media has been shown to give a significant energy saving over existing Carbolite media. The results summarised in Table 5-2 show that there are a number of phenomena to consider:

- Considering the Carbolite media; there is an efficiency benefit to be gained from reducing the grinder impeller speed from 1410 rpm down to 600 rpm. Imerys is aware that there are grinding efficiencies possible from the lower speeds. However, production plants are run at the higher speed in order to increase throughput, and thus improve the overall plant efficiency.
- At 600 rpm, it can be seen that increasing the density of spherical media from 2.71 (Carbolite) to 3.60 g/cm^3 (Carbo HSP) improves the grinding efficiency and also reduces the total batch grinding time (due to a higher power draw on the motor). However this particular media has a highly detrimental effect on the final powder brightness (Brightness reduced from 95.0 to 92.1).

- Moving from the Carbo HSP media to the Alodur 92 media, it can be seen that there is a further benefit on the batch grinding efficiency. Furthermore, the batch grinding time has been reduced further, which would allow for a potentially higher throughput within a production cascade, and increase the plant efficiency further still.

Table 5-2: Summary of the effects of separately changing the motor speed, media density and media shape on the grind efficiency. Motor speed is 600 rpm unless otherwise stated, grinds are for 150 kWh/t.

Media	Media Volume Conc'n (%)	Time for 150 kWh/t input (min)	%< 2µm (Sedigraph)	%< 1µm (Sedigraph)	Surface Area (m^2/g)	Bright-ness	Yellow-ness
Alodur 92	51	36	84.0	56.4	11.7	93.8	1.0
	50	37	83.0	55.1	11.0	94.4	1.0
	49	40	78.2	51.9	9.9	93.8	1.1
Carbolite 20-40	51	95	70.8	51.5	8.5	95.0	1.2
Carbo HSP 20-40	52	75	77.1	54.7	9.1	92.1	2.2
Carbolite 20-40 (1410 rpm)	52	22	62.9	40.5	8.0	95.-	1.2

5.2.3 Effect of media density (spheres)

In the previous section, the rod-shaped Alodur 92 media were compared with the spherical Carbolite media. This section will now consider the role of media density on lab scale

grinding efficiency. Therefore a range of spherical media are considered with the same range of diameters (as specified by manufacturers).

Figure 5-3 highlights the relationship between the grinding media physical density and the resulting fineness of the calcium carbonate after grinding, whilst Figure 5-4 highlights the surface area generation over the same experiments.

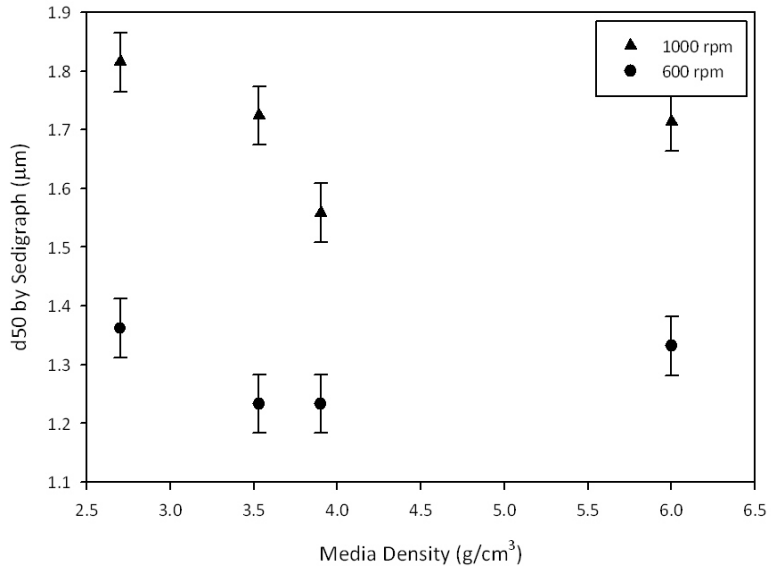

Figure 5-3: Effect of media physical density on the fineness of a ground calcium carbonate after 100 kWh/t of energy input. Error bars are systematic measurement/sampling errors, not from experiment repetition.

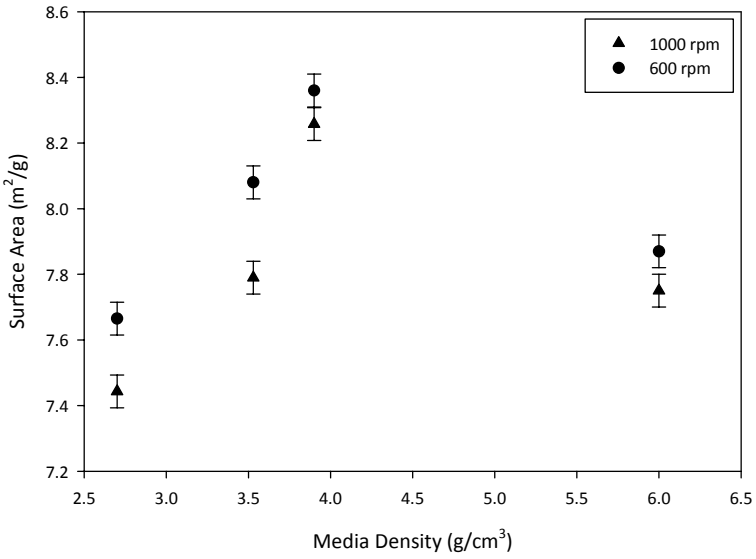

Figure 5-4: Effect of media physical density on the surface area of ground calcium carbonate samples after 100 kWh/t of energy input. Error bars are systematic measurement/sampling errors, not from experiment repetition.

The results for lab scale grinding with a range of grinding media with the same size distribution in each case, shows that there is a significant effect on grinding efficiency with the media density. Broadly, it is seen that the higher density media produces a finer particle size for a given energy input (Figure 5-3 and Figure 5-4). However, there is a consistently anomalous data point in the case of the Silibeads YZ material, with a density of 6.0 g/cm^3. This media does not appear to corroborate the trend of higher density giving a finer particle size distribution. This suggests that there are further effects to consider than simply the media density in this respect. In the grinding process, it may be considered that grinding 'events' are more likely to have the requisite energy to fracture adjacent mineral particles. However, if the shear forces in the interstitial fluid between media particles are the key to grinding, then the effect of surface roughness as well as media density is

significant. The smooth surface of the yttrium-stabilized zirconia media could lead to a weaker shear field between media particles.

Given that there is the same volume of media in each experiment (and media are of approximately equal size in all cases), there are approximately the same number of media particles in the grinder for all experiments. When this is related to some of the theories of stirred media milling, as discussed in Chapter 2, these experiments clearly demonstrate that there is an effect of grinding on the momentum which each media particle has, or its kinetic energy. These factors will be considered alongside the radioactive tracking data in the next section.

The theory discussed in Chapter 2, also considers the frequency of collisions as being beneficial to the grinding efficiency. This is known to have an optimum which is related to the media volume concentration but has not been further considered with respect to spherical media.

5.2.4 Effect of media density (rods)

The rod shaped media formulated at the Imerys Kiln Furniture facility in Lomba, Spain can be tested by the same method as the spherical media. Figure 5-5 highlights the relationship between the d_{50} and the physical density of the media, where it is seen that there is only a weak relationship and large errors in repeatability. Similarly, Figure 5-6

highlights the effect on surface area, and it is again seen that there is a poor relationship. There are large error bars in the results, which may be the effect of an initial deterioration of the rod shape, with corners of the rods breaking apart etc.

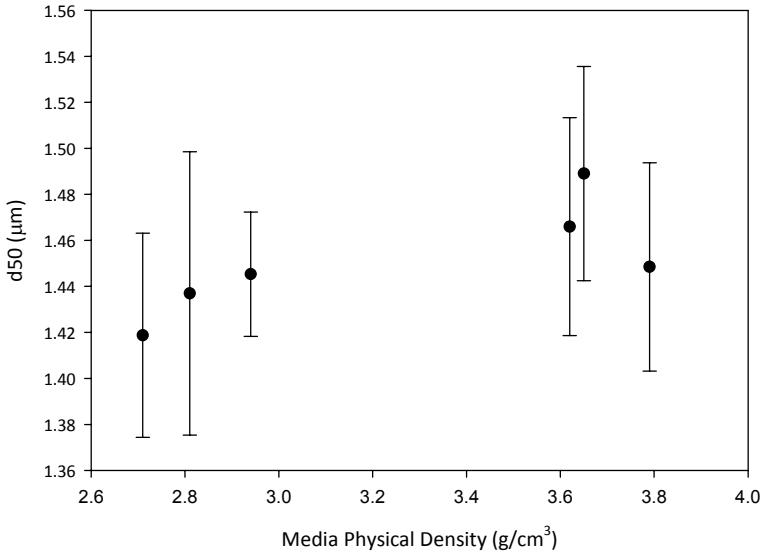

Figure 5-5: Effect of media physical density on the fineness of calcium carbonate ground for 100 kWh/t with rod shaped media. Error bars are two standard deviations of results from three repetitions.

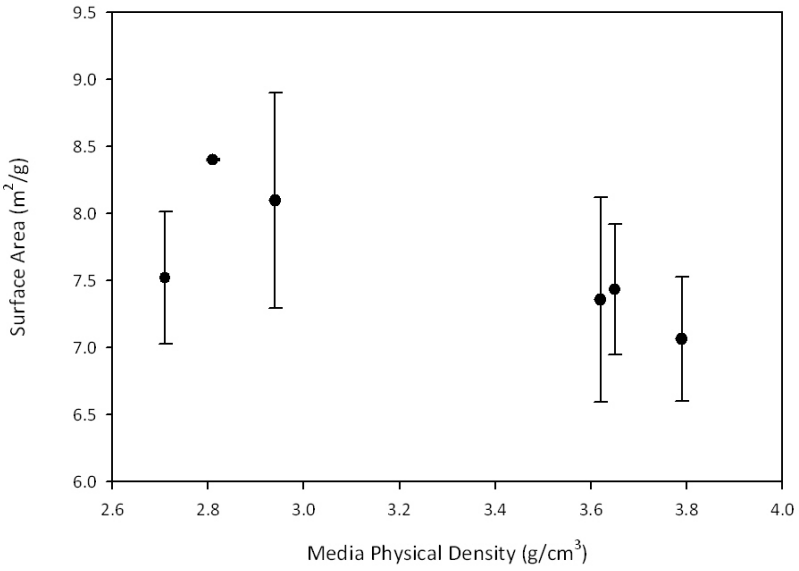

Figure 5-6: Effect of media physical density on the surface area of calcium carbonate ground for 100 kWh/t with rod shaped media. Error bars are 2 standard deviations of results from 3 repetitions (N.B. only one data point available at a density of 2.81 g/cm^3).

Data for the rod shaped grinding media, which are shown in Figure 5-5, show that the effect of density with these media is less significant. This could be due to the fact that the rod length distribution has become prevalent above the density effect, which may be a contrasting and competitive effect alongside the physical density of the material. Furthermore, it may be hypothesised that the difference in efficiency from the rod shaped media is related to the flow patterns within the mill, and that the density is less of a factor in the new regime.

5.2.5 Effect of Motor Speed

The speed of the motor affects the rate of energy input into the system, having concomitant effects on the process efficiency. In Figure 5-7 it is seen that increasing the

motor speed gives a less efficient grind, as there is a larger median particle diameter after 100 kWh/t. This also shows that over the range of motor speeds used, the Alodur 92 gives a more efficient size reduction, except at 600 rpm, where the very close data points show the Carbolite media as slightly more efficient. In Figure 5-8, where the surface area of the final product is considered, there is a similar pattern, except that here there is an anomalous result at 600 rpm, where the surface area is seen to be considerably lower than might be expected given the other data in the series.

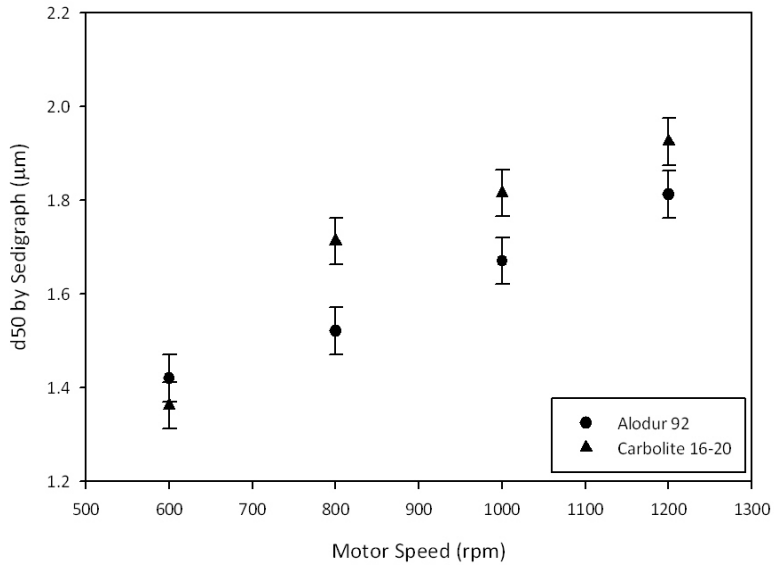

Figure 5-7: Effect of the motor speed on the median particle diameter after 100 kWh/t of grinding. Error bars are systematic measurement errors, not from experiment repetition.

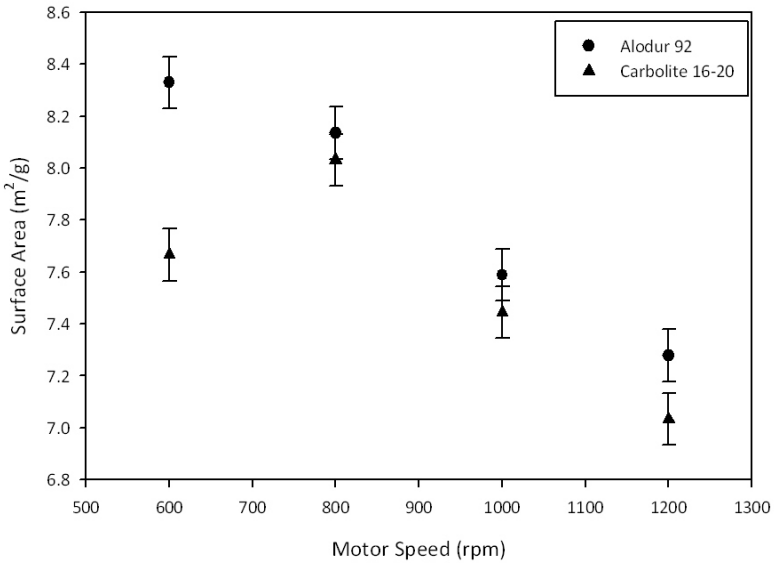

Figure 5-8: Effect of the motor speed on the BET surface area generation after 100 kWh/t of grinding. Error bars are systematic measurement errors, not from experiment repetition.

In Figure 5-7, it is seen that there is a progressive decrease in efficiency when a higher motor speed is used in the grinder. Over the range of motor speeds used in these experiments, there appears to be a linear relationship between factors. However, outside the range which is practical and has been used here, it would be expected that the linear (or near-linear) relationship would break down. At very low motor speed, the system would be unlikely to have the required energy to lead to any breakage, and there would also be very poor mixing in the system, leading to sedimentation of the various materials present. The behaviour at very high speed may not be so clear, although it might be expected that the efficiency continues to decrease until there are practical limitations to the increases (such as the material leaving the chamber). Higher speeds are likely to cause

a move away from the stable flow patterns which are seen over the range used here, and there would be further problems with cavitation etc.

It is also seen in Figure 5-7 and Figure 5-8 that the rod shaped media tend to always give a more efficient size reduction than the spherical control, corroborating observations discussed in Section 5.5.1. However, a lower speed is only more efficient when considering the grind energy. If the control was the total volume of material which achieves the required size reduction in a given period of time, then the effect result may favour higher speeds. For this reason, full scale plants at Imerys use higher motor speed – enabling greater plant throughput, and thus increasing overall plant efficiency. Note that the optimum with respect to financial efficiency is further complicated in relative fluctuations in energy prices, product demand, currency exchange rates etc.

5.3 Pilot Plant Results

5.3.1 Size reduction and surface area generation

The pilot grinder at Gothers Pilot Plant was used as described in Chapter 3, with direct recirculation of the material from the bottom screen into the top of the grinder, via a centrifugal pump. Figure 5-9 shows the increasing fraction of material with particle diameter less than 2 μm throughout the range of specific grinding energies (0-200 kWh/t). It is seen that in order to reach 90% <2 μm, Alodur and Cenotec media require approximately 140 kWh/t, whilst the Carbolite media requires 175 kWh/t.

In Figure 5-10, the increasing surface area of samples taken after progressive energy inputs is shown, where it is seen that with the Alodur 92 grinding media, there is a continuing increase in surface area over the whole range, whereas using the other two media, the surface area heads to a plateau. This plateau appears to be at approximately 11 m^2/g for Carbolite and 13 m^2/g for Cenotec.

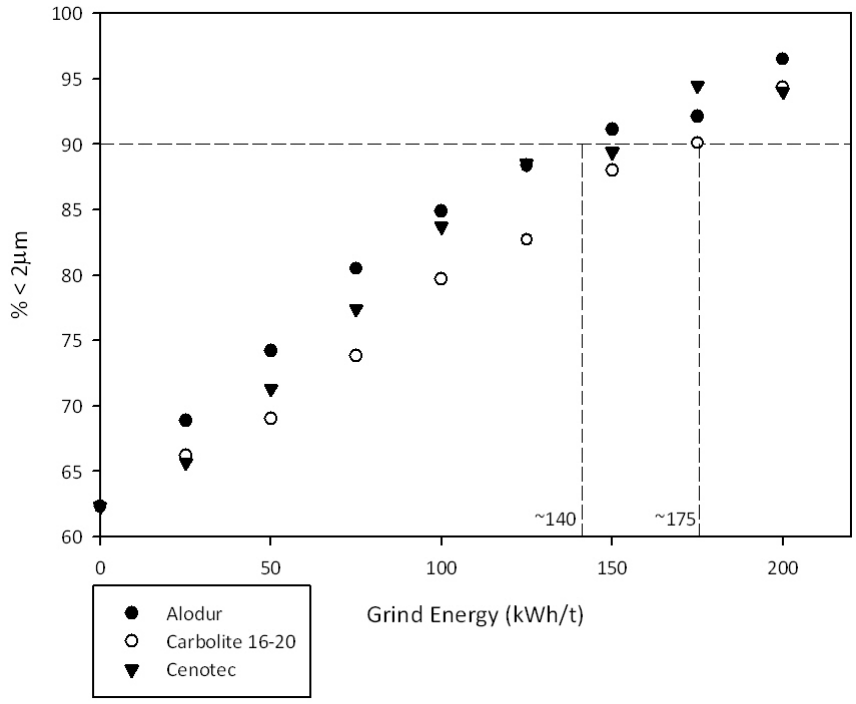

Figure 5-9: Evolution of the percentage of particles with a diameter under 2 µm as measured by Sedigraph. Error bars in size measurement are small (~±0.2%) and omitted for clarity. Errors through repetition of the experiment were not feasible for this scale of experiment.

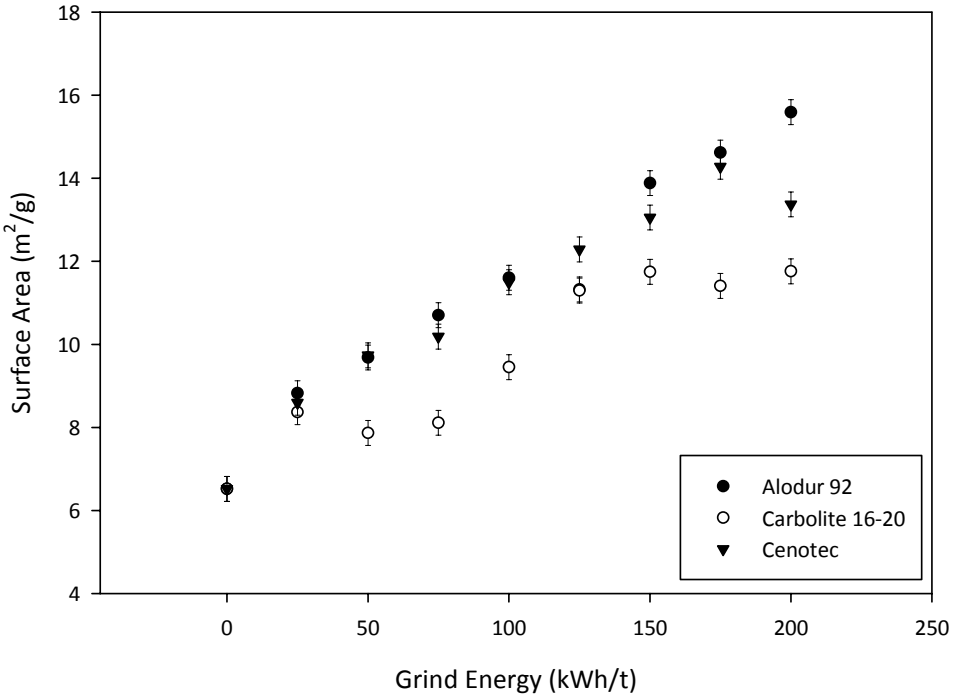

Figure 5-10: Evolution of BET surface area with increasing grind energy. Errors are systematic measurement errors only, as repeating the experiment was infeasible.

5.3.2 Product brightness during grinding

The colour properties of the final product are important specifications for all of Imerys' white minerals. Figure 5-11 shows the progression of the powder brightness with increasing grind energy from the pilot scale trial. It is seen that there is a steady decrease in brightness with Alodur 92 and Cenotec as the grinding media, whereas the decrease is not as pronounced when the Carbolite media was used.

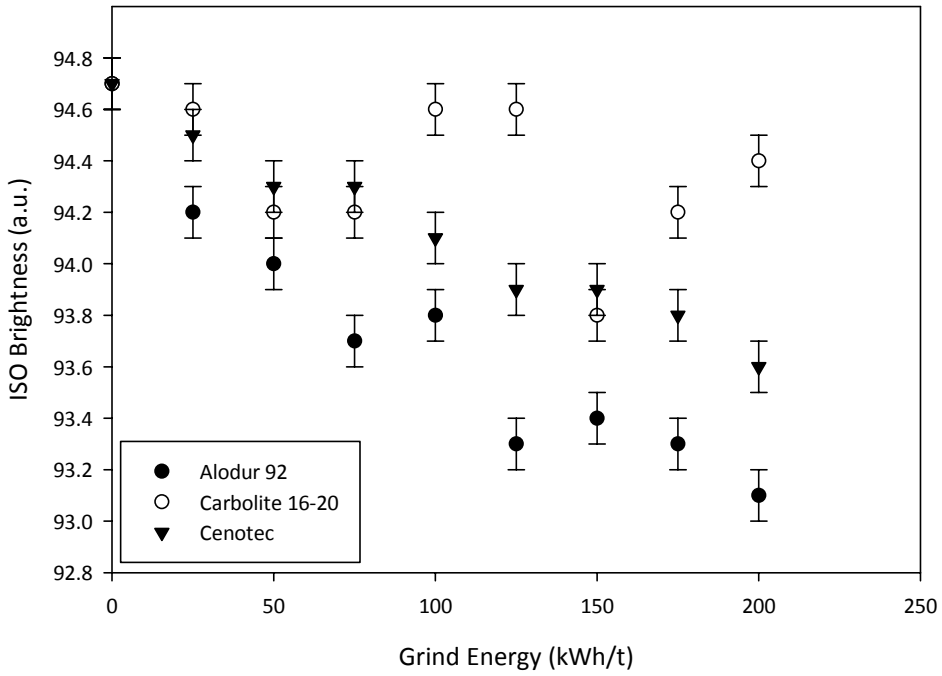

Figure 5-11: Effect of grinding energy on powder brightness from the pilot scale trial, as measured by DataColour. Error bars represent systematic measurement errors, as repeat trials were not feasible.

In Table 5-2, the brightness data are shown for a typical lab scale experiment. The Alodur 92 media is seen to produce a carbonate powder with a lower brightness than that ground with Carbolite media, agreeing with the pilot scale results. There is too much loss of brightness with the Alodur grinding media to meet Imerys' product specification. However, the rod shaped media which were made at Imerys Kiln Furniture, Lomba, Spain (see Chapter 4), give improved powder brightness for the carbonate, as seen in Figure 5-12.

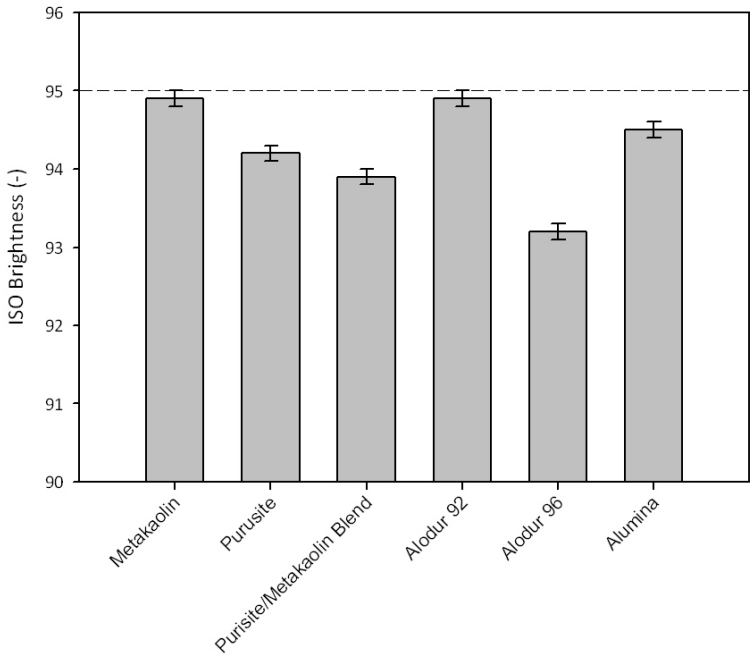

Figure 5-12: Brightness results of the carbonate ground with various rod shaped media after 100 kWh/t. Error bars are the known values from the Imerys Brightness test method.

The Alodur 92 media, which has been used with the pilot scale grinder at the pilot plant, has a dark colour (see Table 5-3). Abrasion of the grinding media is likely to contribute to the progressive colour reduction of the final powder, as is seen in Figure 5-11. In this Figure, it is also seen that the white Cenotec media also contributes to a reduction of the powder brightness. It is possible that the Cenotec spheres are breaking down into large enough pieces to cause scattering of the light during brightness measurement and reducing the perceived colour. It is also possible, with both the Cenotec and the Alodur rods that the media are contributing to the abrasion of the steel lining of the mill, which is consequently contaminating the product.

5.4 Media Wear Examination

The economics of a grinding media are driven not only by the efficiency in particle size reduction (and other properties of the product), but also through the lifespan of the media itself. Table 5-3 gives progressive microscopy images of the Alodur 92 media over the first 320 kWh/t of its lifespan. There is evidence of some surface smoothing and of the corners of the cylinders being rounded by the grinding process.

Table 5-3: Optical microscopy images of the media after progressive amounts of grind energy up to 320 kWh/t. In all images, the field of view is 5 mm. Any apparent change of colour is likely an artefact of changes in the lighting on the microscope.

 Fresh Media	 32 kWh/t
 100 kWh/t	 320 kWh/t

For the quantification of the wear rate of the grinding media, the water rinse experiment can be conducted on the laboratory grinder adjusted to have a top-screen. The media is

fed with a continuous supply of clean water in the grinder, which overflows through the top screens and is collected in a large tank where it is allowed to sediment over several days. The excess water is then removed, and the remaining sediment can be weighed and analysed. Then amount of material collected after successive phases of the rinse-grinding are shown in Table 5-4.

Table 5-4: Summary of the wear values for Carbolite and Alodur 92 in the rinse-grinding experiment.

	Alodur 92						Carbolite 16-20				
	Day 1	Day 2	Day 3	Day 4	Day 5		Day 1	Day 2	Day 3	Day 4	Day 5
Weight collected (g)	35	30	22	28.9	18.9		21	12	5.6	5.6	3.6
Wt. Per kilo media (g/kg)	2.33	2.00	1.47	1.93	1.26		1.75	1.00	0.47	0.47	0.30
Energy Input (Wh)	1100	1100	1100	1200	1050		1100	1500	1050	1200	1000
Wt.Res per kilo media per kWh (g/(kg.kWh))	**2.12**	**1.82**	**1.33**	**1.61**	**1.20**		**1.59**	**0.67**	**0.44**	**0.39**	**0.30**
Cumulative Energy Input (Wh)	1100	2200	3300	4500	5550		1100	2600	3650	4850	5850
Cumulative Mass Collected (g)	35	65	87	115.9	134.8		21	33	38.6	44.2	47.8
Cumulative % loss	**0.233**	**0.433**	**0.580**	**0.773**	**0.899**		**0.175**	**0.275**	**0.322**	**0.368**	**0.398**

The material which is collected is examined in the Scanning Electron Microscope to help the understanding of the form of the material which is eroding. These images are shown in Figure 5-13.

Figure 5-13: SEM images of the rinse residue material from the rinse-wear experiments

Alodur 92 Residue	Carbolite 16-20 Residue
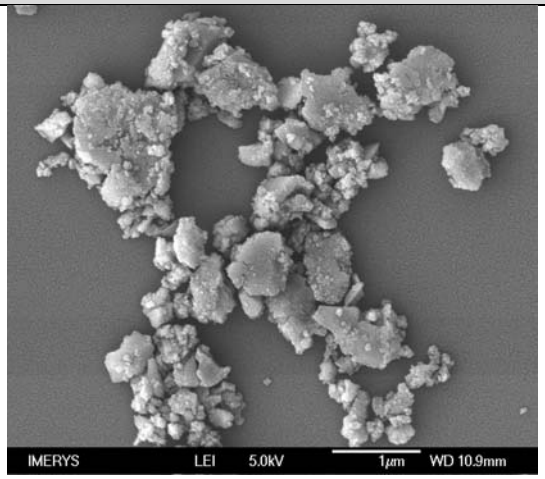	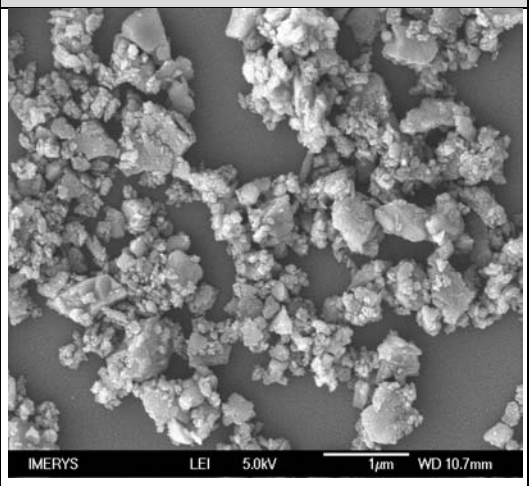

5.4.1 Acid Insoluble Residue (AIR) analysis

Final samples from the pilot scale grinds (as well as the feed carbonate) were analysed for their acid insoluble residue (AIR). Table 5-5 highlights the compositions of the dried slurries for the key species present (CO_2 is lost during the process, which would constitute the remaining weight). It can be seen that the AIR and iron content is higher with the Alodur residue, whilst the Cenotec (zirconium silicate) media gives a relatively large presence of zircon in the product. This must be the result of wear of the zirconium silicate media into the product.

The information given in Table 5-5 suggests that the Alodur grinding media has broken down into the product more than the other media, as there is a significantly higher acid insoluble residue. The higher iron content of the carbonate slurry ground by Alodur 92 affirms this, as it has been seen previously that the Alodur 92 has relatively high iron content (see Chapter 4, Section 4.2.3).

The Cenotec, zirconium silicate, media is seen to produce a carbonate product which has higher zircon content, again suggesting some contamination into the product from the media. All three grinding media are seen to somewhat increase the iron and chromium content of the carbonate slurry, and these materials could be a contaminant arising from the abrasion of the steel lining of the mill and pipe work.

Table 5-5: Summary of the chemical analyses of the feed slurry, as well as the final slurry after grinding to 200 kWh/t with the various media.

Sample	CaO (wt.%)	MgO (wt.%)	Fe_2O_3 (wt.%)	AIR (wt.%)	Cr (ppm)	Zr (ppm)
Carbital 60 (Feed)	54.4	1.1	0.013	0.27	<0.5	1.2
Alodur 92 (ground $CaCO_3$)	54.0	1.0	0.024	0.35	7.3	1.2
Carbolite (ground $CaCO_3$)	54.0	1.0	0.017	0.27	6.1	2.1
Cenotec (ground $CaCO_3$)	54.5	1.0	0.018	0.27	9.7	16.4

5.5 Discussion

5.5.1 Efficiency Benefits of Alodur 92

The benefits of the energy savings can be seen if it is considered how much energy would be required on the pilot scale grinder, to produce the Carbital 90 grade of material, which is Imerys' ground calcium carbonate grade with the (approximate) specification that 90% of the material is under 2 µm (as measured by Sedigraph). Reading from Figure 5-9, taking a reference line at 90% <2 µm, it can be seen that the Cenotec and Alodur media would

both require approximately 140 kWh/t, whilst the Carbolite would require 175 kWh/t. Now a saving of 35 kWh/t represents a significant benefit to the company. At the time of writing, energy costs are around 10 p per kWh in the UK, and a saving of £3.50 per tonne would represent a substantial industrial advantage.

The Alodur 92 media also offers a higher power draw than is seen with the Carbolite media, and indeed the equivalent density spherical media (Carbo HSP). This can be attributed to the different shape of the media particles leading to different flow patterns, a subject for analysis in the next chapter. This appears advantageous in reducing the batch grinding time at a lower speed. However, this means that the Alodur 92 media cannot be used at high speeds (1410 rpm) in the small laboratory grinder as the motor is unable to provide sufficient torque. With the pilot scale work, even with the added mass of media, the grinder is capable at operating at the standard speed, and the grinding is still seen to be more efficient. It is not clear at this stage whether the Alodur 92 media would be usable within a production facility, as these grinders typically operated near to their maximum available power, and may not be able to accommodate the extra power requirement of the Alodur 92 media if it is added on an equivalent volume basis to Carbolite media.

5.5.2 Wear Rates of the media

The media wear rates which are summarised in Table 5-4 show that the wear rate for the Alodur 92 media is worse than for Carbolite media – after 5550 Wh of grinding, the Alodur has worn by 0.9 wt.% compared to on 0.4 wt.% with the Carbolite. Obviously this has

serious ramifications for the economics of this particular recipe of grinding media, however, that calculation is beyond the scope of this discussion, as the relative costs of the media are not yet determined.

However, the problem with wear is not simply the rate of media loss, but also the ramifications on the final product. Downstream from the grinder cascade is a centrifuge for removing large contaminants, as well as an air flotation system to remove some larger hydrophobic material. Ultrafine (< 1 μm) material may be acceptable in the product, depending on their effect on product abrasiveness and brightness. In Figure 5-13 it is seen that the residue from abrasion is a fine material, and so the particles should be removed through the downstream separation processes, or else acceptable as a small contaminant in the product.

In Table 5-5, the chemical analysis of the carbonate slurry is shown, in order to ascertain whether there is a significant contribution of contamination. The Acid Insoluble Residue (AIR) is seen to be quite consistent for all media, except for the Alodur 92 media, where it is 0.35 wt.% compared to 0.27 % with the other media. To clarify whether there is contamination from wear of the stainless steel lining of the mill, the amount of iron oxide and chromium is also given. Again it is seen that there are higher iron levels with the carbonate samples ground with the Alodur media, although it is not clear whether this is due to contamination from the mill liner, or from the iron present in the media. The

carbonate sample ground with zirconium silicate media is seen to have higher levels of zircon present, as might be expected.

5.6 Conclusions

This work has shown that there are considerable energy savings available to Imerys in the stirred media milling process, without significant capital expenditure. Although already known to the company, results are shown which demonstrate that there are significant energy savings to be made through varying the motor speed. However, it is understood that this would have ramifications for plant throughput, and hence overall process financial efficiency.

Of greater importance within this work is the role which the grinding media plays in process efficiency. It is seen that with spherical media of the same size, there are some significant changes which can be made to the process efficiency, especially using the Magotteux MT1 or Cenotec zirconium silicate media. However, the effect of density is not the only change between the media, as it is seen that the high density (6.0 g/cm^3) yttria-stabilized zirconia media does not provide the high efficiency in these experiments which might be expected.

Rod shaped media are seen to give improvements in process efficiency above and beyond their increased density. This is seen both in the laboratory mill and the pilot scale grinder.

The Alodur 92 media matches the performance of Cenotec media, which has a significantly higher density. The media also causes a higher power draw, which enables the grinders to be run at a higher throughput, which could have further process efficiencies. This could also allow the plant to be run at a lower speed, which would bring further efficiencies as seen in Figure 5-7.

However, in order for this technology to be taken forward by Imerys, there must be an improvement in the product brightness, which is also related to the media wear. The use of rod shaped media with a different recipe has been demonstrated in the lab, and it is seen that the efficiency benefits of the Alodur 92 media are maintained, whilst the original brightness of the mineral feed is maintained. At this stage, there has been insufficient of these samples to use them for pilot scale testing, where the efficiency benefits would hopefully be corroborated.

5.7 References

[1] O'Driscoll M. A bright carbonate future. Industrial Minerals. London, 2007. p.24.
[2] Harben PW. Industrial Minerals Handybook: A Guide to markets, specifications and prices: Metal Bulletin PLC, 2002.
[3] Falcon-Steward HR. A Review of the technology of ultrafine wet grinding in agitated media mills. Imerys Internal Research Report, 1989.
[4] Jens K. H. Lichter GD. Selection and sizing of ultrafine and stirred grinding mills In: A.L. Mular DNH, D.J. Barratt, editor. Minerals Processing Plant Design, Practice, and Control, vol. 1. SME, 2002. p.783.
[5] Asquith JP. The Unit Process of Mixing. North Western Branch of the Institute of Chemical Engineers. Manchester: IChemE, 1945.
[6] Conway-Baker J, Barley RW, Williams RA, Jia X, Kostuch J, McLoughlin B, Parker DJ. Measurement of the motion of grinding media in a vertically stirred mill using positron emission particle tracking (PEPT). Minerals Engineering 2002;15:53.

[7] Muller F. Parameters influencing generation of steep particle size distributions in stirred media mills - stata of knowledge and research. In: Kwade A, editor. Grinding and Dispersing with Stirred Media Mills. Braunschweig, Germany: iPat, 2007.
[8] Deniz V, Ozdag H. A new approach to Bond grindability and work index: dynamic elastic parameters. Minerals Engineering 2003;16:211.
[9] S. Behl SN, M.J. Willis, J.P. Berberich. Delaminated Kaolin pigments, their preparation and use in paper filling applications. In: USPTO, editor. USA: Engelhard Corporation, 1995.
[10] Gale Graves BF. Evolution of Ceramic Grinding Media. Industrial Minerals: IM, 2007.

6 POSITRON EMISSION PARTICLE TRACKING IN A LAB STIRRED MEDIA MILL

6.1 Introduction

Throughout Chapter 5, there was an in depth investigation into the role of grinding media for wet stirred media milling of calcium carbonate. That chapter investigated the effect of media density, shape, and to some extent size, through measuring the final properties of the slurry after grinding. In this chapter, the role of the grinding media is further investigated, however, the stirred media mill is no longer considered a 'black box' and instead the dynamics of flow within it are investigated with a view to further understand the effect of the media.

Positron Emission Particle Tracking (PEPT) (see Chapter 3), has been developed within the University of Birmingham as a unique method for the investigation of particle motion within a system which may be optically opaque[1]. By directly irradiating a single grinding media particle it is possible to track its position in real time. Therefore PEPT lends itself well to studying the role of grinding media in the stirred media mill.

6.1.1 Scope

PEPT has been used in this application before, by Conway-Baker *et al.*[2, 3] and the role of rotational speed and impeller design were investigated, resulting in a range of visual

images of the flow directions and mass distributions. The analysis of the PEPT data in this case was completed using the *Track* software developed by Parker *et al.* within the Dept. of Nuclear Physics at the University of Birmingham[4].

The present work focuses on the effect of density and shape of the grinding media, in order to help understand the results of Chapter 5. Additionally, the effect of motor speed on measured parameters is discussed. Instead of the *Track* software, separate data analysis routines are used, some of which are based on previous work within the Department of Chemical Engineering at Birmingham[5, 6] and are modified to fit the geometries of this work. Other routines in MatLab are developed especially for this work. All relevant analysis code is given in the Appendices.

6.2 Analytical Process

6.2.1 Experimental Configurations

Table 6-1 summarises all configurations that are discussed in this work. The range of media densities covers the standard feasible range of materials which are currently marketed.

Table 6-1: Summary of the experimental configurations used in the PEPT work.

Media Name	Principle composition	Specific gravity (g/cm^3)	Diameter (mm)	Shape	Motor speeds used (rpm)
Carbolite 16-20	Mullite	2.71	0.85-1.2	Spherical	600, 800, 1000, 1200
Carbo HSP	Sintered bauxite	3.52	0.85-1.2	Spherical	600, 1000
Magotteaux MT1	Zircon	3.90	1.0-1.2	Spherical	600, 1000
Silibeads YZ	Yttria stabilized zirconia	6.00	1.0-1.2	Spherical	600, 1000
Alodur 92	Alumina (92%)	3.63	0.85 (X-sect)	<3 mm rods	600, 800, 1000, 1200

6.2.2 Data Preparation

As the size reduction of the slurry is not explicitly being considered in this work, there is no need to run the experiments for prolonged periods of time. Upon start up, sufficient time (at least 1 min) is given to allow for mixing and a steady state flow to be achieved. Then for each condition, the process is allowed to run for 10 min, in order to collect sufficient data for good time averaging of the particle location and velocity around the mill. Whenever, the conditions are changed, 1 min is allowed for transient effects before the PEPT data is gathered for the new condition.

During data collection, the live positional data is followed to ensure that the media particle is never stuck and stationery within the system; due to, for example, being trapped in a dry cake of material against the chamber wall, or entrapped between impeller and shaft. This check is verified by examining all the position data in the *Track* software for large periods

of stagnation. In this work, there was never any evidence of the tracking particle getting stuck in this way.

The next stage of data processing is to remove noise from the system. A simple filter developed by Chiti [5] is used here, *filtra.m*, which first plots a histogram of the distances between consecutive locations, and allows a maximum step to be defined by the user. If the data exceed this limit, then the relevant data points are removed as noise.

With high impeller tip speed (1200 rpm ≈ 6 m/s here), it can be necessary to interpolate between consecutive positional data. The representation in Figure 6-1, demonstrates how a particular cell can be missed when the particle is moving at high speed. This is due to the data collection rate of the PEPT camera being largely independent of particle speed. The algorithm developed by Chiti [5] checks if consecutive data points are separated by a distance greater than the cell dimension, a linear interpolation adds a further data point to the corresponding cells.

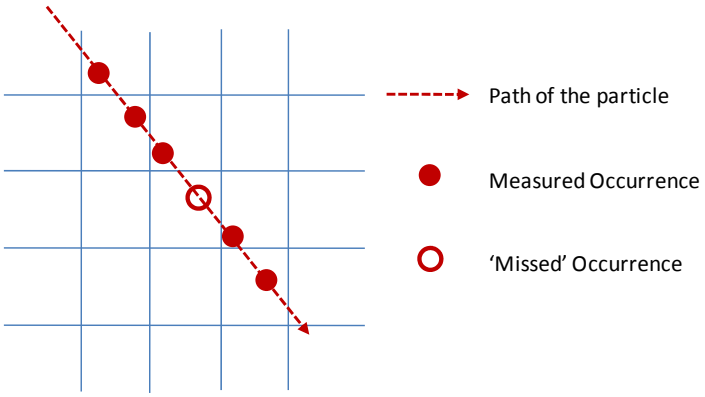

Figure 6-1: Representation of requirement for data interpolation at high speeds.

6.2.3 Data Representation

After filtering and removing noise from the data, it is possible to visualise the properties of the flow inside the mill. The data is displayed as a vertical slice through the mill, and it is assumed that there is good radial symmetry. Figure 6-2 represents the plane through the chamber which the images generated represent. Throughout the analysis, the cylindrical polar coordinate system is used as is appropriate to this system. Instead of breaking down the space into units of equal two-dimensional area; the cells are based on an equivalent three-dimensional volume. Therefore, cells appear larger closer to the impeller, and smaller adjacent to the chamber wall.

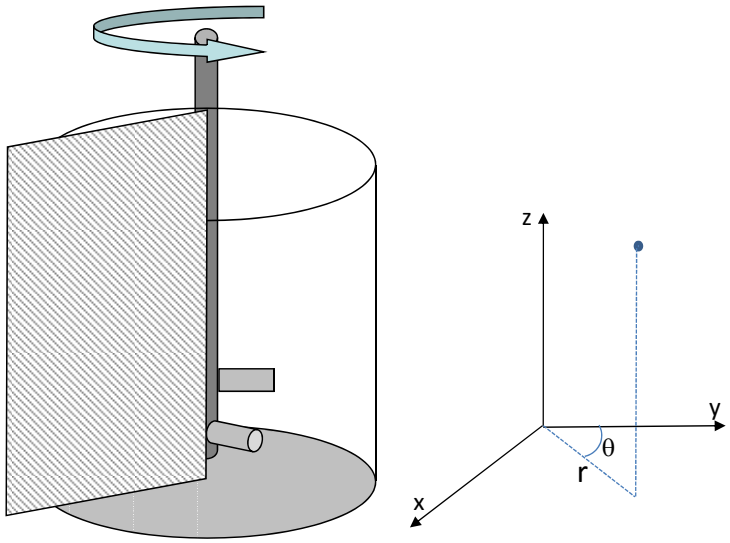

Figure 6-2: Representation of the radial slice which can then be integrated about the axis to visualise flow within the chamber. Radial symmetry is assumed. The cylindrical coordinate system is also given for reference.

6.2.4 Measurable Parameters of the flow field

A number of parameters of the flow can be visually displayed:

- **Occupancy** – this is given as the fraction of time spent in each pixel of the flow field. Therefore, the sum of the occupancy for a given system is 100%. By assuming a good time averaging of the system, the occupancy of a pixel also gives a measure of the relative weight of a given cell.
- **Velocity –** the three components of velocity in cylindrical polar coordinates can be individually determined. This allows areas of high and low velocity to be determined, and by considering only radial and vertical components of velocity, it is also possible to see circulation patterns within the mill. By considering the magnitude of the complete velocity vector, a dimensionless velocity, V*, can be derived, based on the tip speed of the impeller. This allows a measure of the efficiency of the impeller in transferring momentum to the media particles.
- **Kinetic Energy –** By considering the occupancy as representing a mass distribution and combining it with the square of the magnitude of the velocity vector, a representation of the kinetic energy in the system is achieved. This is modified proportionately to the mass of material in the grinder (which depends on the media density). The result is a distribution function for the kinetic energy in the grinder, which has arbitrary units, but gives a good representation of where the areas of high energy are in the system.
- **Bed Height –** The level of the bed within the grinder is vitally important to a number of processing scenarios, as well as signifying a difference in the flow

patterns in the mill. For each experimental arrangement the height of the bed can be measured from the recorded PEPT data as the range of the z-values.

- **Time in Lower Region –** The lower region of the chamber is defined by the horizontal plane mapped by the uppermost edge of the upper impeller. The time spent in this region may be considered to relate to the time nearer to the impellers, and therefore time spent here could be related to the grind efficiency.

6.3 Results

For the purposes of flow visualisation a first approach is made to track the location of the particle within the mill with time. The resulting video (*see compact disc attached to this document, file: 'PEPT Video.wmv'*) demonstrates the location of the tracked particle with time, as well as displaying a 'tail' which includes the previous 30 locations of the tracer. Therefore, there is a good representation of the motion of the particle, and it can be seen that it moves up smoothly and quite slowly alongside the wall of the mill chamber, whilst falling rapidly and somewhat chaotically through the central vortex.

6.3.1 Poincaré Plots

By examining horizontal planes within the bed at different heights, (z), it is possible to examine where the tracked particle is moving up and down. This in turns helps to visualise the areas where the flow is more chaotic and changing with time, as well as those areas

where the flow is more consistent over time. These images shown in Table 6-2 highlight a number of points:

- In both cases, at z=40 there is chaotic behaviour and lots of mixing. This is seen by the apparently random mixture of vertically up and down occurrences. This is close to the position of the impellers. As well as direction being random, this area has the largest number of occurrences.
- In the upper regions (z=80), there is greater segregation of the flow, with material moving up near the circumference of the chamber, and down closer to the centre. This behaviour is very well established, and there are no cases of the particle moving in an unexpected direction at either the centre or the circumference.
- At z = 20, there are fewer occurrences than with z = 40, however, there is evidence of some segregation. Unlike at z = 80, the material is moving down at the circumference here, and up in the centre. There are significantly more occurrences at z=60,80,100 with Alodur than with the spherical Carbolite media.

Table 6-2: Poincaré plots for rod shaped and spherical media showing vertically up (red) and down (blue) movements through the selected planes. Each dot represents a single pass through the given plane. Data cover the experiment duration.

z = Height above the base (mm)	Alodur 92 at 1000 rpm	Carbolite 16-20 at 1000 rpm
20	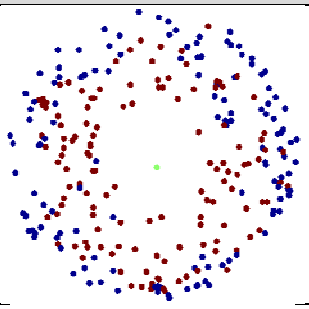	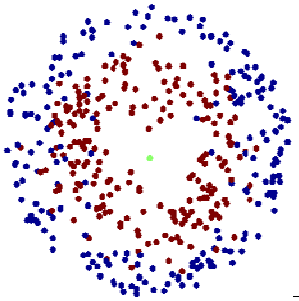
40	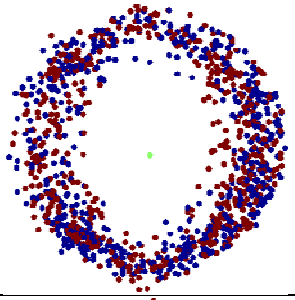	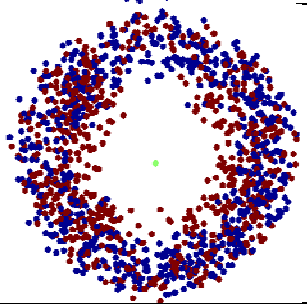
60	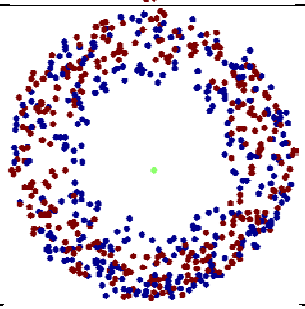	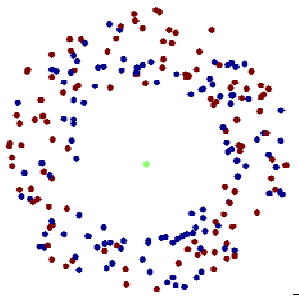
80	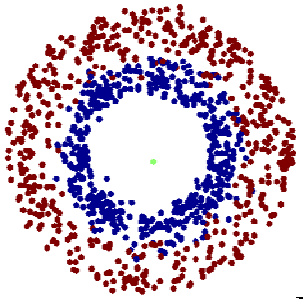	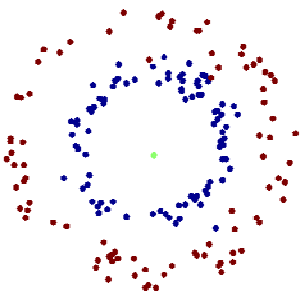
100	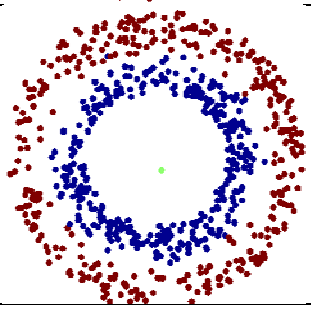	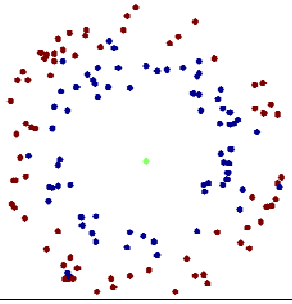

6.3.2 Carbolite 16-20 and Alodur 92 – Flow Representations

To demonstrate the various images which can be generated by the PEPT camera, the range of parameters discussed in Section 6.2.4 are shown for both Alodur 92 media and Carbolite 16-20 media in full, at 600 rpm. Figure 6-3 shows the occupancy distribution for the two flows, where it can be seen that there is a more even distribution of the material with the Alodur 92 media, which may entail greater levels of circulation, a theory reinforced by the recirculation patterns seen in Figure 6-4. The components of the velocity can be separately examined also; Figure 6-5 compares the vertical components of the velocity where it can again be seen that there are stronger recirculation patterns with the Alodur 92 media. Figure 6-6 highlights the transmission of the angular component of velocity from the impeller to the rest of the mill chamber. Given that the motor speed of 600 rpm corresponds to a tip speed of 3.1 m/s, it is clear that there is a region close to the impeller where the media is moving close to the speed of the impeller. It is also clear in Figure 6-6 that this region is significantly larger with the Alodur 92 media than with the Carbolite 16-20 media. This may suggest that the rod shaped media results in better transmission of velocity from the impeller to the media.

Figure 6-7 demonstrates the field of kinetic energy within the mill. As might be expected, this is focussed about the impeller region of the mill. Again it is seen that the high energy region close to the impeller is both larger and of higher energy with the Alodur 92 media compared to the Carbolite media.

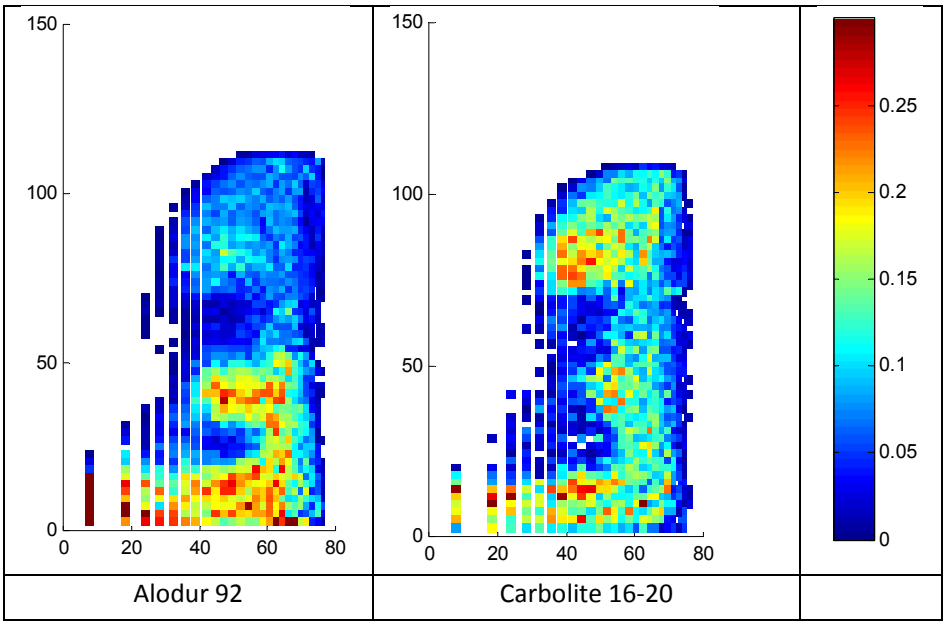

Figure 6-3: Time normalised occupancy data for Alodur and Carbolite 16-20 media at 600 rpm. Scale bar represents percentage time in each cell.

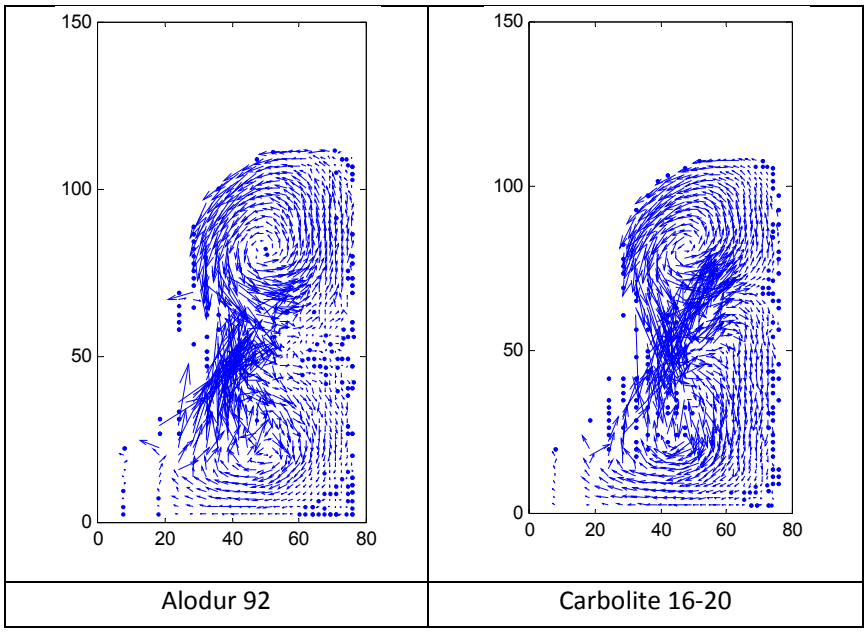

Figure 6-4: Vector Plots for the motion of the particle in the r-z plane at motor speed 600 rpm.

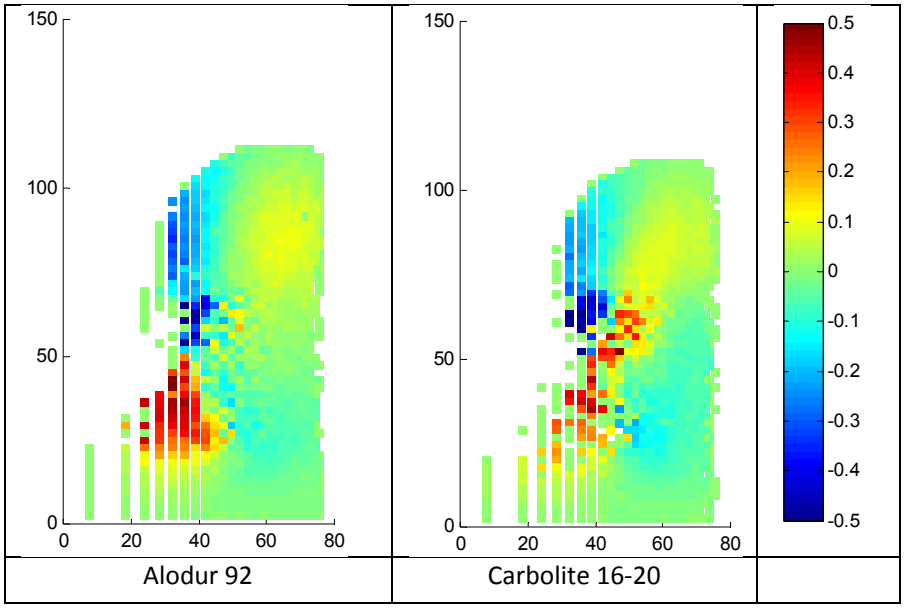

Figure 6-5: Vertical component of velocity for both media at 600 rpm. Scale bar gives speed in m/s, up positive numbers correspond to upward movement.

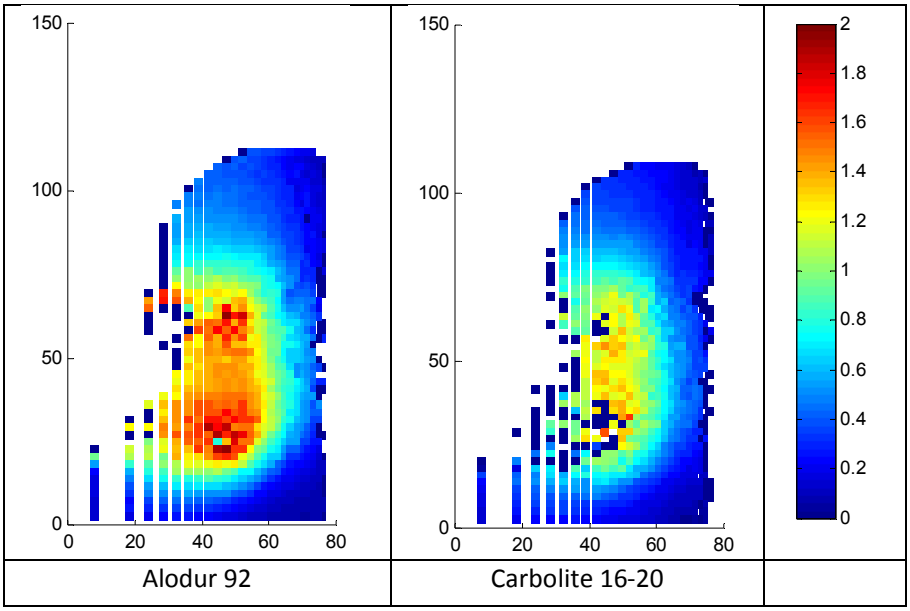

Figure 6-6: Angular Velocity map of the flow field for Alodur 92 and Carbolite 16-20 media at 600 rpm. Scale bar show speeds in m/s.

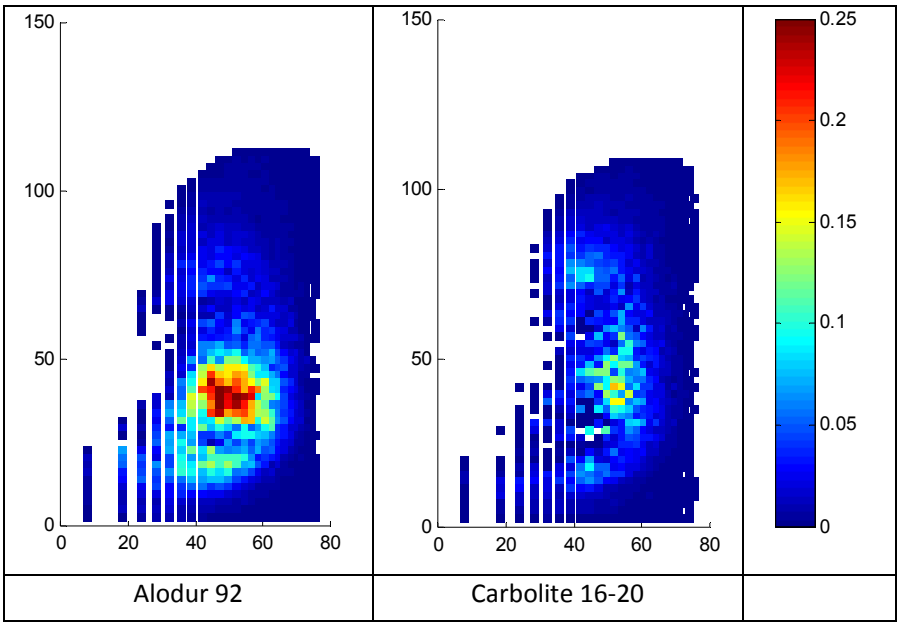

Figure 6-7: Kinetic Energy map of the flow field for both media at 600 rpm. Units are arbitrary yet consistent.

The flow images shown first highlight the use of PEPT to demonstrate the flow of media within the stirred media mill. The various figures, also demonstrate that there are some differences between the flow characteristics of the mill with Alodur 92 and Carbolite media. Of course these effects can be attributed to either the density of the media or the different shape of the Alodur media.

In Figure 6-3, where the different occupancy plots are shown, it is clear that the tracked particle does not spend time in all areas equally. In this example, there is evidence that more time is spent in the lower regions of the flow field with the Alodur media compared to Carbolite media. It is possible that by spending more time in this lower region, closer to the impellers, where there are higher velocities, there would be a positive impact on grinder efficiency.

The vector plots shown in Figure 6-4 do not display any obvious discrepancies between the two media, but give an excellent understanding of the motion within the mill. In both cases, there are clear indications of two re-circulating loops, both above and below the top level of the impeller. It can also be seen that there is a region of much higher velocity in the immediate vicinity of the impellers, as would be expected. In the impeller region, the flow is much more chaotic, and the clear circulation loops are not seen. Figure 6-5 and Figure 6-6 corroborate this, showing that the motion in this region can be many times greater than in the top region of the chamber – up to an order of magnitude higher.

6.3.3 Effect of Motor Speed and Media Shape

Carbolite 16-20 and Alodur 92 media are both analysed at a range of motor speed. Therefore, by considering the measured parameters over this range, it is possible to simultaneously consider the effect of the motor speed and compare the differences in flow with the rod shaped media. Table 6-3 summarises the effect of the speed on the occupancy plots for the positional data of the tracked media particle.

Table 6-3: Effect of motor speed on the occupancy plots. Scale bar units are % of total time.

Motor Speed (rpm)	600	800	1000	1200
Alodur 92	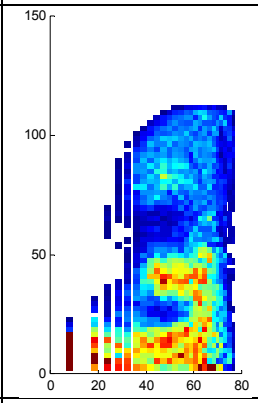	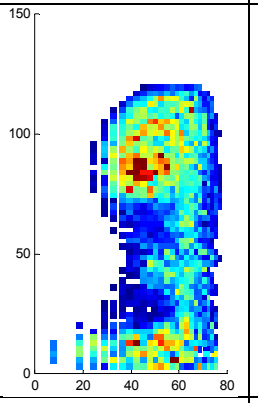	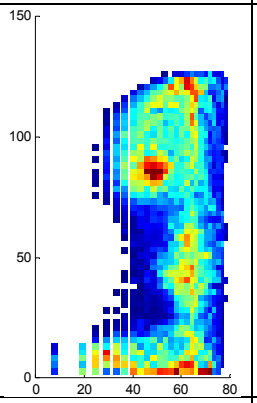	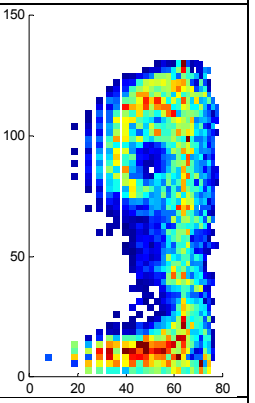
Carbo-lite 16-20	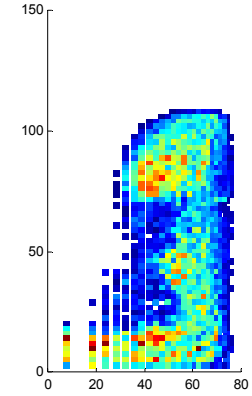	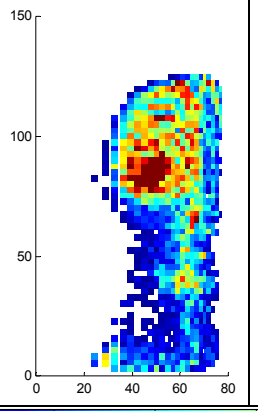	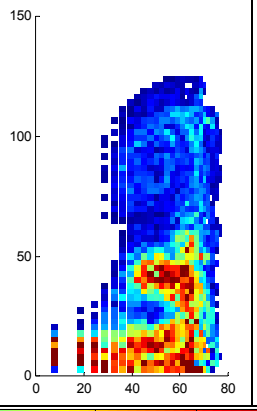	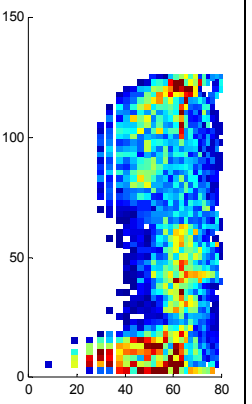
	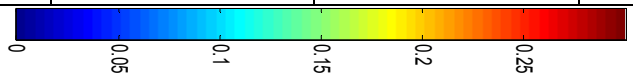			

The occupancy plots shown in Table 6-3 show that there is a change in the occupancy distribution between motor speed and between the two shapes of media. There are two examples (Alodur media at 600 rpm and Carbolite media at 1000 rpm) where there is a much larger amount of time spent in the lower region of the chamber, an observation reinforced by the data in Figure 6-9. As has been discussed in the data analysis section (Section 6.2), long periods of the particle being stationary have been removed from consideration. However, it is possible that there is an issue with the mobility of the particle

from the lower to the upper region. The vector plots shown in Figure 6-4 indicate that movement from the lower section (z < 75 mm) to the upper region of the chamber only occurs in the chaotic region of the impeller.

6.3.3.1 Bed height and time in lower region

In Figure 6-8 it can be seen that with both the Alodur 92 and the Carbolite media, there is an increase in bed height above 600 rpm. The Alodur media is seen to continue to increase in height above this level, whilst the Carbolite media does not appear to exceed 125 mm. In Figure 6-9 it is seen that with the Alodur media, the time in the lower region reduces to a steady plateau, whilst with Carbolite media there is no discernable relationship with the motor speed.

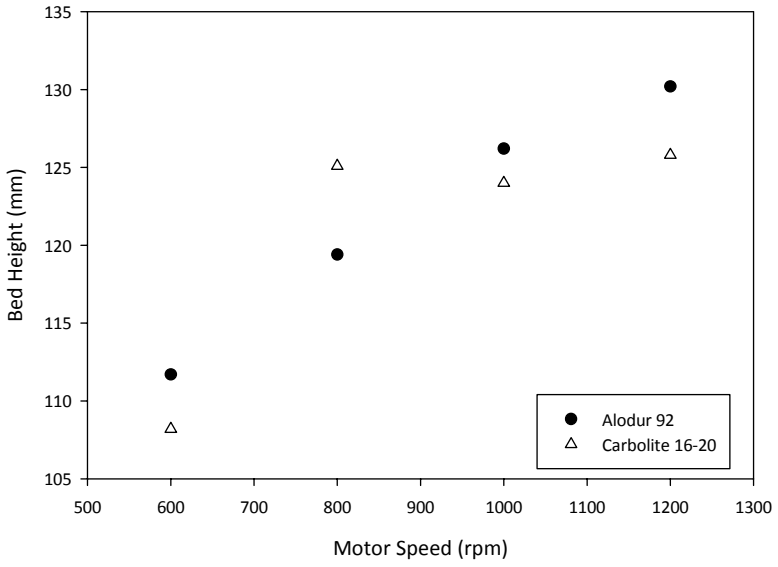

Figure 6-8: Effect of the motor speed on the maximum height of the bed. As this is the maximum range in z coordinate of the tracer, and the experiments have not been repeated, errors in the bed height are not appropriate.

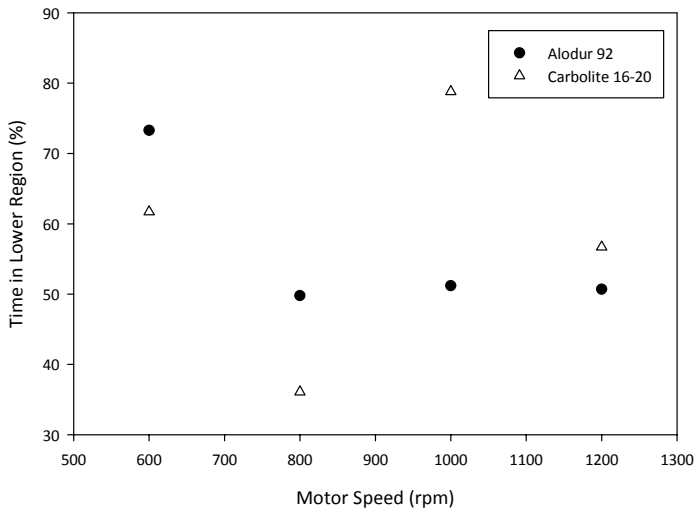

Figure 6-9: Time in the lower region for both media as a function of motor speed.

The rise in bed height with motor speed, which is displayed in Figure 6-8 demonstrates a progressive increase in the bed height with motor speed. This is an expected result, as the increased rotational speed of the impeller will cause increased centrifugation of the mill loading. As this material nears the chamber wall, it is forced to move either up or down, and that material which is forced upwards has more energy, and hence will travel further before returning back into the central vortex. Combining the findings, from Figure 6-8 and Figure 6-9, it can be seen that with increasing speed, the bed tends to gain height, and also the particle spends less time in the lower region. This pattern is clearer with the Alodur media than it is with the Carbolite media, which is less consistent in these trends. The reason for this may be that the rod shaped media is interlocking with neighbouring particles, creating a 'log-jamming' effect which causes this media to have different vertical mobility than the spherical media. This may lead to the measure of time in the lower

region being essentially random and independent of motor speed for the Carbolite media. Unfortunately a good estimation of the errors in the measurements is not feasible given the practicalities of the PEPT experiment, so this observation may not be verified.

6.3.3.2 Effect on velocity and kinetic energy

Figure 6-10 shows that with increasing motor speed, there is a tendency for the mean dimensionless velocity to decrease. Alodur media is often seen to give a higher mean V* over the motor speeds investigated here. Similarly Figure 6-11 shows the maximum speed which is achieved in the grinder by the tracked particle, and it is clear that there is an expected increase with motor speed. Once again, it is seen that the Alodur media has a higher, or similar, maximum particle velocity than the Carbolite media does.

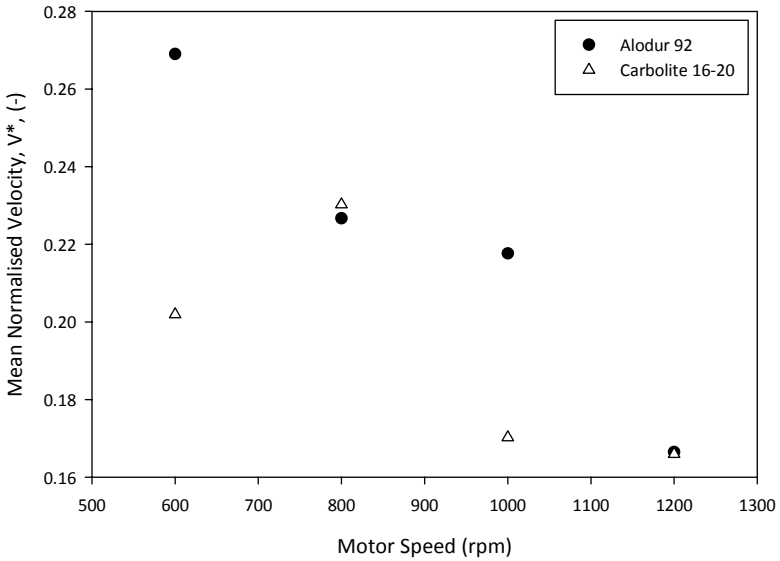

Figure 6-10: Effect of the motor speed on the mean V* (normalised by impeller tip speed) of the different grinding media. Random errors cannot be calculated without repeating

the experiments. Errors in V^* are estimated at 10%, based on the variation in Carbolite experiments.

In Figure 6-12 the total kinetic energy in the system is given, and there is a trend of the kinetic energy increasing with higher speed. There are no discernable and consistent differences between the Alodur and Carbolite media.

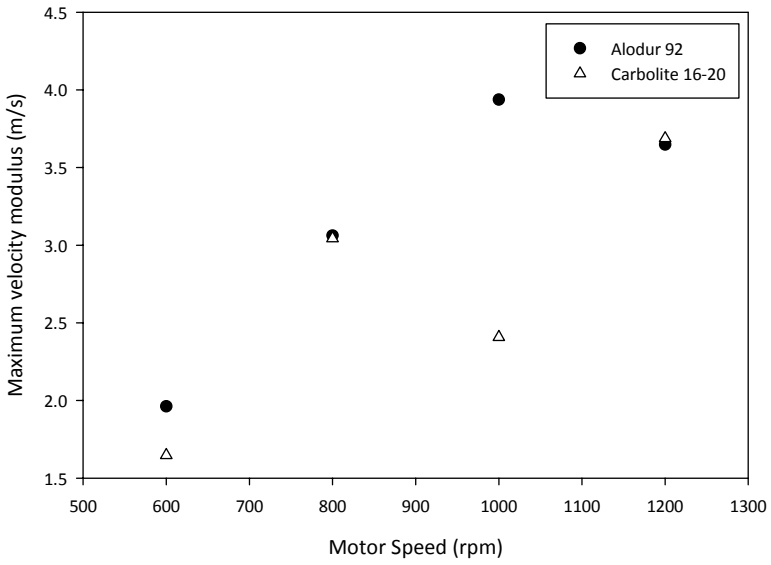

Figure 6-11: Maximum absolute velocity of both grinding media, V_{abs}, as measured in the chamber.

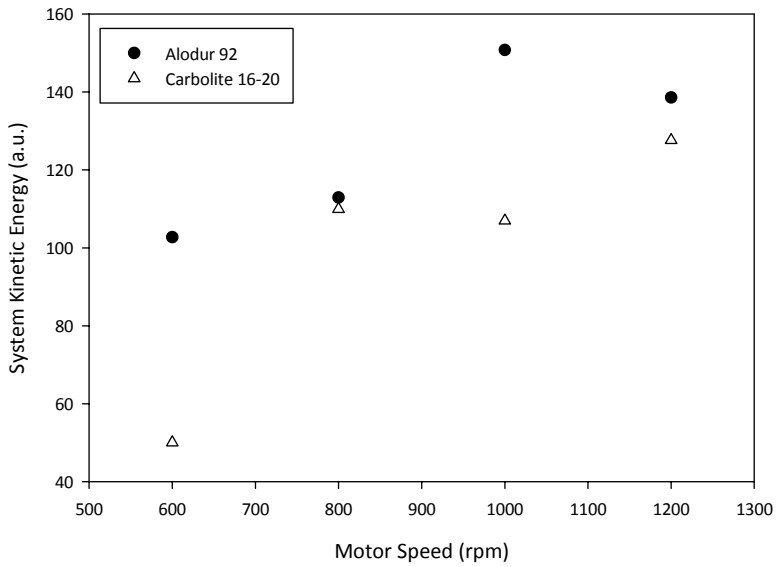

Figure 6-12: Measure of the total kinetic energy in the system for both media over a range of motor speeds. Units are arbitrary yet consistent. Random errors cannot be calculated without repeating the experiments. Errors in are estimated at 5%, based on the variation in Carbolite experiments.

When considering velocity, it is possible to consider both the true velocities which are present in the system, and a normalised velocity, based on the tip speed. In Figure 6-10 it is seen that the mean normalised velocity in the mill decreases with increased impeller speed. This infers that at higher speeds, the transmission of velocity from the impeller to the mass of media is less efficient. For the Alodur media, there is a drop from V* = 0.269 to V* = 0.166 with the motor speed increasing from 600 to 1200 rpm. This is a drop of nearly 40%. Therefore, despite the increase in the true mean velocity, there is now a possible contributing factor as to the decrease in efficiency with higher rotational speeds; the grinder is set to input an equivalent total energy in all cases, therefore it is important that this energy is transformed into grinding within the chamber.

Figure 6-11 investigates the maximum absolute velocity which is found within the mill. As this is the largest single velocity which is found, it is widely susceptible to experimental noise of a single large data point. However, there is a good broad experimental trend of the maximum observed velocity increasing with the motor speed, as would be expected. Similarly, higher motor speeds would be expected to give an increase in the kinetic energy of the system, and this is largely observed in Figure 6-12.

6.3.4 Effect of physical density on flow with spherical media

Table 6-4 summarises the occupancy plots for media of increasing density, at both motor speeds. The changing patterns in recirculation loops and areas where the tracked media particle begin to spend more or less time are apparent. As well as evidence of a change in the interior distribution of the flow, there is some evidence of a change in the total shape of the flow, which may correspond to a change in the size and shape of the central vortex in the mill.

Table 6-4: Summary table of the effect of media physical density on the occupancy plots for congruent spherical media. Scale bar shows % time in a cell.

Media Density (g/cm^3)	2.71	3.53	3.90	6.00
600 rpm	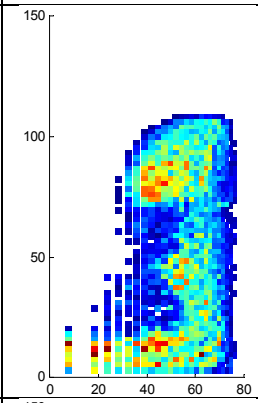	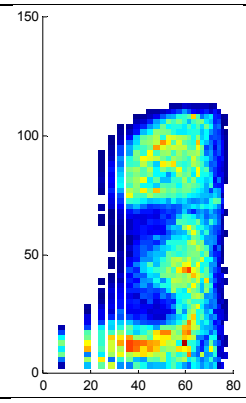	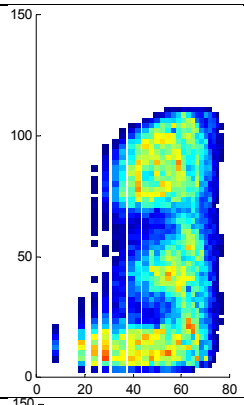	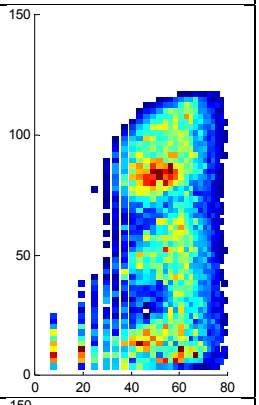
1000 rpm	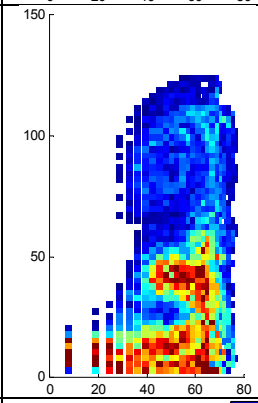	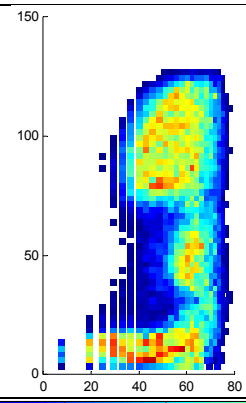	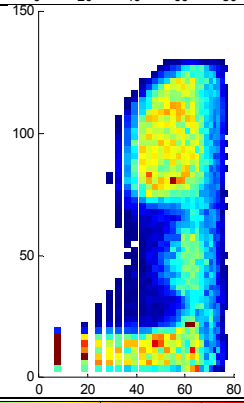	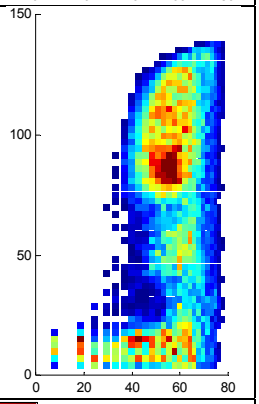
	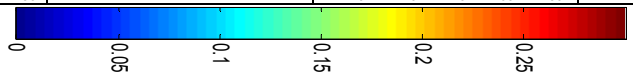			

6.3.4.1 Bed height and time in lower region

Figure 6-13 illustrates the effect of the media on the height of the media bed within the mill chamber. It is seen that there is an increase in the bed height with media density, although the form is less obvious at 600 rpm. In Figure 6-14 it is again seen that with the higher density media (and thus larger bed height) there is a decrease in time spent in the lower region of the mill.

The occupancy figures given in Table 6-4 highlight trends in the media distribution with changing density. Aside from an unusual distribution with the Carbolite media at 1000 rpm, the form of the occupancy plot remains quite consistent. In each plot, the location of the impellers is clearly visible with the two 'indentations' – areas of low occupancy where the media is forced out by the impellers. The tracked particle is also seen to spend very little time at the chamber wall, which has an area of low occupancy along its height. This suggests a built up region at the wall which is not perturbed by re-circulating media.

Aside from these, the particle spends time in three main areas along the height of the chamber. Initial observations suggest that with increasing media density, there is a greater time fraction in the upper section of the mill. This is reinforced by the observation in Figure 6-14 which suggests that for both motor speeds there is a decrease in the time spent in the impeller region, as the density of the media increases.

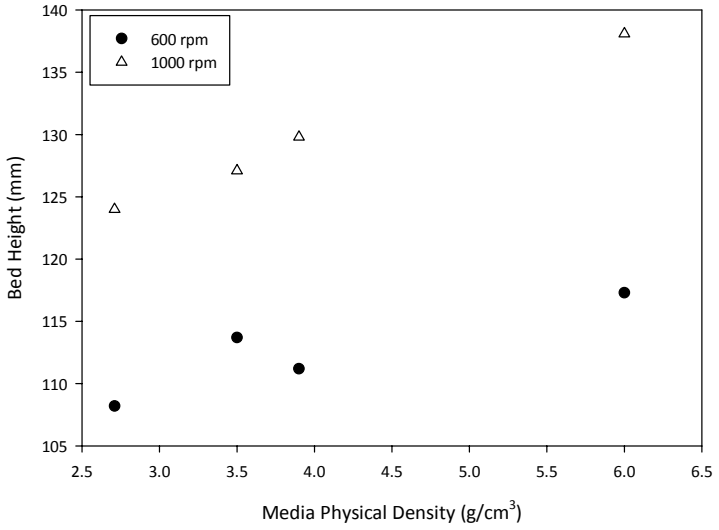

Figure 6-13: Relationship between the media density and the bed height at both speeds. As this is the maximum range in z coordinate of the tracer, and the experiments have not been repeated, errors in the bed height are not appropriate.

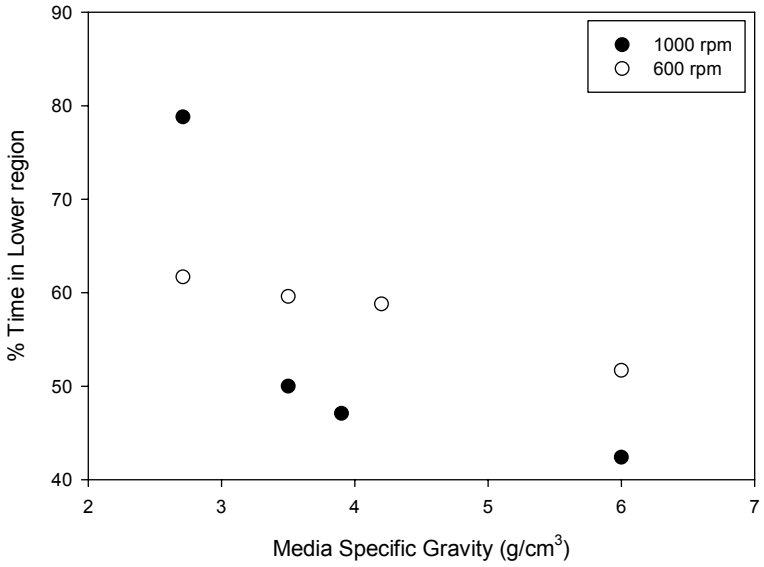

Figure 6-14: Time spent in the lower (impeller) region of the mill as a function of media density.

Figure 6-13 suggests that the overall height of the bed increases with media density. These observations may be explained by considering the energy situations where the particle gains energy. Predominantly, this will be from rapid acceleration in the proximity of the impellers. As the impellers move at the same speed regardless of the media density, the media particles are likely to gain the same velocity in this region, regardless of density. Therefore, higher density particles have more kinetic energy here than their lower density counterparts. This may mean that more vertical distance is travelled before all the kinetic energy is lost in the vertical plane.

As was witnessed with the effect of the motor speed, Figure 6-14 demonstrates that there is a concomitant relationship between the height of the bed and the time spent in the impeller region of the mill, whereby the increase in media density increases the height of the bed, as well as dramatically reducing the time spent in the lower region of the mill.

6.3.4.2 Effect of media density on velocity and kinetic energy

In Figure 6-15, the relationship between media density and the mean normalised velocity is seen. There is no pattern which can be confidently attributed to this data, although there is a similar form to the data points at 600 and 1000 rpm. The average decrease in the mean normalised velocity V*, when changing from 600 to 1000 rpm, is 16% (±5). As may be expected, the maximum velocity found within the mill is higher (regardless of media density) at 1000 rpm than 600, as is shown in Figure 6-16. However, the data does not have a clear form.

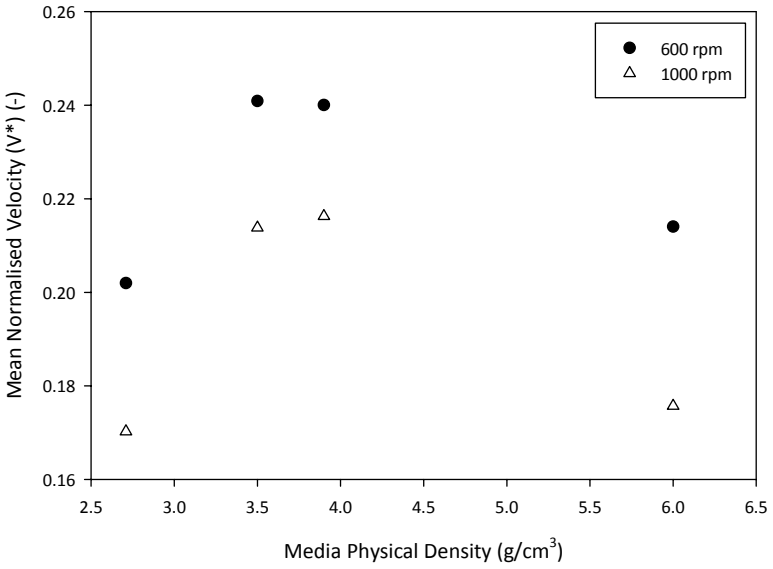

Figure 6-15: Effect of media density on the mean V* (normalised by tip speed). Random errors cannot be calculated without repeating the experiments. Errors in are estimated at 10%, based on the variation in Carbolite experiments.

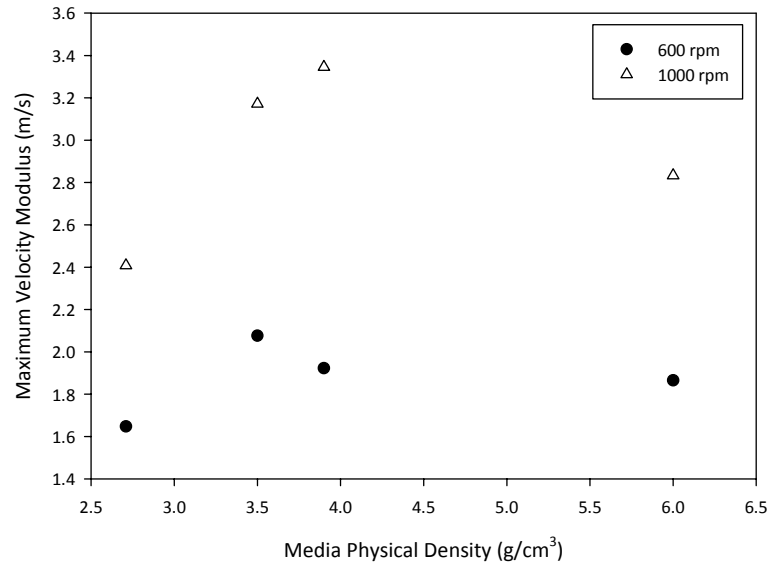

Figure 6-16: Maximum absolute velocity measured in the chamber at both motor speeds as a function of density.

Figure 6-17 examines the relationship between media density and the system kinetic energy. As may be expected, the higher motor speed results in a higher system kinetic energy. There is also a progressive and clear increase in system kinetic energy with increasing media density, and the regression analysis (although limited by a very small data set) shows affirms this relationship. The kinetic energy at 1000 rpm is on average 88% (±8) greater than at 600 rpm. Given that there is a 66% increase in motor speed, the kinetic energy might be expected to increase by the square of the motor speed. However, it does not, and only increases at a slightly greater rate than the linear increase in speed.

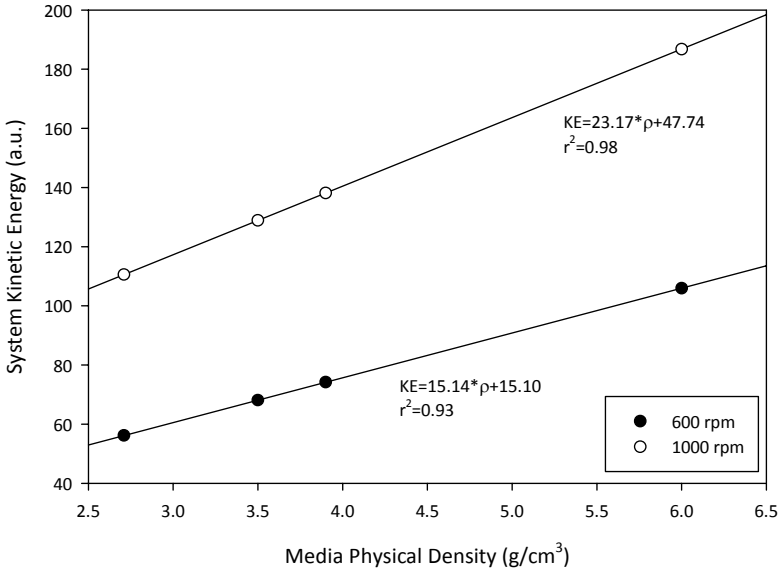

Figure 6-17: Total system kinetic energy as a function of media density for both motor speeds. Units are arbitrary but consistent. Random errors cannot be calculated without repeating the experiments. Errors in are estimated at 5%, based on the variation in Carbolite experiments.

The normalised velocity in the mill is a good measure of how effectively the tip speed is being transferred to the grinding media. It is seen in Figure 6-15 that initially there is an increase with mean V* with media density, however, the highest density media (6.0 g/cm^3) does not concur with this pattern. Interestingly, the same media performs worse than expected in the grinding tests shown in Chapter 5. This suggests that there may be some further feature of this media which differentiates the flow form from other media, which could potentially be related to surface roughness and drag factors.

The system kinetic energy is seen to increase in a linear fashion with the higher density. The higher density of the particles will of course directly have an effect on the kinetic energy (due to the mass consideration of kinetic energy), but nevertheless this confirms expectations of the process.

6.3.5 Correlation of PEPT data with real size reduction data

In the introduction to this chapter (Section 6.1) PEPT was introduced as a method for investigating the effect of the grinding media on the flow, and reducing the 'black box' approach to dealing with the sand grinder. In this section, the experimental data for the size reduction of the carbonate slurry are compared with characteristics of the final slurry from the grinding with spherical media results from Chapter 5. It is possible to analyse the relationship between the various measured parameters in order to predict the size reduction or surface area generation. The data used in this discussion is that presented in Chapter 5, combined with the PEPT parameters.

A multiple linear regression tool was used in Excel[7] allowing investigation of the various measured parameters with the generated surface area. The regression analysis shown in Figure 6-18 shows that a good relationship between the measured PEPT parameters and the surface area can be realised with a high degree of confidence. There are three obvious outliers from the fit, two of which are the Magotteux MT1 media at 600 and 1000 rpm, whilst the third is Alodur 92 media at 800 rpm (as indicated in Figure 6-18).

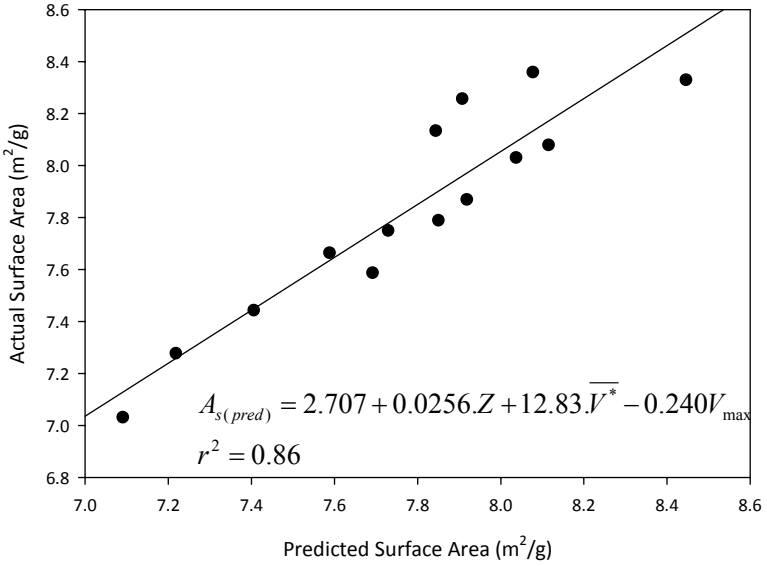

Figure 6-18: Multiple Linear Regression analysis of the bed height (Z), mean normalised velocity ($\overline{V}^*$) and the maximum velocity, V_{max} for surface area, for all data points. Three outliers are circled, corresponding to the Magotteux MT1 media.

The Magotteux MT1 data appear to both be anomalous, and if it is removed and the data is re-analysed, then the results are shown in Figure 6-19, where there is a very good fit to the measured surface area (r^2 value of 0.92 compared with 0.86). The measurement of

surface area through the BET method has an associated error of 0.1 m^2/g at this level, showing that the fit to this line of the real data is good.

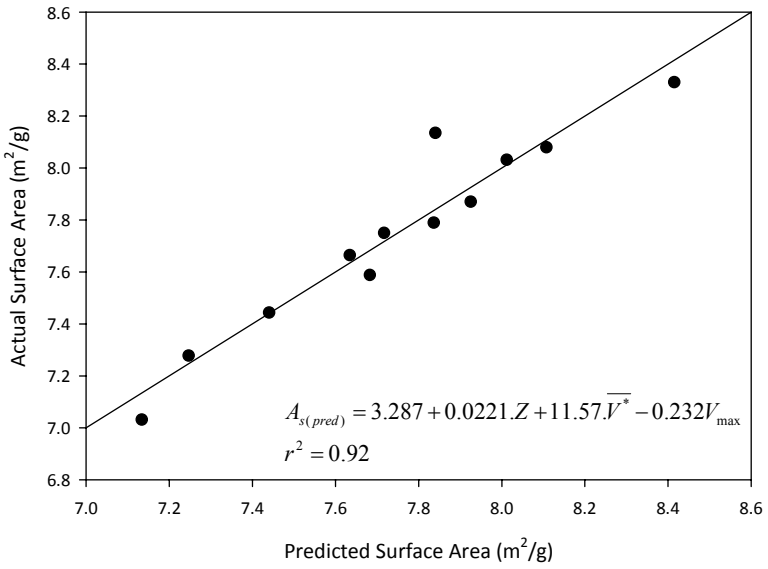

Figure 6-19: Second Iteration of multiple linear regression as in Figure 6-18, without MT1 media.

The chosen parameters for the linear model are related to the key parameters from the initial model of Kwade, discussed in Section 2.4.2.4. The voidage is difficult to derive from the PEPT data, but it is related to the bed height, Z. The maximum velocity in the PEPT data relates to the tip speed considered in the PEPT data. Finally the normalised velocity gives a measure of the degree of transfer of the impeller velocity to the grinding media.

6.4 Conclusions

6.4.1 Differences with shape.

The limitation of a small sample size means that it is difficult to hypothesize with confidence as to the differences with these data between the rod shaped and spherical media. This is further complicated as there are of course other parameters changing between the two media, including the density and the surface roughness. As the diameter of the rods is essentially the same as the diameter of the spheres, yet there is an aspect ratio of approximately 3 with the rods, each rod shaped particle has a higher volume than in the spherical examples.

Nevertheless, there are some differences in the behaviour of the two media, which may or may not be significant in the differences in efficiency which are witnessed. The rod shaped media is seen to give a higher mean V* at both 600 and 1000 rpm, whilst at 800 and 1200 rpm the two media give very close results. However, there is on average 10% higher mean V* with the Alodur media compared to the Carbolite media. This represents an improved transmission of tip speed to the motion within the bed.

With kinetic energy, it is difficult to discern any significant difference between the rods and the spherical media. Although the Alodur media is seen to have on average a 10% more kinetic energy at any instant, the scatter in the data is too great to confidently assert any difference. As kinetic energy is essentially a combination of occupancy and the squared

velocity vector, this is evidence that there is an attributable and significant difference in the occupancy data.

6.4.2 Effect of specific gravity on spherical media

Whilst considering the effect of the media density on the flow patterns, it is assumed that there are no further differences between the media. The reality is likely to be different, and effects such as the surface roughness and the size distribution of the media may come into play. Indeed, such effects may relate to some of the deviations seen in trends with the following results.

6.4.3 Summary

Positron Emission Particle Tracking (PEPT) has been seen to be an excellent method for visualising the motion of media particles within a stirred media mill. This alone enables examination of high and low velocity sections of the mill, as well as complete dead zones. Furthermore, a number of additional parameters may be extracted from the PEPT data to further relate the raw data to the effectiveness of grinding. These parameters, such as kinetic energy, and normalised velocities, have been considered in relation to the speed of the motor, as well as the density of the media. Kinetic energy, and normalised velocity have been shown to be dependent on these variables, although the high density yttria-stabilised zirconia media, the trend was bucked, suggesting that there are other contributing factors at play.

Many authors cite the overall power density of a mill [8] as a key factor in determining its efficiency. This work has shown that the reality may be more subtle than this. The kinetic energy map in Figure 6-7 demonstrates that the energy of certain areas of the mill may be at least one order of magnitude greater than the remainder of the flow bed. This information, combined with the evidence of very good circulation shown in Figure 6-4 proves that the overall bulk energy density may be an over-simplification.

PEPT also allowed comparison of the behaviour of rod-shaped Alodur 92 media with spherical Carbolite media. Although there may not be a clear cut explanation for the improved efficiencies seen in Chapter 5, there is strong evidence that the rod shaped media results in a higher average velocity (normalised) and larger kinetic energy. This may be attributable to a greater transmission of forces and motion between the media, causing a larger zone of high kinetic energy.

The grinding efficiency data from Chapter 5 has been combined with the PEPT measurements, and it is seen to be possible to predict the generated surface area of a slurry through a combination of measured PEPT parameters. This has demonstrated that it is desirable to aim for higher mean normalised velocity within the chamber, a parameter which this work has demonstrated to be related to higher density media, as well as the rod shape of Alodur 92.

6.5 References

[1] Parker DJ, Hawkesworth MR, Broadbent CJ, Fowles P, Fryer TD, McNeil PA. Industrial positron-based imaging: Principles and applications. Nuclear Instruments and Methods in Physics Research Section A: Accelerators, Spectrometers, Detectors and Associated Equipment 1994;348:583.
[2] Barley RW, Conway-Baker J, Pascoe RD, Kostuch J, McLoughlin B, Parker DJ. Measurement of the motion of grinding media in a vertically stirred mill using positron emission particle tracking (PEPT) Part II. Minerals Engineering 2004;17:1179.
[3] Conway-Baker J, Barley RW, Williams RA, Jia X, Kostuch J, McLoughlin B, Parker DJ. Measurement of the motion of grinding media in a vertically stirred mill using positron emission particle tracking (PEPT). Minerals Engineering 2002;15:53.
[4] Parker DJ, Hawkesworth MR, Beynon TD. Process applications of emission tomography. The Chemical Engineering Journal and the Biochemical Engineering Journal 1995;56:109.
[5] Chiti F. Lagrangian Studies of turbulent mixing in a vessel agitated by a Rushton turbine: PEPT and CFD. Dept of Chemical Engineering, vol. PhD. Birmingam: University of Birmingham, 2007. p.241.
[6] Bakalis S, Cox PW, Russell AB, Parker DJ, Fryer PJ. Development and use of positron emitting particle tracking (PEPT) for velocity measurements in viscous fluids in pilot scale equipment. Chemical Engineering Science 2006;61:1864.
[7] Ltd. A-IS. Analyse-It for Excel. 2009. p.Data Analysis Software.
[8] Wills B, Wills' Mineral Processing Technology. Oxford: Elsevier, 2007.

7 High Surface Area Talc

7.1 Introduction

Talc is a key industrial mineral, with a uniquely hydrophobic surface, as well as having a high aspect ratio, due to its crystal structure and chemistry (see Chapter 4). The hydrophobic surface chemistry means that additional chemicals, such as wetting agents and dispersants, are required for the effective wet grinding of the mineral, as is familiar from the grinding of calcium carbonate and kaolinite. Nevertheless, micronized talc has a number of benefits within a number of applications[1]. There a number of routes for achieving this micronisation, such as jet milling and ball milling. This chapter examines the dry stirred media milling of talc as a method for generating a high surface area talc mineral.

7.1.1 Effect of dry grinding phyllosilicates

Intense mechanical treatment of a mineral through dry grinding can result in alterations to the mineral structure, and this phenomenon has been well documented [2-5]. When platy minerals such as talc or kaolinite are ground, the initial grinding is seen to increase surface area and decrease particle size; however, with extended grinding times, the crystallinity of the mineral is reported to decrease and agglomeration may occur, resulting in a coarse, amorphous phase[2] – an effect which may be tracked by X-ray diffraction.

With intense dry grinding of kaolinite, formation of hydrogen gas is reported[6], which is attributed to the mechanochemical reaction of surface water with radicals formed by bond rupture on the surface. Specifically when considering the surface chemistry, Infra-Red (IR) studies of the surface bonding in kaolinite [7, 8] have shown that disruption and rearrangement can occur.

With respect to talc, structural properties have been studied, as well as the optical properties of the treated material, where it is seen that optical properties improved concomitantly with grinding time[9]. Mechanochemically activated talc which is subsequently leached in an acid solution has been shown to produce a porous structure with an extremely high surface area[10]. However the resulting material can no longer be considered as talc mineral, having been fundamentally transformed into porous silica. This work focuses on the dry grinding of talc and subsequent soaking in water to produce a high surface area material.

7.1.2 Application of high surface area talc

The cost of generating a high surface area material through a 'top-down' approach must be justified in order for the route to be industrially viable. Thermodynamically, surfaces have a higher associated energy than the bulk material, and this is also reflected in the energy costs of production. There are application benefits to be gained from higher surface area materials. This work highlights a key application of the high surface area talc – as a reinforcing agent in polymer systems.

Applications for high surface area talc should also exploit the highly hydrophobic surface chemistry – enabling compatibility with a number of media, especially polymers and oils. High surface areas are exploited in catalytic supports, whereby greater amount of surface for a unit mass or volume increases the rate of reaction, and thus plant efficiency increases. As well as these mentioned, there are many other fields where a high surface area, hydrophobic material could have application, such as removal of impurities from non-aqueous systems, i.e. oil filtration.

7.1.3 Polymer Application Testing

One of largest applications by volume and by market share for talc, is as a reinforcing agent in polymer systems[1]. The performance of any mineral filler in a polymer system is related to a number of factors [11], and one of these key factors is the chemical interaction between the particulate surface and the mineral filler. For this reason, hydrophilic minerals such as calcium carbonate are often treated with a surfactant to improve the interaction between the mineral surface and the bulk polymer.

One of the advantages of talc as a filler for polypropylene is that the chemically inert surface is naturally compatible with the hydrophobic polypropylene. This enables the introduction of talc into polymer systems without the added process step (and hence financial cost) of first surface treating the mineral.

7.1.4 Mechanical Properties testing

Mechanical testing can be performed in order to ascertain the reinforcement properties of the composites. Modes of measurement considered here are:

- Flexural properties – i.e. stiffness or resistance to bending.
- Tensile strength – i.e. resistance to longitudinal extension.
- Impact properties – near-instantaneous properties of the composite upon impact with a falling weight. Impact measurements are made with full test bars as well as with notched samples which have a carefully measured indentation along the line of fracture, with the intention of removing the crack initiation energy from the measurement.

As the results below will demonstrate, the impact properties of virgin polymer are often decreased through addition of a high aspect ratio filler, such as talc or kaolin[12], whilst these same minerals improve the flexural modulus[11]. Other minerals[11] with a low aspect ratio may be used to improve the impact properties of a polymer, whilst increasing the brittleness. Much of the current work into nanometre sized fillers attempts to move towards improving flexural and impact properties simultaneously [13-16].

7.2 Experimental

Dry grinding was performed in the modified lab sand grinder as described in Chapter 3, where stainless steel is found in place of all of the polyurethane to account for the high temperatures and levels of abrasion. Beihai talc with an initial surface area of approximately 3 m^2/g was ground for controlled amounts of energy, up to 850 kWh/t with Carbolite 16/20 as the grinding media. Throughout this work, the ratio of media to mineral was maintained at 5:1, using 1500 g of the grinding media. After grinding, the media is removed by dry screening, and the talc is soaked in tap water. In order to measure surface area, the final slurry is filtered and dried at 80 °C. The resulting cake is easily broken up by mortar and pestle.

For the mechanical testing of the polymer compounds, the feed talc is compared with the high surface area talc after dry grinding and soaking. Furthermore, an Imerys kaolin product (Polsperse 10) is used to indicate a typical set of results for all experiments, as well as offering a comparison with the talc.

7.3 Results

7.3.1 Eliminating sampling errors

As may be expected from Figure 7-1, there is an increase of surface area with energy input into the dry grinding process. In fact, the dry grinding for 850 kWh/t results in a surface area of 35 m^2/g. Subsequent soaking of this material overnight in tap water resulted in

70 m^2/g surface area. So the surface area is seen to double, without further mechanical input.

In order to resolve any issues with sampling errors, or retention of fines on the grinding media; samples from the powder prior to soaking were collected from different regions of the grind pot – material stuck to walls, at the top of the media, and at the bottom. Material stuck to the grinding media was also collected separately and weighed, before the surface area was measured. The combination of these results eliminated any issues with sampling errors, as there was little difference in the unsoaked material from any region of the grind pot (summarised in Table 7-1).

Table 7-1: Surface area of the dry ground material at different regions of the grind pot (unsoaked).

	BET Surface Area (m^2/g)
Top of the chamber	34.6 ± 0.5
Chamber walls	32.7 ± 0.6
Removed from grinding media	39.8 ± 1.2

7.3.2 Surface area increase with energy input

Talc was ground for different grind energies, and soaked in water overnight in each instance. The relationship between grind energy and surface area is shown below in Figure 7-1.

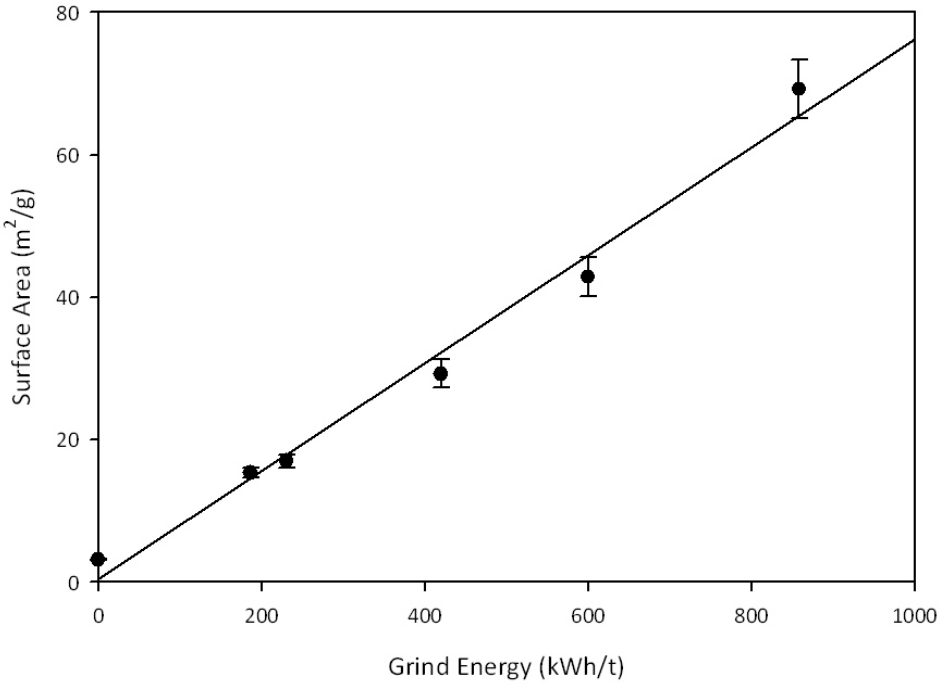

Figure 7-1: Relationship between surface area and the energy input for the dry ground, soaked talc.

7.3.3 Material Characterisation

The dry ground material has been characterised by a number of techniques, to verify that the effect is not an experimental artefact, and to enable understanding of the phenomenon.

7.3.3.1 Dynamic Vapour Sorption

Adsorption of octane onto the mineral surface allows for an alternative measure of the BET surface area, which has been previously measured with Nitrogen adsorption. As well as calculating the BET surface areas, the mass change as a function of target partial pressure

of octane can be seen, in Figure 7-2. The results in Table 7-2 compares the BET surface areas with Nitrogen as the gas and with octane vapour.

Table 7-2: Comparison of BET surface areas by N_2 and Octane adsorption. Error bars are based on only 2 repeats for the DVS measurements.

	N_2 BET Surface Area (m^2/g)	Octane BET Surface Area (DVS) (m^2/g)
Feed talc	3.2 ± 0.1	3.8 ± 0.2
Dry Ground 850 kWh/t	35.4 ± 2.1	25.2 ± 1.9
Dry Ground & Soaked 850 kWh/t	72.2 ± 3.4	76.5 ± 4.5

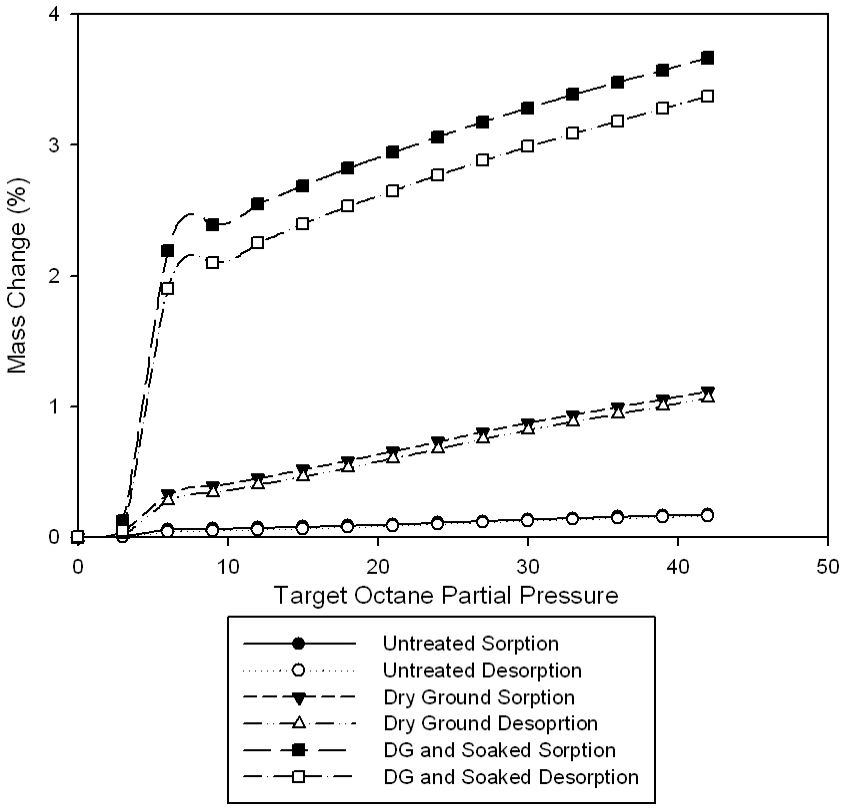

Figure 7-2: DVS adsorption/desorption curves for the talc at the three process stages (850 kWh/t of dry grinding).

7.3.3.2 Electron Microscopy

Scanning Electron Micrographs (SEM) of the mineral at the key stages of the process are shown in Figure 7-3. The dry grinding process causes platelet breakage, and generation of some fines, whilst some larger platelets remain. With the limitation of the extremely small sampling size with SEM, it is difficult to conclude that there is any noticeable difference in morphology between the intermediate and final product.

Figure 7-3 does show that there are a number of very fine particles in the final product, alongside the larger platelets. A single example of these is shown in Figure 7-4.

Unground Feed	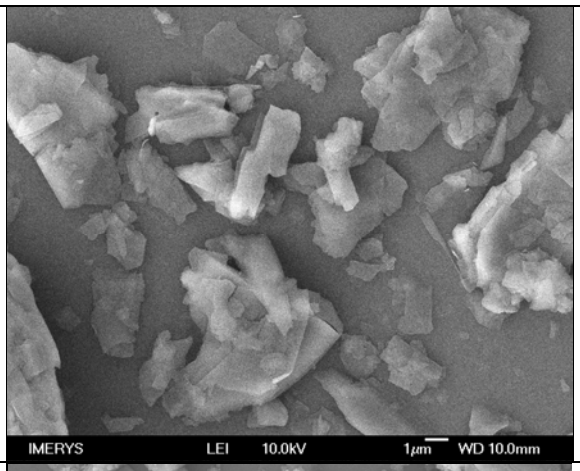
Intermediate (Dry Ground 850 kWh/t)	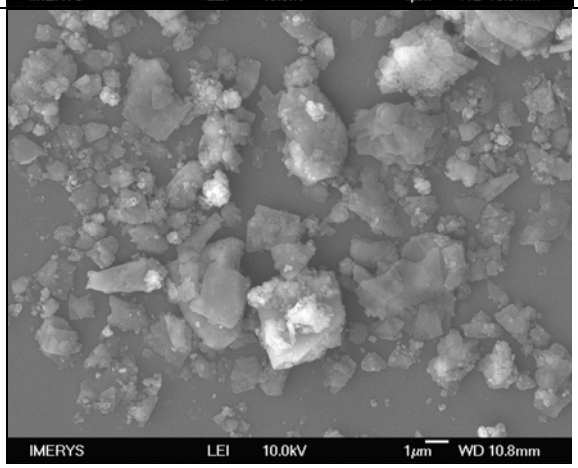
Final (Dry ground and soaked)	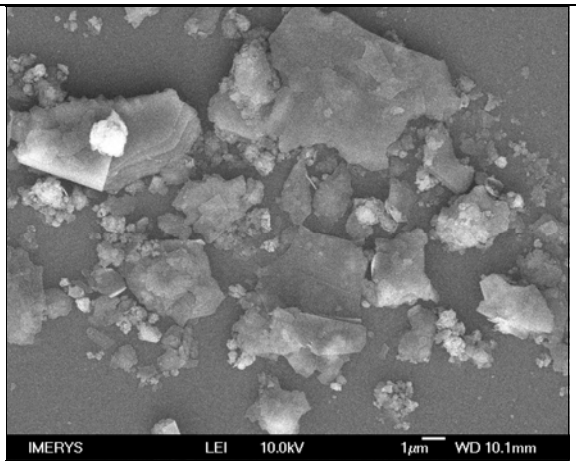

Figure 7-3: SEM images of the talc at 3 stages of the process. Field of view is 25 µm.

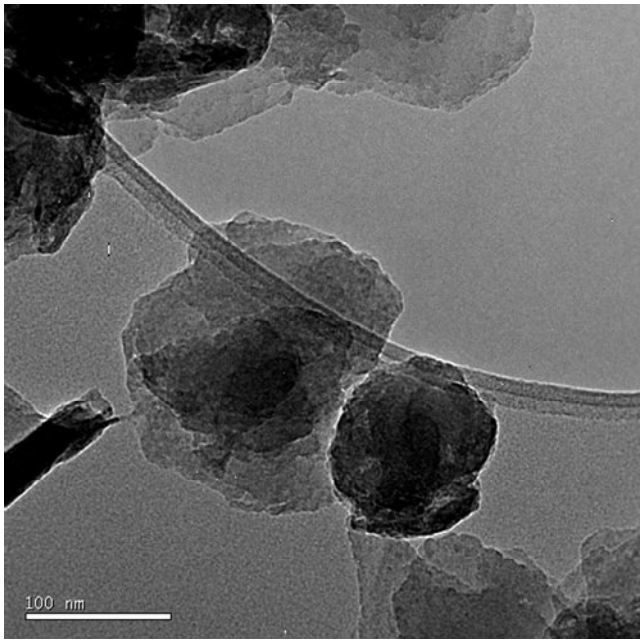

Figure 7-4: TEM image showing a close up image of two of the ultrafine particles. Field of view is approximately 500 nm.

7.3.3.3 Atomic Force Microscopy (AFM)

Atomic Force Microscopy (AFM) images of the feed are shown in Table 7-3, with the height images (vertical displacement of the cantilever) and the amplitude images (alteration of cantilever tapping amplitude). The first row of images shows the typical large plates which are present, as well as some smaller broken particles. The second row of images clearly show the step dislocations which occur on the surface of the large platelets.

With the final product talc material, there are still some large platelets remaining, as has been seen with the particle size analysis and SEM work (See Section 7.3.3.2). The images of the plate surfaces show that there are many fine particles found on the surface of the

plates, and the smooth surface plates have been replaced by many dislocations and adhered particles.

Table 7-3: AFM images (height and amplitude views) of the feed talc material. Field of view is shown below each image, as well as a vertical (z) range. (Images taken with much assistance from Dr J. Bowen).

Height Image	Amplitude Image
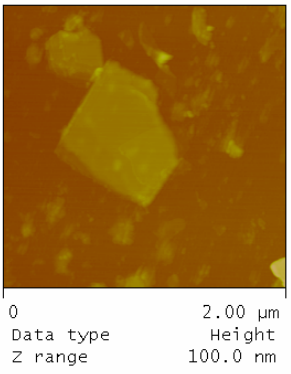	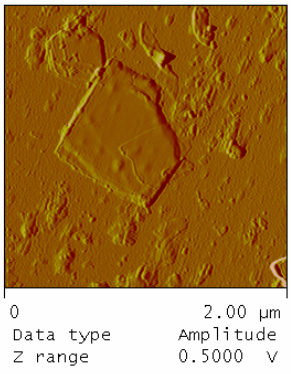
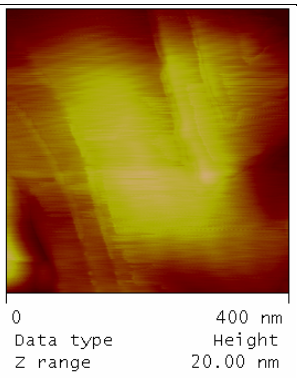	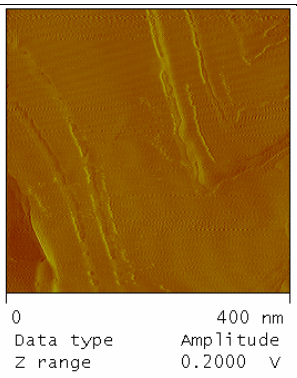

Table 7-4: AFM images (height and amplitude views) of the final product talc material. Field of view is shown below each image, as well as a vertical (z) range. (Images taken with much assistance from Dr J. Bowen).

Height Image	Amplitude Image
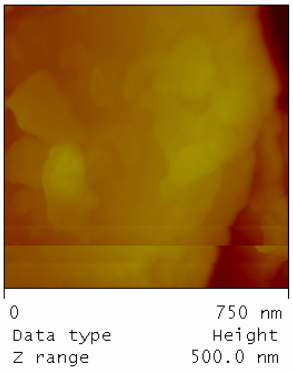	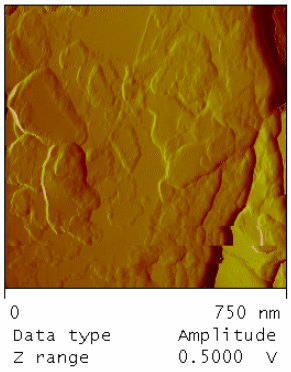

7.3.3.4 Particle Size Measurement

Particle size measurements by dynamic light scattering (CILAS, see Chapter 3) were performed on the feed and product material. As the technique works in the aqueous phase, it is inappropriate to measure the intermediate product in this way. The distributions are shown in Figure 7-5.

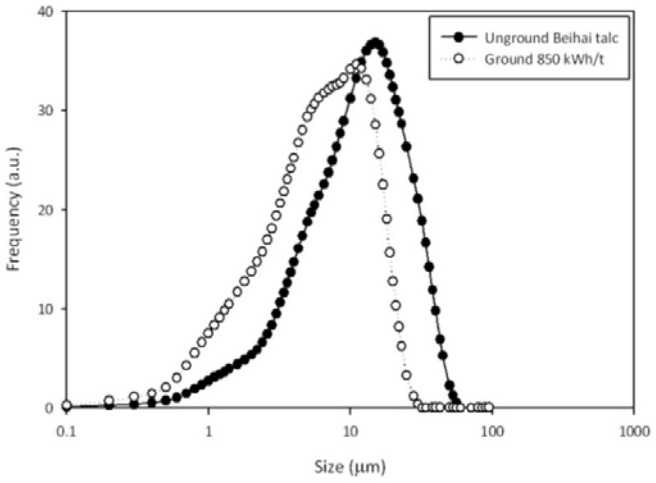

Figure 7-5: CILAS size measurements of the talc, before and after the dry grinding and soaking process.

7.3.3.5 X-Ray Diffraction (XRD)

The crystallinity of the samples of the three key stages of the process (feed, dry ground for 850 kWh/t, and the final soaked material) were characterised by X-Ray Diffraction (XRD). The combined trace in Figure 7-6 show that the crystallinity trace remains constant throughout the process, and the trace below is that of high purity talc. There is limited peak broadening and little evidence of amorphisation.

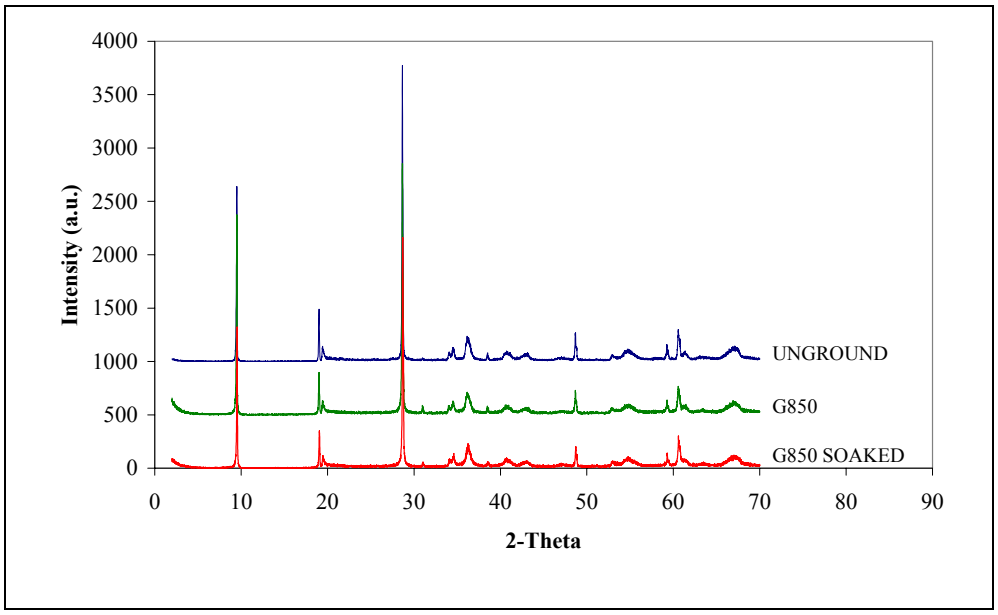

Figure 7-6: XRD trace for all three samples.

7.3.3.6 Mercury Porosimetry

Mercury is used as a probe to investigate whether the soaked material has a higher porosity than the material at other stages of the process. The results shown in Figure 7-7 indicate that there is no significant increase in porosity through the soaking process, in fact there is a smaller volume of the finest pores compared to both the feed and the dry ground intermediate.

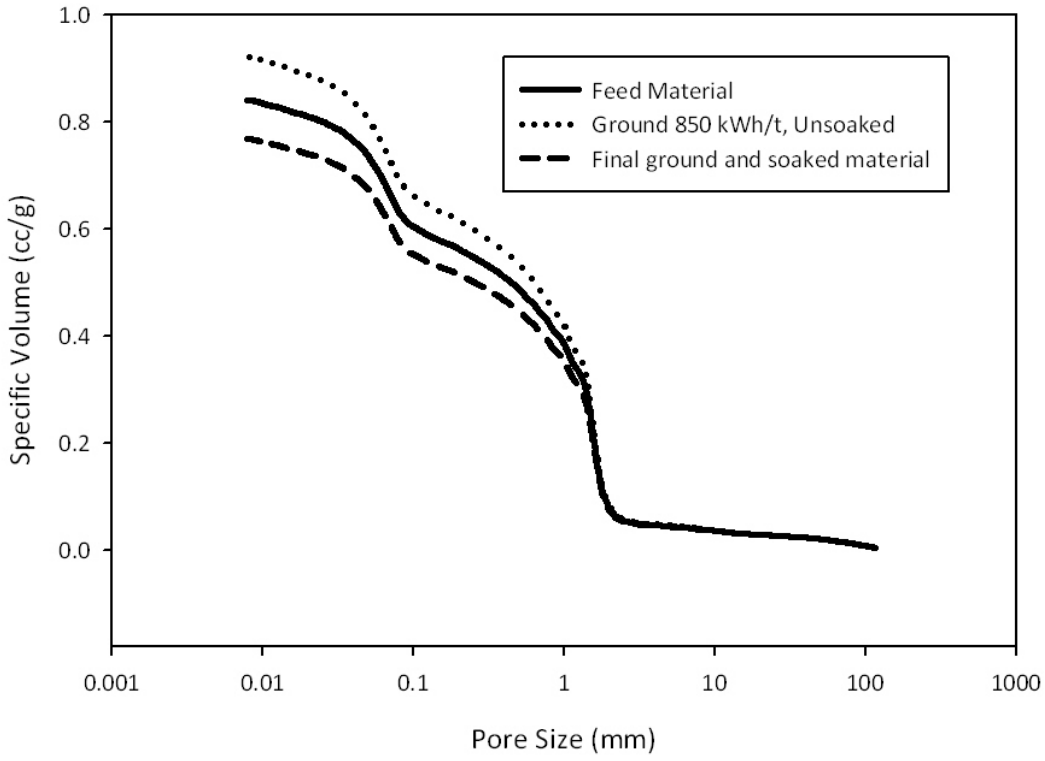

Figure 7-7: Mercury porosimetry data for the talc at the three stages of processing.

7.3.3.7 FTIR Analysis

Fourier Transform Infra-Red spectroscopy (FTIR) spectra of the three samples are shown in Figure 7-8. Throughout the process, there are no major changes to the spectra. The larger amount of residual water is seen with a broadening around 3500 cm^{-1}, and there is some indication that there may be a difference between the feed and the other products around 1550 cm^{-1}.

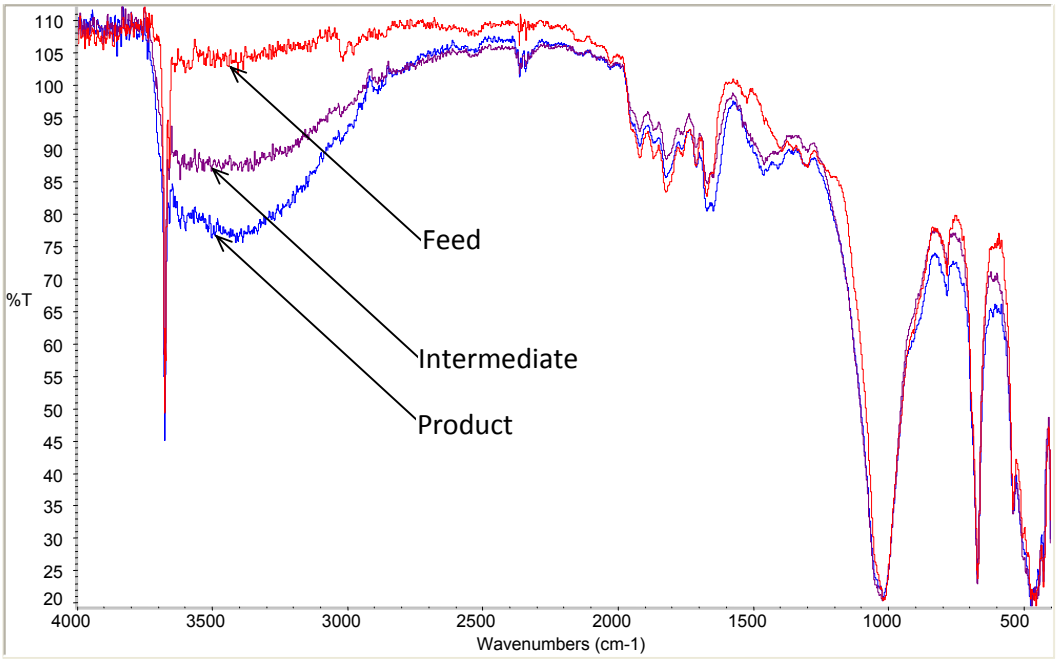

Figure 7-8: FTIR Spectra of the three samples, (grinding for 850 kWh/t). Spectra taken with great assistance from J. Hooper, Imerys.

7.3.4 Discussion – Talc Characterisation

The analyses have shown that there is an unexpected increase in surface area when talc which has been dry ground in a vertically stirred media mill is subsequently soaked in water. It has been shown that this effect is not an experimental relic, so the near doubling in surface at this latter stage must be attributable to one or more genuine mechanisms.

Crystallographic measurements (XRD) have shown that the material remains as talc throughout, and that there is no comprehensive amorphisation or phase transformation of the material. However, it is possible that there is a significant amount of ultrafine material

present which would not contribute significantly to the particle size distribution (which is inaccurate below 0.2 μm), but would have a relatively large impact on surface area.

Microscopy images from SEM, TEM and AFM suggest that there has been some alteration of the structure of the particles. Dry grinding in a stirred media mill is likely to have poor recirculation, due to material caking, and it is seen many large platelets remain in the system. However, AFM studies, although very limited in their sample size, have shown that platelets in the feed material have a uniform and flat surface, and clear edge dislocations are visible. The final ground and soaked product does not have these flat crystal planes, instead it appeared that there were many final particles on the surface. It is unclear at this stage whether these are new discrete particles or new surface features of the platelets.

7.4 Results – Polymer application testing

7.4.1 Flexural Modulus

The data shown in Figure 7-9 illustrate the change in flexural modulus with increasing filler content. It is seen that all three fillers increase the flexural modulus (i.e. stiffen the composite) and that the talc is more effective than the treated kaolin. There is little distinguishable difference in the performance of the talc before and after grinding.

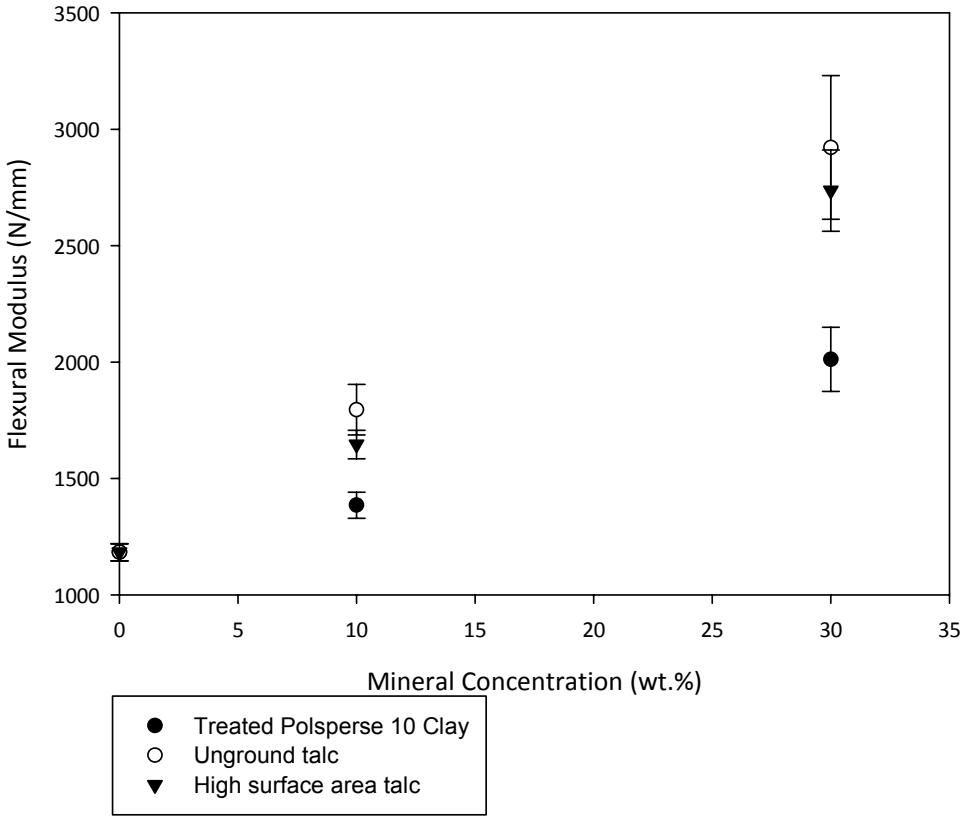

Figure 7-9: Flexural Modulus of the filled composites over the range of filler concentrations. Error bars are one standard error. Data points are the average of 5 repetitions.

7.4.2 Tensile Strength

Figure 7-10 shows the tensile properties of the injection moulded test pieces. It is seen that the kaolin filled composite leads to a slight reduction in the strength, whereas both talc samples increase this slightly. Similarly to the flexural modulus, there is little difference in the performance of the ground and unground talc filled samples, although again the mean value for the unground talc is slightly higher.

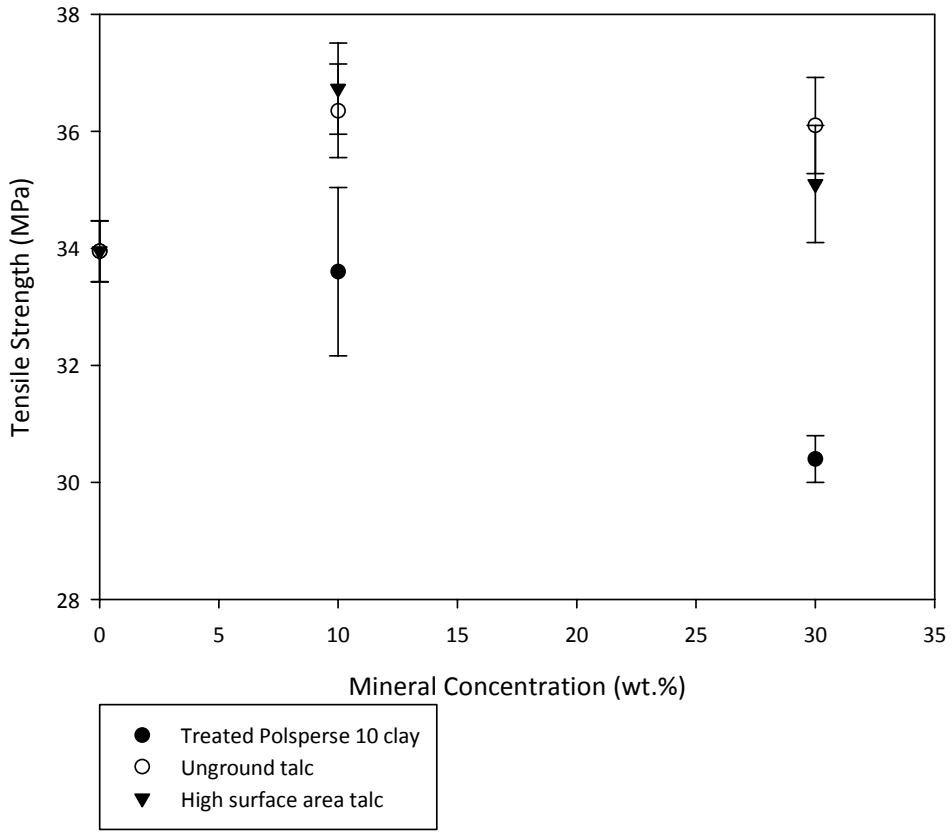

Figure 7-10: Tensile strength of the composites over the range of filler concentrations. Error bars are one standard error. Data points are the average of 10 repetitions.

7.4.3 Impact Testing

Impact testing gives three different measures of the impact properties of the composite – peak stress, peak energy and peak deflection. Figure 7-11 demonstrates the behaviour of the peak stress across the range of filler concentrations. It is seen that the addition of the talc has little effect on the peak stress of impact failure. In these tests however, the mean peak stress for the high surface area filled composites is higher than for the unground material. However, the difference is small given the deviations in the measurements.

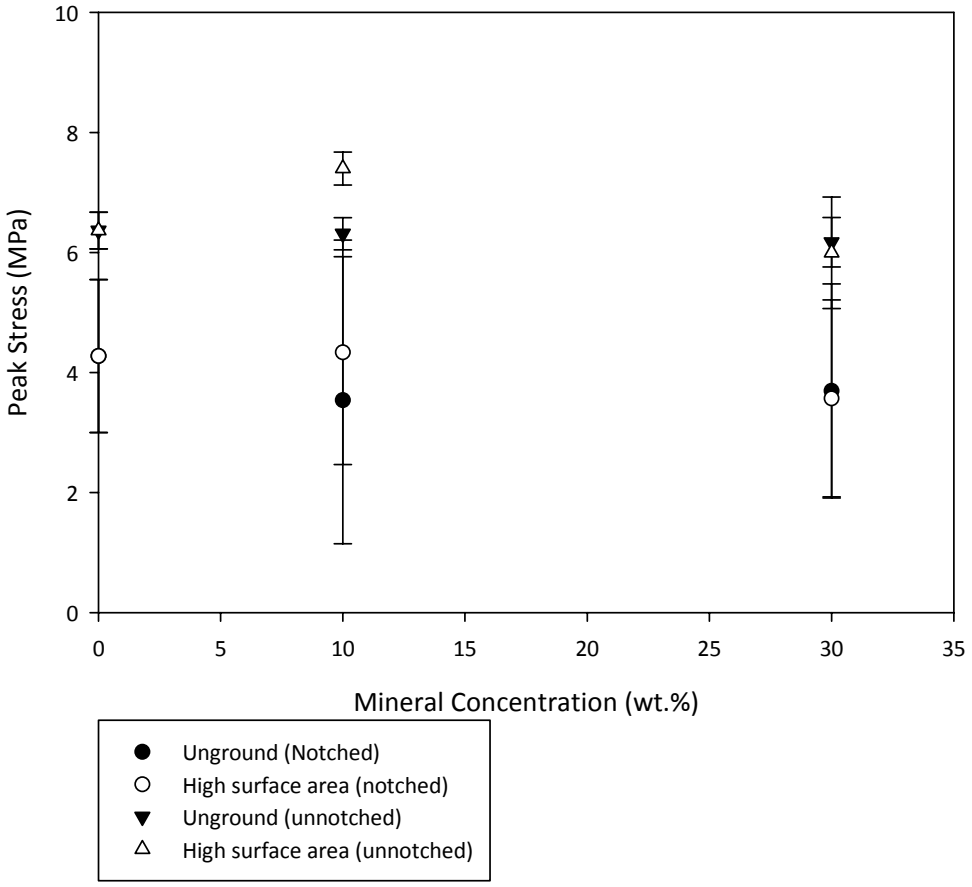

Figure 7-11: Peak stress across the cross section of the test piece during impact. Results are also given for test pieces which have been notched prior to impact. Error bars are one standard error. Data points are the average of 20 repetitions.

The peak energy is a measure of the total energy required for impact failure, and it is shown in Figure 7-12 that there is a slight decrease compared to the virgin polymer upon addition of the talc filler. The notched results do not demonstrate any clear difference between the ground and unground samples; however, with the un-notched samples (when crack initiation is part of the failure mechanism), it is seen that the high surface area talc requires more energy for fracture than the unground talc filled composite. This suggests

that the high surface area talc reduces the crack initiation energy for failure. Peak deflection data are not reported here due to the large errors bars on test results.

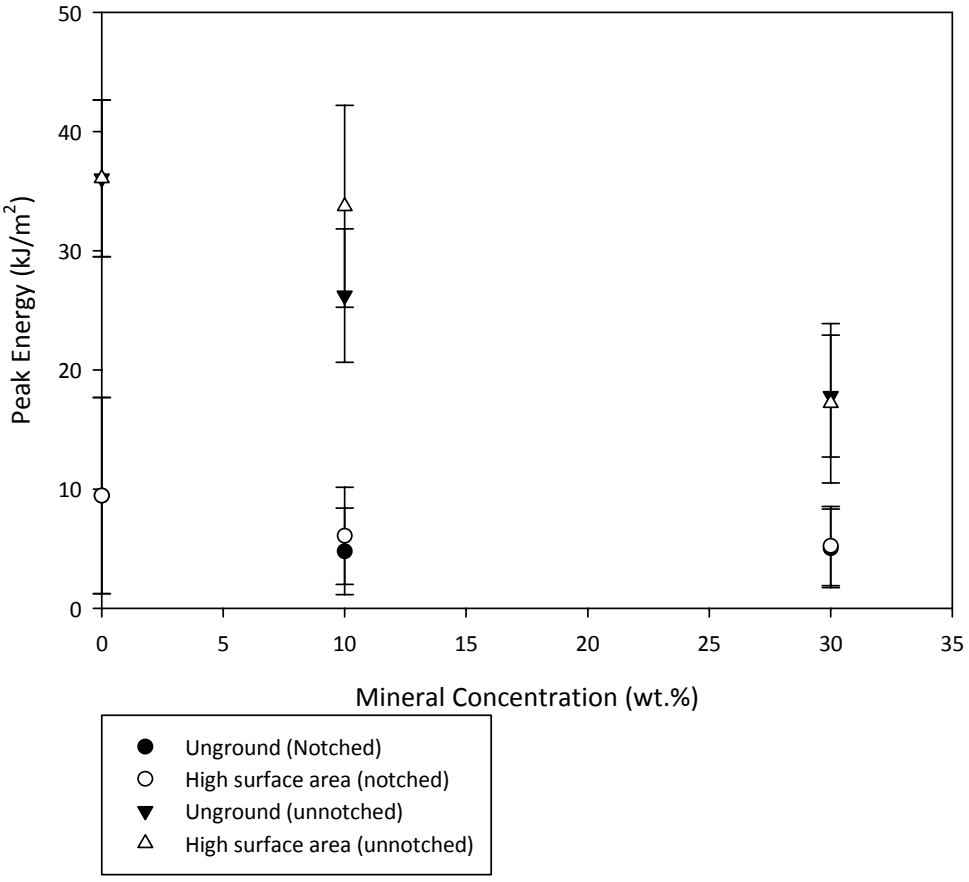

Figure 7-12: Peak energy during impact failure of the polymer composites. Results are also given for test pieces which have been notched prior to impact. Error bars are one standard error. Data points are the average of 20 repetitions.

7.4.4 Discussion – Polymer application testing

The polymer application testing has shown that the talc material can have beneficial reinforcing effects on the compound in polypropylene. However, there are few significant differences between the performance of the unground talc and the high surface area

material. This was unexpected, given the much higher surface areas which have been reported, as this surface area could be considered as a greater opportunity for interaction between the mineral filler and the polymer matrix. The lack of evidence for this effect may corroborate another conclusion from the talc characterisation – that there are a large number of ultrafine particles (which dominate the high surface area) but also a large number of coarse particles remaining. These coarse particles may dominate the mechanical properties of the filled compound, and thus prevent any expected improvement in the reinforcement of the compound. However, the high surface area talc is seen to reduce the un-notched impact strength, especially at low loadings (10 wt.%). This means that there has been a reduction of the crack initiation energy with this material which could be of industrial benefit. Furthermore, if the remaining coarser particles could be removed then it is expected that greater benefit would be seen from the high surface area material.

As a control material, the ultrafine surface treated kaolin, Polsperse™ 10, is used. This is seen to improve the flexural strength with increased loading. However the talc also increases the flexural strength with loading, and the effect is stronger than with the kaolin. None of the materials offer a strong effect of loading on the tensile modulus, however, it is seen that the addition of the different talc minerals increases the tensile modulus, whilst the kaolin causes a slight decrease.

7.5 Conclusions

The dry grinding technique has been shown to effectively and repeatedly produce a high surface area material, and the secondary soaking stage has been shown to generate further surface area, without the need for additional direct mechanical work input. Extensive characterisation of the resulting material has been performed, where it is confirmed that the final material is still predominantly crystalline talc. Various microscopy studies have shown that there are a number of ultrafine materials present, and it is possible that these materials are the source of the high surface area. This work could be extended by concentrating on these fine materials, and looking in more depth at the soaking and drying stages of the process in order to further optimise the surface area generation. If the proportion of ultrafine material can be determined, then there may be the opportunity to elucidate these fines, through a classification process, which could enable the coarser material to be recycled into the mill.

In order to determine the practicality of this approach for the micronisation of talc, the final material must be proven in an end application. This work has shown that in the current form, there is no strong evidence for reinforcement of the polymer compound, despite some evidence of improvement of impact energy at low loadings. However, it is seen that the addition of talc mineral provides an improvement in flexural modulus and tensile strength above the virgin polymer. It is possible that with better classification of the ground material, and removal of the coarser particles, that the high surface area talc would be seen to improve the mechanical properties of the compound.

Furthermore, it would be beneficial to compare the resulting product with equivalent materials prepared by alternative techniques, such as sand grinding. This comparison should be made on the basis of the properties of the product, as well as the energy cost in achieving the given particle size/surface area.

7.6 References

[1] Harben PW. Industrial Minerals Handybook: A Guide to markets, specifications and prices: Metal Bulletin PLC, 2002.
[2] Aglietti EF. The effect of dry grinding on the structure of talc. Applied Clay Science 1994;9:139.
[3] Aglietti EF, Porto Lopez J. Physicochemical and thermal properties of mechanochemically activated talc. Materials Research Bulletin 1992;27:1205.
[4] Zbik M, Smart RSC. Influence of dry grinding on talc and kaolinite morphology: inhibition of nano-bubble formation and improved dispersion. Minerals Engineering 2005;18:969.
[5] Pedro J. Sánchez-Soto M., Effects of Dry Grinding on the Structural Changes of Kaolinite Powders. Journal of the American Ceramic Society 2000;83:1649.
[6] Kameda J, Saruwatari K, Tanaka H. H_2 generation during dry grinding of kaolinite. Journal of Colloid and Interface Science 2004;275:225.
[7] Frost RL, Mako E, Kristof J, Horvath E, Kloprogge JT. Modification of Kaolinite Surfaces by Mechanochemical Treatment. Langmuir 2001;17:4731.
[8] Breen C, Illés J, Yarwood J, Skuse DR. Variable temperature diffuse reflectance infrared Fourier transform spectroscopic investigation of the effect of ball milling on the water sorbed to kaolin. Vibrational Spectroscopy 2007;43:366.
[9] Christidis GE, Makri P, Perdikatsis V. Influence of grinding on the structure and colour properties of talc, bentonite and calcite white fillers. Clay Minerals 2004;39:163.
[10] Yang H, Du C, Hu Y, Jin S, Yang W, Tang A, Avvakumov EG. Preparation of porous material from talc by mechanochemical treatment and subsequent leaching. Applied Clay Science 2006;31:290.
[11] Rothon R, editor Particulate-filled polymer composites: Longman, 1995.
[12] Brown R. Handbook of Polymer Testing: CRC Press, 1999.
[13] Chen BQ, Evans JRG. Impact and tensile energies of fracture in polymer-clay nanocomposites. Polymer 2008;49:5113.
[14] Deshmanea C, Yuan Q, Perkins RS, Misra RDK. On striking variation in impact toughness of polyethylene-clay and polypropylene-clay nanocomposite systems: The effect

of clay-polymer interaction. Mater. Sci. Eng. A-Struct. Mater. Prop. Microstruct. Process. 2007;458:150.
[15] Goettler LA, Lee KY, Thakkar H. Layered silicate reinforced polymer nanocomposites: Development and applications. Polym. Rev. 2007;47:291.
[16] Grecu I, Strat G, Gurlui S, Grecu V, Lihtetchi I, Strat M, Stratulat S, Picealca C. Structure and mechanical properties of nanocomposites based on polypropilene and polyethylene. J. Optoelectron. Adv. Mater. 2008;10:1408.

8 Conclusions and Further Work

This work has examined the stirred media mill, both as a tool for the wet grinding of calcium carbonate, and in the dry grinding of talc. Market data discussed in Chapter 1 has considered the importance of this work, within the context of reducing the energy costs and carbon footprint of comminution processes, as well as for the further understanding of the flow patterns in a stirred media mill.

8.1 Wet grinding of calcium carbonate

Many of the parameters in the wet grinding of calcium carbonate have been considered for the optimisation of grind efficiency, which has been shown to be dependent on the type of grinding media used, as well as the motor speed and ratio of media to slurry. The use of a new, rod-shaped, grinding media has been investigated at length, and this has shown to give significant and repeatable energy savings of 100 kWh/t for grinding a marble flour to a median diameter of 1 µm (when compared to the Imerys *status quo* of Carbolite media). This media has also been shown to be more stable with respect to media volume concentration, and confers a further benefit by grinding the mineral in a shorter time.

In order to confirm the benefits of the material, the process has been scaled up to a pilot scale grinder, and it was seen that at this scale there are still energy benefits from the media. However, the first recipe for the media has a dark colour, which makes it unsuitable

for the grinding of white minerals, as there is significant discolouration. Therefore, new recipes of white coloured, rod shaped grinding media are also developed. These also show energy savings over the Carbolite media; however the prototype materials show large errors in repetition which is attributed to the longer shape, and some abrasion of the fresh surfaces.

When a range of congruent spherical grinding media are considered with different density, it is seen that there is a general trend towards a higher density media giving a more efficient grind. However, there are evidently more of the media properties which are important to efficiency than the density, as the highest density grinding media has been seen to consistently give a worse efficiency than the trend would expect. The reasons for this have not been determined, although it is suggested that the surface roughness and wettability of the media may be important.

Further work in this area can follow one of two clear paths: firstly, the initial Alodur recipe of grinding media can be pursued for applications where the colour is not important (such as with metalliferous ores). Secondly, for comminution processes within Imerys, the white rod shaped media should be developed further. Whichever of these routes is being pursued, there are a number of factors which need further investigation:

- Rod length and aspect ratio: within this work, there has not been the opportunity to fully investigate the role of the length of the rod, or the diameter. Rod shaped

media with a range of cut length and extrusion diameter could be fully investigated in order to ascertain the sensitivity to grind efficiency.

- Wear rates: as is emphasised throughout this work, the commercial viability of the grinding media depends on the efficiency as well as the lifespan of the media. Initial work has been covered in this thesis, however the performance of the mature media, as well as the changing size and shape is another large area to investigate.
- Slurry rheology: the rheology of the slurry has a known effect on the grinding performance, and this is the subject of much research with spherical media. However, the effect of the rheology (from dispersants, and mineral fraction) with the rod shaped grinding media has not been examined here.

8.2 Positron Emission Particle Tracking in a stirred mill

Positron Emission Particle Tracking (PEPT) is very well suited for the studying of motion within a stirred media mill. The grinding beads can be irradiated with sufficient activity to achieve good quality data at the motor speeds which are used. The gathered information has revealed previously unseen properties of the motion within the mill, and highlighted some differences when the motor speed or the media density is altered.

The experimental data gathered for Alodur media has enabled a greater understanding of the mechanisms for the improved grinding efficiency with this media. It is seen that there are appreciable and constant differences in the transmission of impeller velocity to the

grinding media, and consequently higher kinetic energy in the bed with the rod shaped media than spherical media.

The role of density with spherical media is also examined using PEPT, and there are some similarities with the size reduction data gathered in Chapter 5. When a number of the measured parameters are combined, a very good correlation is seen between the grinding data and the PEPT results, however, it is seen that the Magotteux media performs better than the model predicts.

Now that PEPT has been shown as a useful tool for this application, there are a number of other effects which could be analysed, such as the role of the impeller shape, baffles and the media size. Furthermore, the tool could be used for grinding of different minerals, as well as grinding in horizontally mounted grinders. Ideally, the culmination of this would be as a tool for the verification of mathematical models of the stirred mill. If this was completed, then any number of changes to the grinder could be investigated and the benefits could be predicted before a large set of experimentation need take place.

8.3 Dry grinding of talc

The stirred mill has also been used dry in this work, where the dry grinding of talc, with subsequent soaking in water is seen to give an unexpected rise in surface area. The talc material has been fully characterised at all stages of the process in order to aid

understanding of the phenomenon. No significant crystallographic change is seen in the mineral over this process, and it is suggested that the extra surface area is related to the ultrafine material which has been seen through a range of microscopic techniques. The generated material is tested as a filler in polypropylene, where it is seen to give a better performance than the ultrafine kaolin which is used as a control. However, there are no major differences in performance between the high surface area talc and the feed material, which is attributed to the large number of coarse particles which are still present in the product.

This work could be extended in a number of ways to help generate additional surface area, as well as improve performance as a filler in polymeric systems. However, it is important to continue to investigate the reason behind the surface area gained through soaking the dry ground material in water. To confirm the hypothesis that the ultrafine (< 200 nm) material may be the key to the high surface area, a series of classifications could be performed in order to remove all of the coarse material. The fine material can then be examined to determine if the chemical composition and crystallinity is the same as the bulk material.

There is also potential for optimisation of the high surface area, through increasing the grinding time, or following the dry grinding with wet grinding, rather than simply soaking in water. Furthermore, a range of different liquids could be used for the soaking process in order to determine if this can be used to generate a higher surface area.

9 Appendix – Matlab Code For PEPT Analysis

Below is the homemade code 'AllPlots' which is used to generate the z-r plane images of the properties of flow in the mill. A number of additional programs are imbedded within this which have been previously developed within the University of Birmingham by Serafim Bakalis and Fabio Chiti. For these, the interested reader is directed towards Fabio Chiti PhD Thesis, 2007.

```
files = {a20_slow 'Carbo HSP' '600';...
    a20_fast 'Carbo HSP' '1000';...
    a21_slow 'Magotteux MT1' '600';...
    a21_fast 'Magotteux MT1' '1000';...
    a22_slow 'Silibead YZ' '600';...
    a22_fast 'Silibead YZ' '1000';...
    a23_slow 'Carbolite 12-18' '600';...
    a23_fast 'Carbolite 12-18' '1000';...
    a24_slow 'Carbolite 20-40' '600';...
    a24_fast 'Carbolite 20-40' '1000';...
    a25_slow 'Alodur rpt' '600';...
    a25_fast 'Alodur rpt' '1000';...
    a26_slow 'Ottawa Sand' '600';...
    a26_fast 'Ottawa Sand' '1000';...
    a29_600 'Carbolite 16-20' '600';...
    a29_800 'Carbolite 16-20' '800';...
    a29_1000 'Carbolite 16-20' '1000';...
    a29_1200 'Carbolite 16-20' '1200';...
    a30_600 'Alodur 92' '600';...
    a30_800 'Alodur 92' '800';...
    a30_1000 'Alodur 92' '1000';...
    a30_1200 'Alodur 92' '1200'};
%The above gathers all of the data sets which have been saved in Matlab
%format, and matches them with the corresponding media type and motor
speed
DataTable = zeros(23,11); %Empty matrix for the summary values to be
entered into.

for q = 1:1:22
    Array = files{q,1}; %Loads data set
    Media = files{q,2};
    Speed = files{q,3};
    filename = [Media Speed];
    Z = Array(:,3); %Selects appropriate set as 'z' values
```

```
    ZMAX = max(Z);
    ZMIN = min(Z);
    DataTable(q+1,3)=ZMAX-ZMIN; %Determines the bed height, as the range
of z
    ZT = Z - ZMIN; %Normalises to minimum in z
    Array(:,3)=ZT;
    data = Array;
    temp=data(:,3); %Switches the location of z and y so that z is
vertical
    data(:,3)=data(:,4);
    data(:,4)=temp;
    clear temp
    fdata=filtrad(data,'ON'); %Runs the filtrad (Chiti, 2007) routine to
remove noise.

    fdata=intrpselective(fdata,30,50,'on'); %Runs intrpselective (Chiti,
2008) to account for high speed particle

    fdata(:,2)=fdata(:,2)-mean(fdata(:,2)); %Normalises x and y about
central axis
    fdata(:,3)=fdata(:,3)-mean(fdata(:,3));
    fdata(:,4)=fdata(:,4);

    t=fdata(:,1)-fdata(1,1); %Defines start time as zero
    totaltime=fdata(end,1)-fdata(1,1);
    [th,r,z]=cart2pol(fdata(:,2),fdata(:,3),fdata(:,4)); %Converts to
cylindrical polars.
    count=1;
    %to estimate uth add all the components

    delta=0;
    th1=zeros(length(th),1);
    th1(1)=th(1);
    for i=2:length(th) %Ensures all values of theta are in correct range
        if(th(i)-th(i-1)<-pi)
            delta=delta+2*pi;
        end

        if(th(i)-th(i-1)>pi)
            delta=delta-2*pi;
        end

        th1(i)=th(i)+delta;

    end

    cyl=velest(t,r,th1,z,100,4,100); %Runs velest (Chiti, 2007) to
ascertain velocities
    occ=Oaxis(cyl); %Runs Oaxis (Chiti, 2007) to calculate occupancy.


%%The following sections generate plots for a number of different
%%parameters. Some can be chosen as a max or mean output for the
%%'Datatable' array. In all cases, the output is saved if flag = 'on' and
%%isn't if flag = 'off'.

%%
    %Radial Velocity
```

```
    figure(1)
    scatter(occ(occ(:,7)>0,1),occ(occ(:,7)>0,2),35,...
        occ(occ(:,7)>0,3),'s','filled')
    colorbar
    caxis([-0.2 0.5])
    axis equal
    axis([0, 80, 0, 150])
    filenameRV = [filename 'VR'];
    if length(flag)==2
        print ('-dmeta', filenameRV);
    end
    close
    DataTable(q+1,5)=max(occ(:,3));
%     DataTable(q+1,5)=mean(occ((occ(:,7)>0),3));
%%

    % Angular Velocity
    figure(2)
    scatter(occ(occ(:,7)>0,1),occ(occ(:,7)>0,2),35,...
        occ(occ(:,7)>0,4),'s','filled')
    colorbar
    caxis([0 2])
    axis equal
    axis([0, 80, 0, 150]);
    filenameVthe = [filename 'Vthe'];
        if length(flag)==2
            print ('-dmeta', filenameVthe);
        end

    close
        DataTable(q+1,4)=max(occ(:,4));
%         DataTable(q+1,4)=mean(occ((occ(:,7)>0),4));
%%

    % Vertical Velocity
    figure(3)
    scatter(occ(occ(:,7)>0,1),occ(occ(:,7)>0,2),35,...
        occ(occ(:,7)>0,5),'s','filled')
    colorbar
    caxis([-0.5 0.5])
    axis equal
    axis([0, 80, 0, 150])
    filenameVZ = [filename 'VZ'];
        if length(flag)==2
            print ('-dmeta', filenameVZ);
        end

    close
     DataTable(q+1,6)=max(occ(:,5));
%      DataTable(q+1,6)=mean(occ((occ(:,7)>0),5));
%%
    % Vector Plot
    figure(4)

quiver(occ(occ(:,7)>0,1),occ(occ(:,7)>0,2),occ(occ(:,7)>0,3),occ(occ(:,7)>
0,5),8)
    axis equal
    axis([0, 80, 0, 150])
    filenameVec = [filename 'Vec'];
```

```
        if length(flag)==3
            print ('-dmeta', filenameVec);
        end
    close

%%
    % Occupancy
occ(:,7)=occ(:,7) / sum(occ(:,7));
    figure(6)
    scatter(occ(occ(:,7)>0,1),occ(occ(:,7)>0,2),35,...
        occ(occ(:,7)>0,7),'s','filled')
    colorbar
    axis equal
    axis([0, 80, 0, 150])
    filenameOcc = [filename 'Occ'];
          if length(flag)==2
              print ('-dmeta', filenameOcc);
          end
    close
        DataTable(q+1,11)=std(occ(:,6));
%%

    VSQUARED=zeros(size(occ,1),1);
    for i9 =1:size(occ,1)

        VSQUARED(i9)=(occ(i9,3))^2+(occ(i9,4))^2+(occ(i9,5))^2;
    end
    occ(:,8)=VSQUARED;


%%
    occ(:,9)=0.5 * immultiply(occ(:,8),occ(:,6));

    % Kinetic Energy (occ 6)
    figure(8)
    scatter(occ(occ(:,7)>0,1),occ(occ(:,7)>0,2),35,...
    occ(occ(:,7)>0,9),'s','filled')
    colorbar
    caxis([0 0.25])
    axis equal
    axis([0, 80, 0, 150])
        filenameKE1 = [filename 'KE1'];
            if length(flag)==2
                 print ('-dmeta', filenameKE1);
            end
    close
    DataTable(q+1,9)=sum(occ((occ(:,7)>0),9));
%     DataTable(q+1,9)=mean(occ((occ(:,7)>0),9));
    DataTable(q+1,10) = DataTable(q+1,9) / totaltime;

end
```

For the generation of the Poincaré plots, a different routine is used ‘poincare’ which is shown below:

```
%%Program for the generation of Poincare plots for a vertical axis
symmetric
%%problem.
%Richard Tamblyn, University of Birmingham/Imerys 2009

Array = a30_1000; %Here a single data set is chosen for analysis
Media = 'Alodur 92'; %Media and speed inputted manually
Speed = '1000';
%%Section below prepares data as per 'AllPlots'.

filename = [Media Speed];
    Z = Array(:,3);
    ZMAX = max(Z);
    ZMIN = min(Z);
    ZT = Z - ZMIN;
    Array(:,3)=ZT;
    data = Array;
    temp=data(:,3);
    data(:,3)=data(:,4);
    data(:,4)=temp;
    clear temp
    fdata=filtrad(data,'ON');
        fdata=intrpselective(fdata,30,50,'on');
        fdata(:,2)=fdata(:,2)-mean(fdata(:,2));
    fdata(:,3)=fdata(:,3)-mean(fdata(:,3));
    fdata(:,4)=fdata(:,4);
    t=fdata(:,1)-fdata(1,1);
    totaltime=fdata(end,1)-fdata(1,1);
    [th,r,z]=cart2pol(fdata(:,2),fdata(:,3),fdata(:,4));
    count=1;
        delta=0;
    th1=zeros(length(th),1);
    th1(1)=th(1);
    for i=2:length(th)
        if(th(i)-th(i-1)<-pi)
            delta=delta+2*pi;
        end

        if(th(i)-th(i-1)>pi)
            delta=delta-2*pi;
        end

        th1(i)=th(i)+delta;

    end

%%Generation of Poincare plots.
    [xm,ym] = pol2cart(th,r); %Data changed back to Cartesian for 2d plots
    clear M
for Z=0:5:max(z) %Here the step length is defined as 5 mm, however, this
could be adjusted for more or fewer slices
```

```
    fr = Z / 5 + 1;
    SCDATA = zeros(length(th),2);
    direction = zeros(length(th),1);
    for i=1:1:length(z)-1
        alpha = z(i);
        beta = z(i+1);
        %First step determines whether the particle has moved from being
        %below Z to above Z. This is given a positive value (1).
        if alpha < Z
            if beta > Z
                SCDATA(i,1) = xm(i);
                SCDATA(i,2) = ym(i);
                direction(i) = 1;
            end
        end
        %Second step determines is it has moved from above to below Z,
this
        %is given a negative value (-1).
        if alpha > Z
            if beta < Z
                SCDATA(i,1) = xm(i);
                SCDATA(i,2) = ym(i);
                direction(i) = -1;
            end
        end
    end
%The data for this slice is plotted as a scatter plot
scatter(SCDATA(:,1),SCDATA(:,2),30,direction,'filled')
axis equal
axis([-80,80 -80,80])
title([' Height Z = ',num2str(Z), 'mm']);
%Each frame is compiled into a movie of the images.
M(fr) = getframe(gcf);
close
end

movie2avi(M,'poincareslow.avi','quality',95,'compression','none','fps',3);
```